

<https://doi.org/10.15388/vu.thesis.187>
<https://orcid.org/0000-0003-1552-8433>

VILNIUS UNIVERSITY

Agnė
JANONIENĖ

Exploration of carbonic anhydrase IX
inhibitor influence on cancer cell
migration and suitability to use in
anticancer agent delivering nanosystems

DOCTORAL DISSERTATION

Technological Sciences
Chemistry Engineering (T005)

VILNIUS 2021

The doctoral dissertation was prepared at the Institute of Biotechnology, Life Sciences Center, Vilnius University, during 2014–2020.

The research was supported by the Research Council of Lithuania with grant for academic achievements P-DAP-20-119 and mobility funding P-DAK-20-45.

Scientific supervisor: Prof. Dr. Vilma Petrikaitė (Vilnius University, Technological Sciences, Chemistry Engineering – T 005).

Scientific adviser: Prof. Dr. Linas Mažutis (Vilnius University, Natural Sciences, Biochemistry – N 004).

<https://doi.org/10.15388/vu.thesis.187>
<https://orcid.org/0000-0003-1552-8433>

VILNIAUS UNIVERSITETAS

Agnė
JANONIENĖ

Karboanhidrazės IX slopiklio įtakos
ląstelių migracijai ir priešvėžinio poveikio
nanosistemų tiksliniam pristatymui
įvertinimas

DAKTARO DISERTACIJA

Technologijos mokslai
Chemijos inžinerija (T 005)

VILNIUS 2021

Disertacija rengta 2014-2020 metais Biotechnologijos institute, Gyvybės mokslų centre, Vilniaus universitete.

Mokslinius tyrimus rėmė Lietuvos mokslo taryba - skyrė paramą už akademinis pasiekimus P-DAP-20-119 bei paramą akademinėms išvykoms P-DAK-20-45.

Mokslinis vadovas: Prof. dr. Vilma Petrikaitė (Vilniaus universitetas, technologijos mokslai, chemijos inžinerija – T 005).

Mokslinis konsultantas: Prof. dr. Linas Mažutis (Vilniaus universitetas, gamtos mokslai, biochemija – N 004).

ACKNOWLEDGEMENTS

I would like to acknowledge my supervisor, Prof. Vilma Petrikaitė, for guiding and advising me during my PhD studies as well as for tasty and good-humored breaks between experiments. Also, I would like to thank Prof. Linas Mažutis for his helpful consultations. I am thankful to the lab colleagues, especially Greta, Vaida, Lina, Joana, Aušra, Aurelija, and others for the friendly atmosphere and supporting talks.

I would like to thank Dr. Lina Baranauskienė (for CA IX binding and inhibition experiments together with consultations regarding it), Dr. Augustas Vaitkevičius (for spectroscopic confocal microscopy measurements), Dr. Vytautas Petraukas (for advice regarding the format of the dissertation), Dr. Remigijus Vasiliauskas (for academic career advices).

I would like to express my gratitude to colleagues from Helsinki University: Prof. Helder A. Santos, Dr. Zehua Liu, Prof. Hongbo Zhang, for a fruitful collaboration and constructive discussions. I am deeply thankful to the lab members for their kindness and empathy during my stay.

I acknowledge the Research Council of Lithuania for conference funding and scholarship.

I would like to thank my friends, Milda, Monika, Jolita, and my mother, for encouraging me. I am deeply grateful to my husband Vytautas for his incredible impact on our joint family building project, which inspires me every day, and my daughter Ūla for being my everyday teacher of core values.

Yours sincerely,



TABLE OF CONTENTS

ABBREVIATIONS	9
1 INTRODUCTION	10
1.1 The Goal of the study	12
1.2 Objectives	12
1.3 Scientific novelty	13
1.4 Publications and personal contribution	14
1.5 Conferences	15
2 LITERATURE OVERVIEW	18
2.1 Challenges in cancer treatment	18
2.2 Hypoxia in tumors	20
2.3 Role of carbonic anhydrase IX in tumors	21
2.4 Inhibition of CA IX in order to hinder the growth of the tumor	24
2.5 CA IX as a target for antimetastatic drugs	26
2.6 Tumor targeted nanosystems	30
2.6.1 Organic nanocarriers targeting CA IX	33
2.6.2 Inorganic nanocarriers targeting CA IX	35
3 MATERIALS AND METHODS	38
3.1 Materials and cell culturing	38
3.2 Optical microscopy studies	38
3.2.1 Immunofluorescence staining	38
3.2.2 CA IX inhibitor accumulation in cells by confocal microscopy	39
3.3 Cell migration assay	40
3.3.1 Migration in a μ -dish	40
3.3.2 Migration in microfluidic device	40
3.4 Preparation of functionalized NS	42
3.4.1 Chemical modification of PSi based NS	42
3.4.2 Chemical modification of Zn-CuO based NS	43
3.4.3 Characterization of NS	43
3.5 Inhibition and binding studies of CA IX	43
3.5.1 NS binding of CA IX study	44
3.5.2 NS inhibition of CA IX study	44
3.6 NS influence on medium acidification	45
3.7 Drugs loading into PSi and release	45
3.8 Cell viability studies	46

3.9	Evaluation of FRET effect	47
3.10	NS uptake by cell and drug release	48
3.11	Statistical analysis	48
4	RESULTS AND DISCUSSION	49
4.1	Visualization of CA IX in cells by immunofluorescence	49
4.2	Properties of CA IX inhibitor accumulation in cancer cells	49
4.3	Impact of CA IX inhibition to cell migration	53
4.3.1	Influence of CA IX inhibitor on cancer cell velocities	53
4.3.2	Influence of CA IX inhibition on cell chemotaxis	56
4.4	Characteristics of prepared NS	60
4.5	CA IX targeting capability of the prepared NS	62
4.6	Influence of the NS on medium pH changes	64
4.7	Properties of NS drug loading and release profiles	65
4.7.1	Properties of paclitaxel loading and release	65
4.7.2	Properties of doxorubicin loading and release	66
4.8	NS caused cytotoxicity	68
4.8.1	Paclitaxel loaded NS	68
4.8.2	Doxorubicin loaded NS	69
4.8.3	Zn-CuO based NS	71
4.9	FRET effect	72
4.10	Cell uptake of VD-PSi and intracellular doxorubicin release	75
5	CONCLUSIONS	77
	REFERENCES	78
	CURRICULUM VITAE	102

ABBREVIATIONS

Abbreviation	Meaning
ACN	acetonitrile
BSA	bovine serum albumin
CA	carbonic anhydrase
CDI	carbonyldiimidazole
DMEM	Dulbecco's Modified Eagle's Medium
DMF	<i>N,N</i> -dimethylformamide
DNA	deoxyribonucleic acid
DOX	doxorubicin
DOX@PSi	DOX uploaded PSi NP
DOX@VD-PSi	DOX uploaded VD-PSi NP
EC ₅₀	half maximal effective concentration
ECM	extracellular matrix
EDC	1-ethyl-3-(3-dimethylaminopropyl)carbodiimide
EGF	epidermal growth factor
EPR	enhanced permeability and retention
FBS	fetal bovine serum
FRET	fluorescence resonance energy transfer
FTIR	Fourier-transform infrared spectroscopy
FTSA	fluorescent thermal shift assay
HER-2	human epidermal growth factor receptor 2
HF	human fibroblasts
HBSS	Hanks' Balanced Salt solution
HIF	hypoxia-inducible factor
NHS	<i>N</i> -hydroxysuccinimide

NP	nanoparticles
NS	nanosystems
PBS	phosphate-buffered saline
PDH	prolyl hydroxylases
PDMS	poly(dimethyl)siloxane
PEG	polyethylene glycol
PG	proteoglycan-like
Prickly@SpAcDX	Prickly NP encapsulated in SpAcDX
Prickly@SpAcDX-PEG	Prickly NP encapsulated in SpAcDX and attached with PEG
Prickly@SpAcDX-PEG-VD11-4-2	Prickly NP encapsulated in SpAcDX, attached with PEG and compound VD11-4-2
PTX	paclitaxel
PTX@PSi	PTX uploaded PSi NP
PTX@VD-PSi	PTX uploaded VD-PSi NP
PSi	porous silicon
RCC	renal cell carcinoma
r.t.	room temperature
SpAcDX	spermine-modified acetylated dextran
<i>t</i> boc-NH-PEG-NH ₂	<i>t</i> -butoxycarbonyl-amine-PEG-amine
TME	tumor microenvironment
UnTHCPSi	undecylenic acid modified thermally hydrocarbonized PSi
VD-PSi	PSi NP attached with compound VD11-4-2

1. INTRODUCTION

The Nobel Assembly has acknowledged the research clarifying molecular pathways of how cells sense and adapt to oxygen deprivation in 2019. Understanding the hypoxia-induced molecular machinery opened new strategies in the development of hypoxia-related diseases such as coronary artery disease, diabetes, and cancer [1]. Oxygen depletion inside the tumor cell results in hypoxia-inducible factors (HIF) dependent on gene and protein expression, which helps the cells survive and proliferate [2].

One such molecule is the hypoxia solid tumor-related protein carbonic anhydrase IX (CA IX). CA IX is found in an exceptionally broad range of tumors [3]. This protein helps oxygen-deprived cancer cells maintain stable intracellular pH by producing bicarbonate ions, which are important for maintaining intracellular pH [4]. CA IX has also been shown to play a role in tumor resistance to therapy, and metastasis [5].

Sulfonamides, sulfamates, sulfamides, coumarins, and other compounds targeting and inhibiting CA IX are intensively synthesized and tested for the suppression of cell proliferation and motility [6]. These compounds can also be used as targeting moieties for conjugates and nanosystems (NS) for tumor detection, and treatment [7]. However, it should be noted that the family of carbonic anhydrases has over a dozen catalytically active isoforms found in different human body tissues [8]. To avoid the possible side effects arising from other CA isoform inhibition, researchers are seeking for isoform CA IX selective agents [9]. Among them, 3-(cyclooctylamino)-2,5,6-trifluoro-4-[(2-hydroxyethyl) sulfonyl] (VD11-4-2) shows picomolar affinity and selectivity toward CA IX, which is greater than other CA IX inhibitors tested so far [10]. Studies *in vitro* showed that VD11-4-2 can inhibit CA IX function

in *Xenopus* oocytes and MDA-MB-231 cells [11]. VD11-4-2 has low toxicity as observed during the studies in zebrafish embryos [12]. Furthermore, compound VD11-4-2 exhibits fluorescence properties - an advantageous feature for *in vitro* studies. Taking all these facts into consideration, compound VD11-4-2 was chosen as a CA IX inhibiting agent of this doctoral project. VD11-4-2 was tested for its antimigratory properties, and it was investigated as a targeting moiety of cancer-targeted NS.

Antimigratory properties of CA IX inhibitor VD11-4-2 were tested by monitoring the motility of individual breast cancer cells. Previous studies have shown that CA IX inhibition can reduce metastases of breast tumors in mice and alter cell migration and invasion during *in vitro* studies. However, most of the CA IX inhibition influence on cell migration studies were done by monitoring the cell monolayer's ability to close an empty growing surface area. Such migration is based on a cell-cell interaction, while tumor metastasis is a single-cell process, related to cell-extracellular matrix (ECM) interaction. Therefore, VD11-4-2 influence on cell migration described in this thesis is based on monitoring the migration trajectories of individual cells located on the ECM matrices. Cell trajectories were recorded, single-cell velocities calculated and compared between the experimental groups at different experiment timepoints. VD11-4-2 diminished velocities of CA IX expressing breast cancer cells, and hindered cell speed increment during the experimental time. VD11-4-2 influence on cell migration toward greater concentration of epidermal growth factor (EGF) as a chemoattractant was studied as well. It was observed that inhibitor reduces the number of CA IX positive cells migrating toward the attractant.

The possible **VD11-4-2 application in NS as cancer cells targeting moiety** was studied and described in the thesis. CA IX catalytic domain is favorably located on the cancer cell cytoplasmic membrane with an active center oriented to extracellular space, and could be used as a target for systems delivering anticancer agents. Two different types of nanoparticles (NP) were functionalized with VD11-4-2, and after the modification reactions, inhibitor VD11-4-2 retained the affinity toward CA IX. Porous silicon (PSi) based NS was tested for drug loading and release properties. NS showed pH-responsive doxorubicin (DOX) re-

lease at acidic conditions while preserving the drug inside the particles at neutral pH values. NP modification with VD11-4-2 did not improve the loading and release properties of another anticancer drug, paclitaxel (PTX). DOX and VD11-4-2 were further found to be suitable pairs for the fluorescence resonance energy transfer (FRET) effect. FRET was successfully applied for monitoring of PSi based NS uptake and drug release within the cell. *In vitro* studies of breast cancer cells showed that inhibitor modified NP were the most effective among all tested DOX formulations in killing the CA IX positive cells. For further confirmation of VD11-4-2 targeting ability, it was attached on zinc-doped copper (also called Prickly) particles coated with a polymer, degrading at acidic conditions. Prickly NP damaged the cells only after their uptake and coating degradation in cell organelles with an acidic environment. VD11-4-2 attachment led to successful NP uptake by CA IX positive cells, resulting in a cytotoxic effect.

Overall, the work presented in this thesis further expands possible applications of the VD11-4-2 and supports the advantages of CA IX as an anticancer drug target.

1.1 The Goal of the study

To evaluate CA IX inhibition influence on cancer cell migration and to study CA IX inhibitor as a targeting moiety of cancer-targeted NS.

1.2 Objectives

- To study VD11-4-2 ability to target CA IX positive breast cancer cells *in vitro*.
- To evaluate CA IX inhibition influence on breast cancer cell migration and chemotaxis at a single-cell level.
- To evaluate the suitability of VD11-4-2 as a CA IX targeting moiety of PSi and Zn-doped CuO based NS, by studying their binding and inhibition of CA IX protein properties, and effect on cell viability *in vitro*.

- To study anticancer drug delivery properties of PTX and DOX loaded PSi based NS *in vitro*.

1.3 Scientific novelty

CA IX inhibition influence on cell migration *in vitro* was investigated for the first time by tracking single-cell trajectories and calculating their migration speeds. Results showed that VD11-4-2 was able to reduce breast cancer cell velocities while not affecting CA IX non expressing cells. The chosen method enabled monitoring of how the cells differing in their phenotypic plasticity respond to VD11-4-2 treatment. CA IX expressing cells in compound treated groups migrated at lower velocities and did not reach a maximum speed compared to compound untreated group. The experiment also led to distinguish CA IX inhibition influence on cells migration from proliferation. Additionally, the experiment showed that the migration suppression effect of VD11-4-2 begins after the second hour of incubation. Moreover, studies in a microfluidic device with gradient flow of EGF were utilized to test CA IX inhibitor influence on cell migration toward chemoattractant. Results confirmed that CA IX inhibition could reduce breast cells chemotaxis.

Application of CA IX inhibitor VD11-4-2 as hypoxic breast tumor cells targeting molecule in NS was carried out for the first time in this doctoral work. VD11-4-2 was attached on two different NS based on PSi and Zn-CuO NP. CA IX inhibitor on the surface of the nanoplatforms showed to be beneficial in delivering drug-loaded NP into the cells and enhancing their anticancer activity *in vitro*. The mechanism of action of these NS was shown to be due to CA IX inhibition, as cell preincubation with free inhibitor led to a reduced anticancer effect. The fluorescence properties of VD11-4-2 and DOX were utilized in pairing them for FRET. FRET effect enabled the possibility of monitoring of NP uptake and DOX release within the tumor cells.

1.4 Publications and personal contribution

Publications related to the dissertation:

- Zhang H., Liu D., Wang L., Zehua, L., Wu, R., **Janoniene A.**, Ma M., Pan G., Baranauskiene L., Zhang L., Cui W., Petrikaite V., Matulis D., Zhao H., Pan J., Santos H. A., “Microfluidic Encapsulation of Prickly Zinc-Doped Copper Oxide Nanoparticles with VD1142 Modified Spermine Acetalated Dextran for Efficient Cancer Therapy”, *Advanced Healthcare Materials*, 2017, 6 (11), 1601406.

I have participated in setting up chemical synthesis reactions and in the arrangement of CAIX binding and inhibition studies. I have conducted immunofluorescence studies and participated in the preparation of the publication.

- **Janoniene A.**, Liu Z., Baranauskiene L., Mäkilä E., Ma M., Salonen J., Hirvonen J., Zhang H., Petrikaite V., Santos, H. A., “A Versatile Carbonic Anhydrase IX Targeting Ligand-Functionalized Porous Silicon Nanopatform for Dual Hypoxia Cancer Therapy and Imaging”, *ACS Applied Materials and Interfaces*, 2017, 9 (16), 13976–13987.

I carried out the synthesis and physicochemical characterization of NP by size, zeta potential changes and Fourier-transform infrared spectroscopy (FTIR) measurements, drug loading and release studies, medium pH changes, cell immunofluorescence, FRET, and a part of cell viability studies. I have participated in the arrangement of CAIX binding and inhibition studies. In the contribution of Zehua Liu, I have prepared the publication.

- **Janoniene A.**, Petrikaite V., “In Search of Advanced tumor Diagnostics and Treatment: Achievements and Perspectives of Carbonic Anhydrase IX Targeted Delivery”, *Molecular Pharmaceutics*, 2020, 17 (6), 1800–1815.

I have analyzed the literature applying CAIX as a target for NS and conjugates, summarized the peculiarities of their structures, and prepared the manuscript.

- **Janoniene A.**, Mazutis L., Matulis D., Petrikaite V., “Inhibition of CA IX suppress breast cancer cell motility at single-cell level”. *Submitted for publishing.*

I have developed the methodology of the experiments, carried out the experiments, analyzed the data, and prepared the manuscript.

Publications not directly related with the thesis:

- Liu Z., Balasubramanian V., Bhat C., Vahermo M., Mäkilä E., Kemell M., Fontana F., **Janoniene A.**, Petrikaite V., Salonen J., Yli-Kauhaluoma J., Hirvonen J., Zhang H., Santos H. A., “Quercetin-Based Modified Porous Silicon Nanoparticles for Enhanced Inhibition of Doxorubicin-Resistant Cancer Cells”, *Advanced Healthcare Materials*, 2017, 6 (3), 1601009.

I have performed a part of the DOX release study and participated in developing DOX resistant cells as well as in flow cytometry experiments.

- Daunys S., **Janonienė A.**, Januškevičienė I., Paškevičiūtė M., Petrikaitė V., “3D tumor Spheroid Models for In Vitro Therapeutic Screening of Nanoparticles”, in: F. Fontana, H.A. Santos (Eds.), *Bio-Nanomedicine Cancer Therapeutics*, Springer. 2021, 1295, 243-270.

I wrote the section “Challenges in testing of the nanoparticles in 3D tumor spheroids”.

1.5 Conferences

The presenting author is underlined.

Poster presentations:

- **Vegyte A.**, Mažutis L., Petrikaitė V.; “Microfluidics as a tool to determine CAIX inhibitory compounds influence for cell migration”; International conference The COINS; March 3-5, 2015 Vilnius, Lithuania.

- **Vegyte A.**, Mažutis L., Petrikaitė V.; “Portable device for testing effect of CAIX inhibitors on cancer cell migration”; International conference Lab-on-a-Chip and Microfluidics; March 17-18, 2015 Berlin, Germany.
- **Vegyte A.**, Liu Z., Baranauskienė L., Petrikaitė V., Santos H. A.; “Porous Silicon Nanoparticles with anchored CAIX inhibitor for the targeting of cancer cells”; XIV Lithuanian Biochemical Society Conference; June 28-30, 2016 Druskininkai, Lithuania.
- **Janonienė A.**, Liu Z., Baranauskienė L., Zhang H., Petrikaitė V., Santos H. A.; “Modified Porous Silicon nanoparticles for cancer targeting via Carbonic Anhydrase IX”; International Conference Nanotechnology and Innovation in the Baltic Sea Region; June 14-16, 2017 Kaunas, Lithuania.
- **Janonienė A.**, Liu Z., Zhang H., Baranauskiene L., Petrikaite V., Santos H. A.; “Porous Silicon based nanoplatform targeting hypoxic cancer cells”; 3rd International Conference Current Trends in Cancer Theranostics; June 25-29, 2017 Pakruojis, Lithuania.
- **Janonienė A.**, Liu Z., Baranauskiene L., Mäkilä E., Salonen J. J., Zhang H., Santos H. A., Petrikaitė V.; “Tumor specific protein CA IX as a target for nanoparticles”; International conference Tumor microenvironment; March 2-4, 2020 Lisbon, Portugal.
- **Janonienė A.**, Matulis D., Petrikaitė V.; “Investigation of CAIX protein inhibitors as an antimigratory agents”; The International Scientific-Practical Conference Achievements of pharmaceutical science and practice; October 16, 2020 Kaunas, Lithuania (Remote conference).

Oral presentations:

- **Janonienė A.**, Liu Z., Correia A., Baranauskienė L., Mäkilä E., Ma M., Salonen J., Hirvonen J., Zhang H., Santos H. A., Petrikaitė V.; “Targeted nanotherapeutics: achievements and perspectives”; 34th congress and international scientific-practical conference of the Lithuanian pharmaceutical association “Role of

pharmaceutical society in the health system: The past, current and future”; October 19, 2019 Vilnius, Lithuania.

- **Janonienė A.**, Liu Z., Baranauskienė L., Staniulytė M., Santos H. A., Petrikaitė V.; “Nanoparticles for targeted drug delivery in chemotherapy”; International Conference Nanotechnology and Innovation in the Baltic Sea Region; June 14-16, 2017 Kaunas, Lithuania.

2. LITERATURE OVERVIEW

2.1 Challenges in cancer treatment

Cancer-related diseases are one of the major health problems worldwide, which caused 10 million deaths in 2020 [13]. This statistics indicates that there is a need to rethink the strategies for overcoming the significant obstacles related to the treatment of cancer patients [14]. There is a significant number of challenges associated with the current malignant tumor chemotherapy, such as severe adverse effects of the chemotherapeutics, cell resistance to them, and the lack of specific cell metastasis hindering drugs. Several possible strategies (**Fig. 2.1**) for overcoming these obstacles will be discussed in this chapter of the thesis.

The vast majority of currently used chemotherapeutics target DNA integrity, and cell division [15]. They effectively treat certain malignancies, but cause **severe side effects** to normal cells due to them being unspecific. It has been shown that nanoformulations with several cytotoxic agents are promising in reducing toxicity and enhancing anticancer effect toward tumor tissues, due to their size-dependent enhanced accumulation in tumor sites [16]. Several of these nanoformulations are designed to release the carried drug in a controlled manner, that is, only after entering the site of interest and can act locally in tumor sites [17].

Another problem leading to the anticancer treatment failure is tumor cell **resistance to free chemotherapeutics**. The main mechanisms behind this phenomenon are increased drug efflux, drug inactivation, mutation of the target, DNA repair, and others [18]. One of the strategies to partially solve this issue is to use a combination of anticancer drugs with a different mechanism of action, which can also be benefi-










Solving strategies \ Challenges	Severe adverse effects	Resistance to therapy	No safe metastasis suppressors
Nanotherapeutics			
Locally acting drugs			
Combination treatment			
Cancer targeted systems			
Mechanical cell damage			
Antimetastatic agents			

Figure 2.1: Current challenges in malignant tumor treatment and several of possible solutions for overcoming these obstacles.

cial in enhancing the safety of the drugs [19]. Cancer-specific molecules can be used as targets for conjugates or nanotherapeutics. Molecular targeting can lead to elevated drug accumulation within the tumor site, enhanced uptake by cells, and increase the amounts of drug within the cell [20]. Systems targeting specific receptors in cancer cells could also be applied in finding and killing the tumor cells circulating in the blood, preventing their further development of metastatic sites [21]. Mechanical cell damage (due to specific geometry, vibration, heating, etc.) causing systems are tested as a possible solution in overcoming cancer drug resistance in tumor cells [22]. In such a case, NP exhibiting a physical damage mechanism is used without an anticancer drug.

Finally, the majority of cancer-related deaths are the result of **metastasis** [23]. Despite this fact, there is a lack of specific metastasis suppressing drugs, which could prevent or delay the metastasis without cytotoxicity [24]. Metastasis suppressing agents could further solve other chemotherapy-related problems (safety and efficacy), because localized solid tumors can be then removed by surgery. Nevertheless, there are no standard methods for testing the antimetastatic effect of a drug [25]. Studies in animals show conventional chemotherapy toward highly resistant metastatic cancer is enhanced when used in combination with antimigratory drugs [26].

One method to solve all the above-mentioned challenges simultane-

ously could hardly be found. However, recent studies have shown that the strategy of targeting components of the tumor microenvironment (TME) could solve several of the different cancer treatment-related problems [27]. TME is a dynamic organization of various cells (tumor, immune, stromal) surrounded by ECM, facing the deprivation of nutrients and oxygen [28]. The cascades of actions arising from the deprivation of oxygen in tumors will be explained in the next chapter.

2.2 Hypoxia in tumors

Oxygen is an important molecule for ATP production during oxidation reactions in mammalian cells. The state when oxygen supply in tissues drops below adequate levels is called hypoxia. Oxygen deprivation in the human body may be generalized process, and could be result of anemia, high altitude, etc., or specific area localized process, for example, after thrombosis, in solid tumors, etc., process. In malignancies, hypoxia occurs due to the tumor-specific immature vasculature and uncontrolled cell division in tumor sites, distanced more than $\sim 200\ \mu\text{m}$ from capillaries [29].

It has been demonstrated that cells can sense oxygen deprivation and change their gene expression in response [30]. For these and other important hypoxia-related findings William G. Kaelin Jr., Sir Peter J. Ratcliffe, and Gregg L. Semenza were nominated for Lasker Award in 2016 and for the Nobel Prize in 2019.

HIFs are key molecules initiating hypoxia-related molecular machinery. HIFs complexes consist of oxygen-dependent HIF- α and non-oxygen-responsive HIF- β subunits. Under normoxic conditions, HIF- α subunit is hydroxylated by HIF prolyl hydroxylases (PDH), and further undergoes degradation in proteasomes (**Fig. 2.2**). Deprivation of oxygen leads to HIF- α stabilization. HIF- α stabilization could also be achieved in normoxic conditions by using compounds inhibiting the enzymatic activity of prolyl hydroxylases (**Fig. 2.2**), so-called hypoxia mimetic agents [31]. One of such agents is CoCl_2 , which inactivates PDH enzymes by replacing iron ions with cobalt in the active site. It has been observed that CoCl_2 in concentrations ranging from 50 to 240 μM induces hypoxia markers, including CA IX, expression in breast

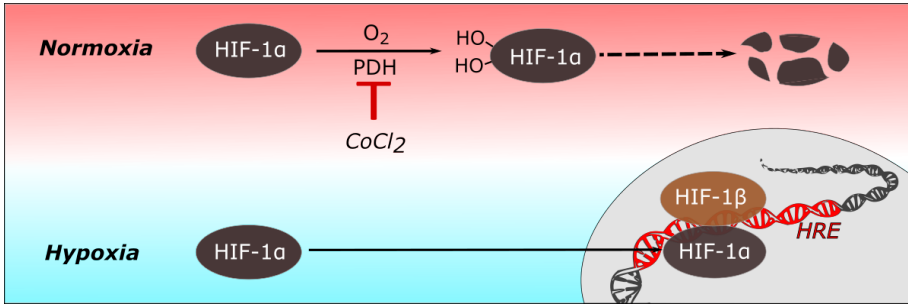


Figure 2.2: HIF-1 pathways in normoxia and hypoxia. In the presence of normal oxygen levels, HIF-1 is hydroxylated by prolyl hydroxylases (PDH) and degraded in proteasomes. In the deprivation of oxygen conditions, HIF-1 α complexes with HIF-1 β in the nucleus, and binds to hypoxia-related element (HRE) region in DNA sequence.

cancer cells [32–35].

Stabilized HIF- α subunit translocates to the cell nucleus, where it binds with HIF- β . HIF complex binds to the hypoxia response element (HRE) region in DNA sequence (**Fig. 2.2**), which results in HIF dependent gene transcription. In cancer cells, HIF up-regulates the translation of tumor-related molecules for the compensation of ATP loss, pro-angiogenesis, cell motility, drug resistance, proliferation, etc. [36]. To maintain the required pH of the cell, HIF activates sodium-proton and anion exchangers, sodium-bicarbonate, and monocarboxylate transporters together with carbonic anhydrases.

2.3 Role of carbonic anhydrase IX in tumors

Human carbonic anhydrases (CA) are a family of enzymes, which has at least 15 different isoforms located in various tissues within the body [37]. Considering the cellular lever, CA isoforms are found in cytosol and mitochondria (CA I, CA II, CA III, CA VII, CA VIII, CA XIII, CA VA and CA VB), while others are located in the extracellular space (membrane-bound CA IV, transmembrane CA IX, CA XII, CA XIV) or secreted (CA VI, CA X, CA XI) [37] (**Fig. 2.3 A**). It should be noted, that isoform CA IX, lacking of several catalytic domain exons, could also be found in cell cytoplasmic membrane or be secreted; however, such variant of CA IX is found only in low amounts and shows diminished catalytic activity [38]. Most of these metalloenzymes are

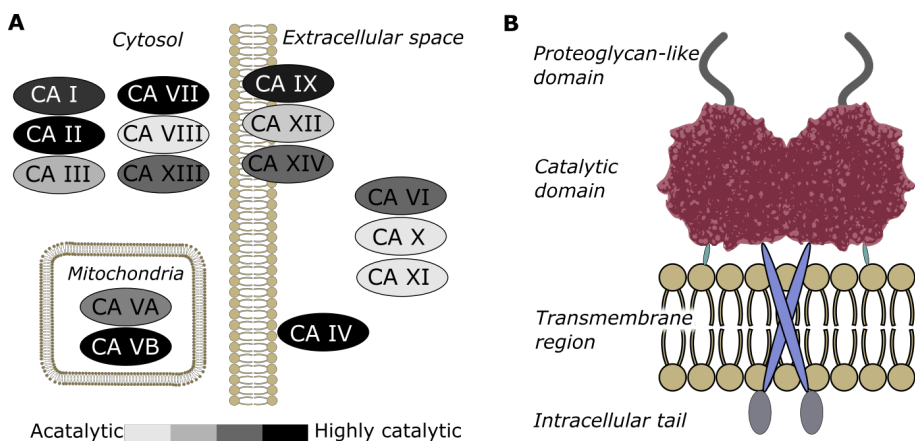


Figure 2.3: Different isoforms of Carbonic anhydrase locations within the cell (A): cytosolic, mitochondrial, transmembrane, membrane-bound, and secreted. Structural outlook (B) of transmembrane CA IX isoform, which has proteoglycan-like and catalytic domains located on the external surface of the cell membrane.

catalytically active and catalyze a reversible bicarbonate and proton ions production from carbon dioxide. This plays an important role in regulating cell pH and participates in lipogenesis, gluconeogenesis, and ureagenesis. Several CA inhibitors are approved as drugs for clinical use and are mainly prescribed as diuretics, antiglaucoma agents, and antiepileptics. Their clinical usage is also extended to the treatment of obesity, intracranial hypertension, sleep apnea, migraine, and altitude-caused sickness prevention [39].

Carbonic anhydrases are also broadly investigated in tumor-related studies [40]. Cancer-related isoforms CA IX and CA XII are used as the targets. Overexpression of CA IX is observed in most of the solid tumor tissues (**Fig. 2.4**). Besides the tumor tissues it is also expressed in some gastrointestinal tract organs and testis (**Fig. 2.4**) [41]. CA XII could also be found in healthy kidneys, pancreas, intestine, eyes as well as in some tumor types (kidney, breast, etc.) [42, 43]. Protein CA IX is considered to be more catalytically active than the CA XII isoform [44]. Because of all of these features, CA IX was identified to be a promising drug target and is being investigated in this thesis.

CA IX is a dimeric protein, consisting of N-terminal proteoglycan-like (PG) and catalytic domains, a transmembrane helix and intracellular tail (C-terminal) (**Fig. 2.3 B**). PG and catalytic domains help cancer

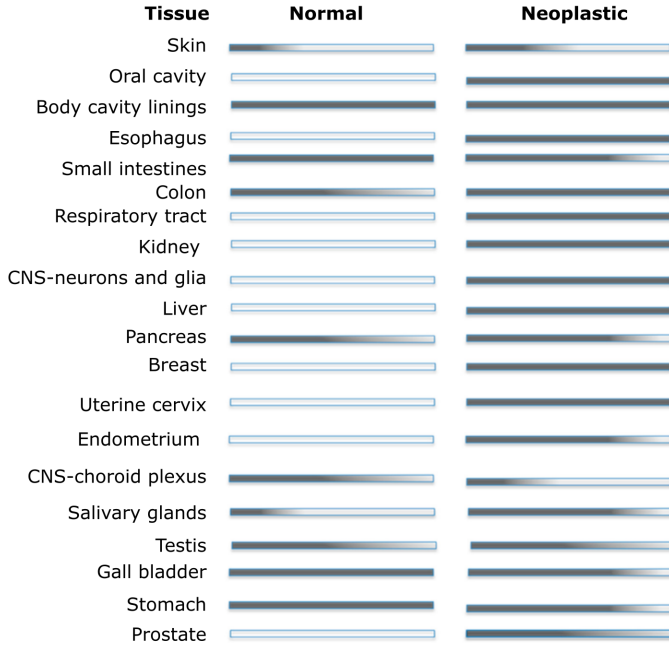


Figure 2.4: Expression of CA IX in normal and tumor tissues in adults. Line darkness marks the intensity of CA IX expression in different tissues. Reprinted with permission from [45].

cells under hypoxia to manage the excess of lactate and protons arising from intensified glycolytic pathways. The catalytic domain produces bicarbonate from the excess of carbon dioxide. Bicarbonate ions enter the cell and help to maintain the required pH by neutralizing excess protons. Meanwhile, protons stay in extracellular spaces and acidify it [46].

PG domain is also called a proton antenna and is found only in CA IX isoform [47]. It facilitates the release of vast amounts of protons and lactate from the cells [48]. Therefore, it enhances the catalytic activity of CA IX in the aspect of extracellular space acidification. PG domain is also involved in cell-cell interaction, and cell invasion [49–51]. The intracellular tail has three phosphorylation sites, two of which (Thr 443 and Ser 448) modulate the catalytic activity of the enzyme [52]. Meanwhile the phosphorylation of Tyr 449 site has been related with EGF receptor-dependent signaling transduction through Act activation in kidney cancer cells [53].

CA IX plays an important role in helping cancer cells to survive and

escape harsh conditions through its catalytic and non-catalytic functions. Silencing or knockout of *CA 9* genes was observed to reduce the growth of tumors and suppress metastasis in animal studies [5, 54–56]. CA IX function in cell and overexpression in diverse types of tumors make it a promising target in translational studies for the development of novel cancer diagnostic and therapeutic agents.

Overexpression of CA IX has been related to a poor prognosis in multiple types of cancer [57–59]. CA IX was tested as a biological marker in diagnosing cervical lesions from liquid biopsies [60]. The levels of CA IX in blood serum have been measured in previous studies in order to estimate the response of renal cancer treatment; however, the clinical trials were terminated [61]. CA IX amount in serum have been shown to correlate with the presence of circulating tumor cells in breast cancer patients [62]. Radiolabeled CA IX specific antibodies are tested as new tumor imaging tools, which could overcome cell carcinoma (RCC) detection limits while diagnosing the stage of disease or evaluating the treatment response [63–65]. Near-infrared fluorescence dye labelled CA IX specific antibodies and nanobodies were investigated in animal studies. They were tested for possibility to improve the detection of breast tumors and their metastasis together with identification of neoplasm margin during surgery and after it [66–68].

CA IX is broadly investigated as a therapeutic target for cancer treatment. Chimeric antigen receptor T-cells targeting CA IX were clinically investigated as a cure of metastatic RCC [69]. Inhibitors and antibodies of CA IX are also tested as components of combination treatment of cancer in clinical and preclinical studies [70–74]. Preclinical studies are extensively exploring the application of CA IX for anticancer, antimetastatic activity, and as a targeting molecule for nanosystems. These applications will be further considered in this dissertation.

2.4 Inhibition of CA IX in order to hinder the growth of the tumor

More than two decades ago, Teicher et al. and Chegwiddden et al. have observed that CA inhibitors acetazolamide, methazolamide, and

ethoxzolamide (clinically approved as diuretics and antiglaucoma drugs), can hinder the proliferation of cancer cells *in vitro* and delay the growth of tumors *in vivo* [75, 76]. The mechanism behind this effect was not clear at that time. After several years, Supuran et al. raised a hypothesis that novel synthesized sulfonamides might reduce the growth of various cancer cell lines by inhibiting the cancer-associated CA isoforms IX and XII [77]. Subsequently, an increasing number of studies were attempting to find novel CA IX inhibitors and evaluate their influence on cancer cell growth [78].

There are several CA IX inhibitors that could be recognized amongst others for their anticancer activity as seen from tests on cancer cells and malignancies. This includes sulfonamides, sulfamates, sulfamides, and coumarins which exhibited anticancer effects in preclinical research and entered clinical trials. Ureidobenzenesulfonamide U-104 or SLC-0111 is the first small molecule, which entered clinical trials as a CA IX inhibitor. It is investigated as a therapeutic agent for use combined with gemcitabine for patients diagnosed with metastatic pancreatic cancer [79–81]. Preclinical studies showed that U-104 affects pancreatic cancer cell viability under hypoxia conditions and reduces orthotopic tumor growth in mice [82]. This compound also potentiates the anticancer effect of conventional chemotherapeutic agents in melanoma, breast, colon cancer cells [83] and reduces orthotopic breast tumor growth in mice alone and in combination with PTX, or sunitinib [72,84]. Further research of U-104 analogues showed their potential in reducing the proliferation of breast, prostate and colorectal cancer cells under hypoxia conditions [85].

CA IX non-selective sulfonamide acetazolamide is also tested for its anticancer effects. Studies showed that acetazolamide, in combination with bevacizumab or rapamycin, reduces colorectal tumor growth in mice [54, 86]. However, Dubois et al. observed that acetazolamide induces tumor regression under irradiation in both CA IX expressing and knocked-down colorectal tumor cells [87]. Indanesulfonamide and nitroimidazole sulfamides were shown to decrease colorectal tumor growth rate *in vivo*, which was significantly enhanced in combination with irradiation [87,88]. A group of ureidosulfamates was shown to be effective as antiproliferative agents against breast cancer cells, and one of them (S4) delayed tumor growth *in vivo* [89]. Ureidosulfamates combined with lan-

soprazole effectively inhibited melanoma cell proliferation [90]. Another group of CA IX inhibitors tested for anticancer activity are coumarins. One of these derivatives inhibited the growth of mouse breast tumors *in vivo* [91].

Another kind of CA IX targeting molecules are antibodies, which are less intensively investigated for anticancer activity than small molecule inhibitors. Monoclonal antibody G250 is the first CA IX binding molecule, which entered the clinical trials for treating patients with non-metastatic RCC after surgery. Phase 2 clinical trial showed that it is well-tolerated, but did not possess a clinical benefit as an adjuvant therapeutic [74]. G250 and its counterparts are broadly applied in the development of various CA IX radio conjugates, and they are undergoing clinical trials for the detection and treatment of CA IX positive tumors [92, 93]. Antibody MabVII/20 was tested in mice colorectal carcinoma xenografts and showed anticancer effect [94].

There is evidence that several CA IX specific molecules could reduce the growth of cancer. However, it should be noted that a cell can compensate for the absence of one protein function. For example, McIntyre et al. showed that knockdown of CA IX protein increases the expression of CA XII in HT-29 cell spheroids [54]. This observation partially explains why such molecules as fluorinated benzenesulfonamide VD11-4-2 have shown a low capacity to induce cancer cell death even while having high affinity and selectivity toward CA IX [95]. Despite that CA IX inhibitors and antibodies can successfully be exploited as CA IX positive cell targeting molecules for cell motility suppression and in conjugates or NS containing cytotoxic agents.

2.5 CA IX as a target for antimetastatic drugs

Tumor cell metastasis cascade consists of several steps (**Fig. 2.5**). Initially, cell-cell adhesion is lost, leading to a cell detaching from the primary site and migrating in mesenchymal mode. This allows the cell to move toward blood vessels by forming protrusions and interacting with ECM [96]. When a cell intravasates the blood vessel, it circulates in the blood until it forms contact with endothelium, transmigrates and invades the new tissue [97].

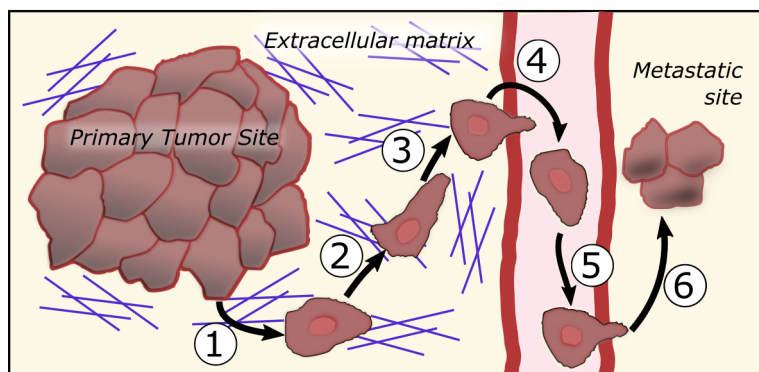


Figure 2.5: Illustrated view of metastasis steps. 1: Separation; 2: Migration and invasion; 3: Intravasation; 4: Circulation; 5: Extravasation; 6: Colonization.

CA IX was shown to be involved in different cell metastasis steps at the molecular level. Protein CA IX was shown to be involved in the cell detachment from primary tumor step (**Fig. 2.5 1**) as the increased amount of CA IX on cell membrane diminishes cell-cell adhesion [51,98].

Protein CA IX was found to be participating in cell migration and invasion (**Fig. 2.5 2**), as it plays a role in the formation of protrusions by interacting with integrins, ion exchangers, and matrix metalloproteinases as well as pH gradient formation needed for the remodeling of cytoskeleton [56,99,100]. CA IX has been related with cell intravasation and extravasation processes, which might take place through PG-like domain interaction with cells or by cell junction disconnection due to catalytic protein function [101]. Thus, this protein was also recognized to play a role in colonization (**Fig. 2.5 6**) steps, as it promotes the metastatic niche formation [102].

CA IX inhibition influence on metastasis was tested in mice using two different models: experimental and spontaneous metastasis (**Fig. 2.6**). Nitrophenyl and fluorophenyl (U-104) ureido benzenesulfonamides and glycosyl coumarins were observed to reduce the metastasis formation in mice lungs after murine breast cancer cells 4T1 injection into the tail vein (**Table 2.1**) [5, 103]. Later on, U-104 has been shown to reduce human breast cancer cell MDA-MB-231 metastasis from the primary site (spontaneous metastasis model) [72, 84]. U-104 also inhibited the growth of primary tumors.

In vivo experiments showed that CA IX inhibitors affect metastasis in

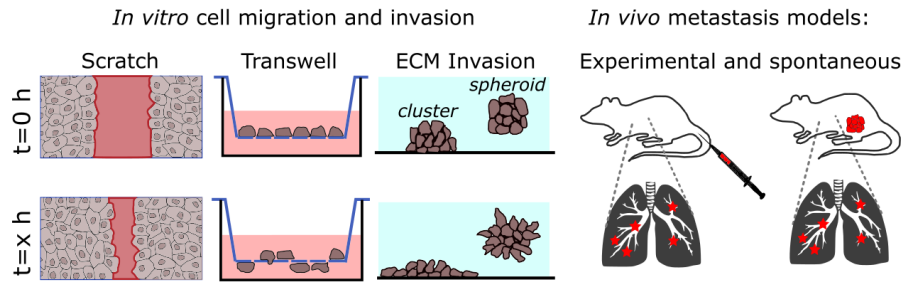


Figure 2.6: Schematic representation of *in vitro* and *in vivo* methods used to test CA IX inhibitors influence on cell motility.

general, while *in vitro* models were used to obtain quantitative analysis recapitulating different steps of metastasis [104]. *In vitro* experiments (**Fig. 2.6**) gave information on affected metastasis step (cell migration, invasion). Matrigel invasion from the MDA-MB-231 cell cluster was reduced after treatment with U-104 (**Table 2.1**) [84]. U-104 has shown the ability to slow down the gap closure of MDA-MB-231 cell monolayer during scratch assay tests [56,105]. Thus, it showed the ability to reduce chemotactic migration or matrix invasion toward EGF of MDA-MB-231 cells stably expressing CA IX or under hypoxia condition during transwell assay, respectively [56].

Several ureido-sulfamates were recognized as human breast and thyroid cancer cell migration suppressors during scratch assays [106]. Ureido phenyl sulfamate S4 was tested in a mice xenograft model and reduced MDA-MB-231 cell metastases in the lung while not affecting primary tumor growth [106]. Ward et al. have demonstrated that ureido-sulfamates could reduce not only breast (MDA-MB-231), but also ovarian (SKOV-3) cancer cell migration during scratch assay in both normoxia as well as hypoxia conditions and inhibited cell invasion from MDA-MB-231 cell spheroids and breast biopsy tissues [107].

Part of this thesis is concentrated on the influence of CA IX inhibition on cell motility. CA IX inhibitors were shown to disturb cell migration during the scratch assay tests, as seen from previous studies by other scientists (**Table 2.1**). This method is one of the simplest and is quite commonly used to study cell migration. A monolayer of cells is formed during these studies, and cell displacement toward the empty space is monitored. This assay is frequently used because of its repro-

Table 2.1 : Summary of studies where CA IX inhibitors were tested for their influence on cell motility and metastasis.

Inhibitor	Method	Results	Ref.
U-104 and glycosyl coumarins	Experimental metastasis	U-104 inhibited and glycosyl coumarins limited metastasis	[5]
U-104	Matrigel invasion and spontaneous metastasis	Reduced invasion and metastases number	[84]
U-104	Scratch and transwell	Reduced migration and invasion in all tests	[56]
U-104	Scratch	Reduced migration rate	[105]
U-104	Spontaneous metastasis model	Reduced metastatic burden	[72]
Ureido sulfonamide	Experimental metastasis	Limited cell colonization in lungs	[103]
Ureido sulfamates	Scratch and spontaneous metastasis	Some inhibitors affected migration	[106]
Ureido sulfamates	Scratch and collagen invasion	Two leading compounds identified	[107]

ducibility. However, several drawbacks of this method could be named. Firstly, the method represents collective cell migration related to cell-cell interactions that are observed more commonly in such processes as tissue recovery. Cell migration during metastasis is based more on the cell-matrix interaction [108]. Also, if the experiment duration is longer than the cell doubling time, it becomes complicated to distinguish between the effects for cell migration and proliferation [109]. Moreover, if the scratch during the assay is made by pipette tip, it harms the cells together with the culture dish or ECM layer [110].

Efforts have been made to test CA IX inhibitors for their ability to disturb cancer cell metastasis. Application of CA IX as a target molecule for NS, as described further in this thesis, could also be beneficial in affecting the metastatic cells.

2.6 Tumor targeted nanosystems

Most of the cytotoxic drugs approved for cancer treatment lack specificity toward the tumor cells. Specificity toward cancer cells could be attained when a cytotoxic drug is uploaded into a targeted nanocarrier [111, 112]. Moreover, loading the anticancer drug into NP can enhance its solubility and stability [113]. NP can also selectively deliver imaging agents to tumor tissues and overcome the existing detection limits [114]. Furthermore, simultaneous therapeutic and diagnostic effects could be achieved by a so-called tumor theranostic approach [115]. One of the main reasons why nanosystems are attractive in anticancer therapeutics research is their preferential passive accumulation in a tumor as compared to healthy tissues. Such accumulation in malignancies is caused by the chaotic and leaky vasculature in tumor sites (see **Fig. 2.7**) [116]. This accumulation manner due to the enhanced permeability and retention effect (EPR) is called passive targeting [117].

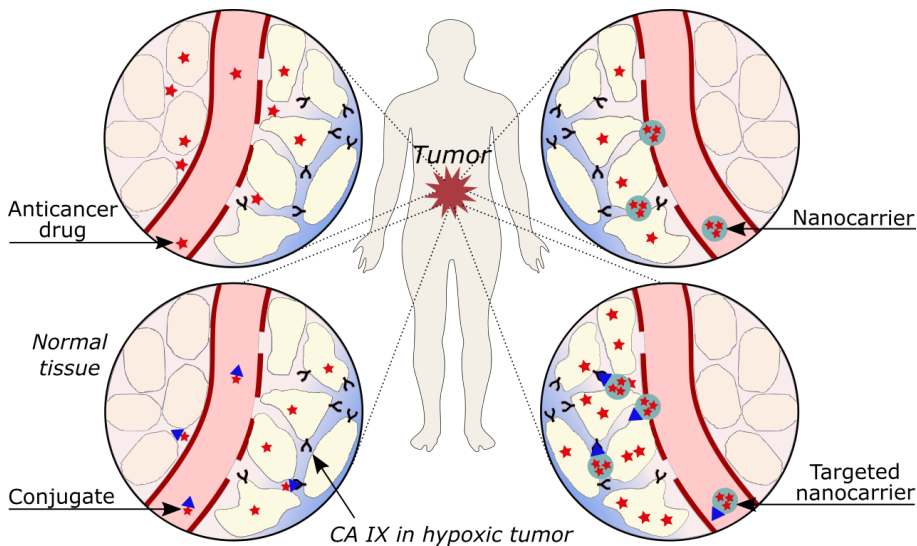


Figure 2.7: Graphical explanation of how cytotoxic drug formulation alters its accumulation in tissues, and cells. Anticancer drug alone accumulates and harms all tissues. Selectivity towards tumor cells is enhanced when it is used in conjugate with a tumor-specific molecule. Nanocarriers tend to accumulate in tumor tissues due to tumor-specific blood vessels. Functionalization of the nanocarrier could enhance its residence in tumor time and alleviate its uptake by cells. Figure is reprinted with permission from [7].

While most NP lack specific active targeting ability, it can be achieved by attaching a tumor-specific molecule to its surface. The targeting moieties can be small molecules, antibodies or their fragments, aptamers, peptides, sugars, etc. Their attachment to the NP results in extended NP residence in tumor and alleviated uptake by cells [118]. The most widely investigated targets are CD20, CD30, CD44, CD47 proteins, folate, prostate-specific membrane antigen, human epidermal growth factor receptor 2 (HER-2), and fatty acid synthase enzyme [119,120]. Several nanosystems are already approved for clinical use, and are in numerous ongoing clinical trials, but none of the clinically approved NS has a tumor-targeted moiety yet (**Fig. 2.8**) [17]. However, targeting capability is just one piece in the puzzle of the rational development of the nanocarrier.

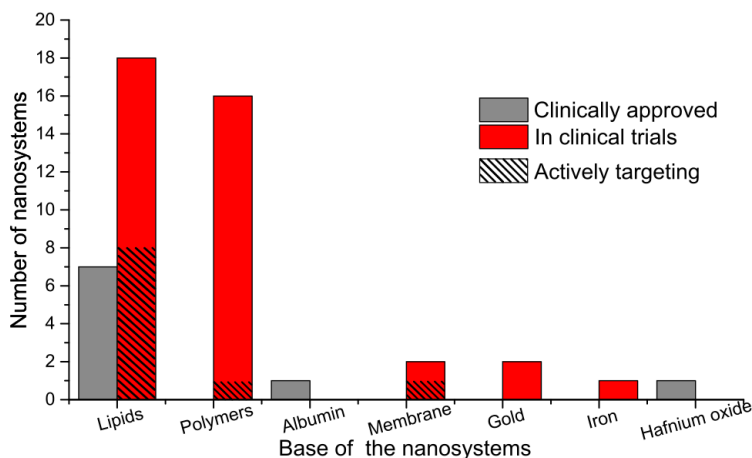


Figure 2.8: Different materials based nanosystems approved for clinical use or in clinical trials for cancer treatment after its intravenous injection (according to the data from [17]).

Ideal nanocarriers should exhibit quite controversial properties [121, 122]. It should be stable in blood and show no aggregation, degradation, and payload release. With these properties, it should also circulate in blood while avoiding opsonization by proteins in blood and phagocytosis by macrophages (**Fig. 2.9 A**) [123]. To avoid instability in blood, NP are often modified with various coatings such as polyethylene glycol (PEG) [124].

After reaching the tumor site, NP should start showing reverse prop-

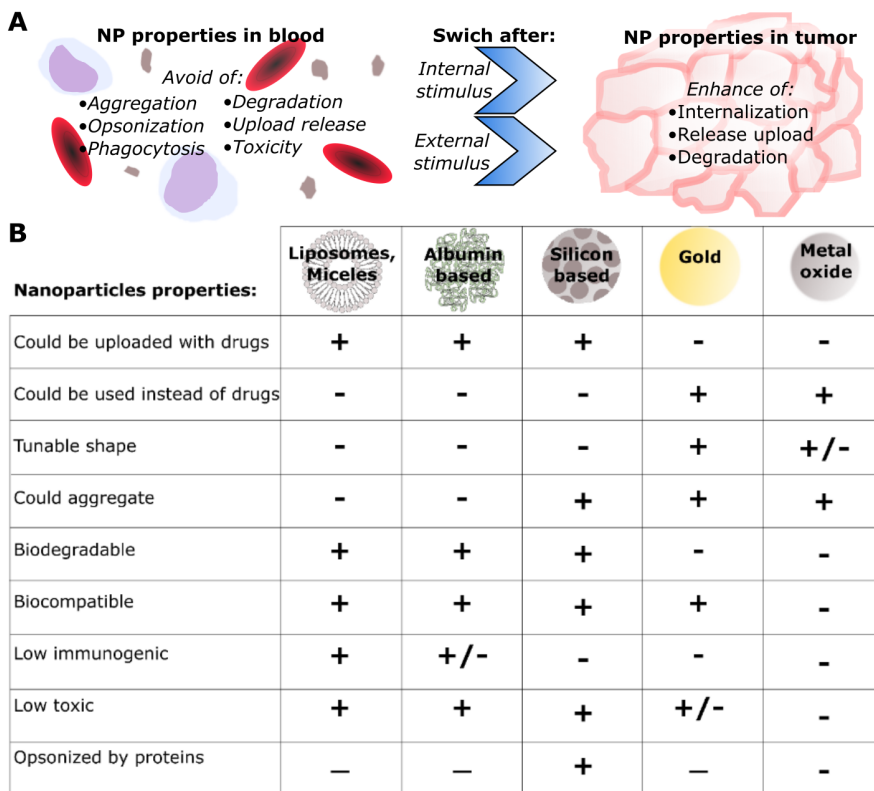


Figure 2.9: The controversial requirements for nanocarrier (A). Properties of the carriers which were applied as a base for CA IX targeted systems and their main advantageous properties (B). Reprinted with permission from [7].

erties: be easily internalized, release uploaded agents, and quickly degrade (**Fig. 2.9 A**). Such complete changes of the NP properties could be achieved by external (temperature, light, ultrasound, magnetic field, electric field) or internal (low pH, temperature, enzyme, oxidative stress) stimuli [125].

Liposome, micelle, albumin, silicon, gold, and metal oxide platforms have been applied in the development of CA IX tumor-targeting systems. They show distinctive features (**Fig. 2.9 B**) which fates their scope of application. CA IX targeting nanocarriers will be described in the next section.

2.6.1 Organic nanocarriers targeting CA IX

Liposomes and micelles are the most widely used drug delivery forms for clinical cancer treatment (**Fig. 2.8**) [17]. These spherical lipids consisted structures are similar to biological membranes, and have attractive biological (biocompatibility, low toxicity, low immunogenicity) and technological (tunable size, surface, charge, lipid organization) properties [126].

Two decades ago, Shinkai et al. constructed magnetoliposomes, and were pioneers in CA IX targeting NS field [127]. Fab' fragment of G250 antibody was attached to magnetoliposomes (**Fig. 2.10 A**) in order to increase the particle uptake by CA IX positive tumors. Functionalization of the magnetoliposomes led to a 27-time increase in their uptake by CA IX positive tumors as revealed in a study in mouse renal cell carcinoma models. Such a significant increase in the accumulation led to a successful mouse renal tumor growth restrain due to hyperthermia after magnetic field irradiation.

Couple of immunoliposomes (**Fig. 2.10 B, C**) were tested as anti-cancer agent carriers targeting CA IX in lung cancer cells. Functionalization with rabbit monoclonal CA IX antibody increased the liposomes' binding to CA IX positive cells and enhanced the impact of an anticancer drug docetaxel on the human lung cancer cell growth [128].

Lin et al. tested how lung tumors can be killed by poorly water-soluble cytotoxic agent triptolide uploaded to liposomes with attached G250 antibody [129]. They were introduced via the pulmonary route in aerosolic form to mice with lung implanted cancer cells. CA IX antibody decorated liposomes suppressed tumor growth, and prolonged mice lifespan more than other triptolide formulations.

Alsaab et al. attached acetazolamide to micelles which were carrying apoptosis inducing agent CFM 4.16 in order to overcome drug resistance in human renal carcinoma cells (**Fig. 2.10 D**) [130]. CA IX directed micelles with anticancer drug sorafenib showed synergistic growth reduction of tumor in mice xenografts and no traceable toxicity to healthy organs (liver and kidney).

Another material used as the base for NP targeting CA IX is **serum albumin**. This protein is most abundant in mammalian blood plasma,

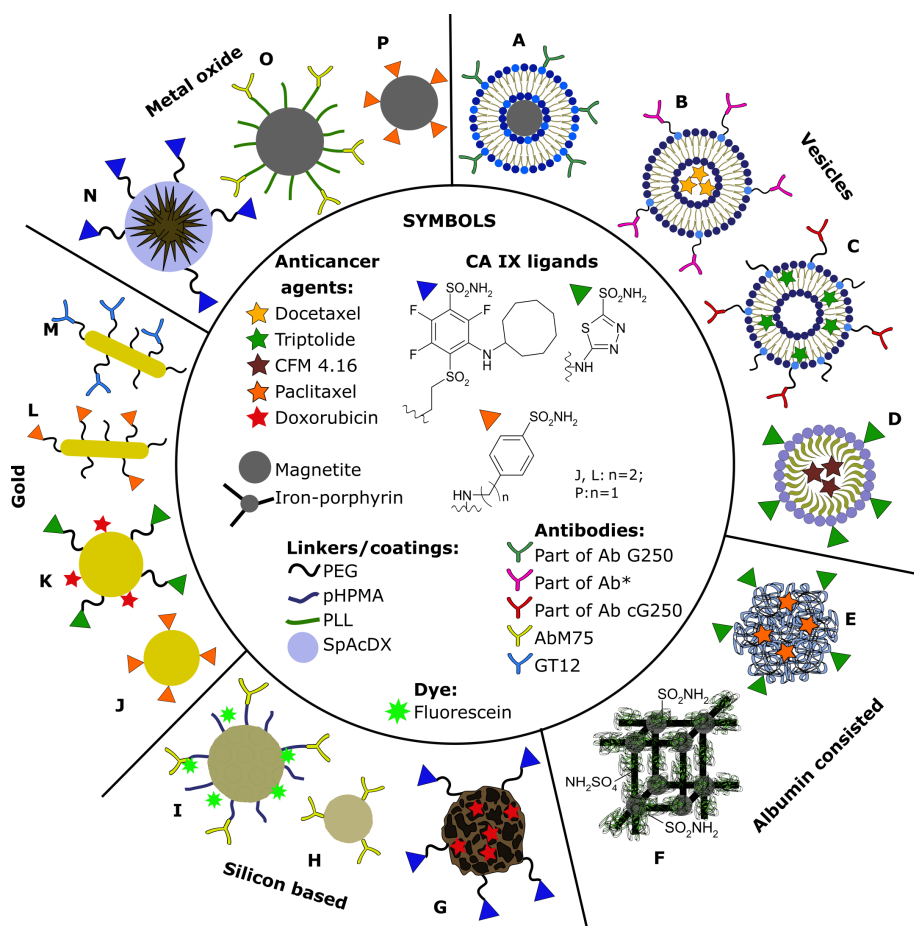


Figure 2.10: CA IX targeting nanosystems which can be found in the literature, reprinted with permission from [7].

therefore, is not toxic and stable in blood. It is eligible for the design of the nanocarrier, because it is soluble in water, stable in various pHs, has low cost, is non-opsonized by serum proteins, is biodegradable, has amino and carboxyl groups, which can be exploited for chemical modifications [131].

Human serum albumin NP uploaded with anticancer drug PTX were tested for the targeting of breast cancer cells [132,133]. PTX uploaded acetazolamide functionalized NP (**Fig. 2.10 E**) showed greater anticancer activity toward CA IX positive cells than PTX alone or uploaded in non-functionalized NP.

Albumin could be used as the coating for other nanomaterials in order to prolong its circulation in blood. In study of Zhu et al. bovine

serum albumin coated iron-porphyrin metal-organic frameworks were used to target CA IX through attached sulfonamide groups (**Fig. 2.10 F**) [134]. These NP in the study of mice bearing mammary gland tumors showed that nanosystem could be applied simultaneously for antitumor effect and the localization of malignancy position.

2.6.2 Inorganic nanocarriers targeting CA IX

Silicon based NP are mostly fabricated from silicon (Si) or silica (SiO₂) materials. They are suitable base for nanocarrier' construction due to the large surface pores that can be easily uploaded with drugs. Silicon NP can be biodegraded in organism and excreted, which makes them biocompatible within living organisms [135, 136]. However, these particles still need appropriate coating or functionalization to bypass non-specific protein adsorption [134].

M75 antibody attached non-porous silica NP (**Fig. 2.10 H**) were tested for the CA IX targeting capability [137]. These NP demonstrated binding to the targeted PG domain of CA IX alone or to CA IX expressing cancer cells. In later studies NP were coated with a polymer, fluorescently labeled and tested for their biodistribution *in vivo* (**Fig. 2.10 I**) [138]. Targeting moiety bearing NP showed ten-fold higher accumulation and longer retention within the human colon tumors in mice xenografts.

Chen et al. have tested mesoporous NP attached with CA IX selective antibody through disulfide linkage for the delivery of DOX to mice breast cancer cells [139]. This NS showed an acidic pH, glutathione triggered drug release, and internalization by cells depended on CA IX presence. CA IX targeted NP carrying DOX exhibited the greatest tumor growth reduction *in vivo*.

Gold NP have a broad scope of applications (imaging, drug delivery, photothermal therapy), which can be obtained by using NP of different sizes and shapes (spheres, rods, shells, cages, stars) [140–142]. The toxicity of these NP to living organisms can be reduced by appropriate coating; however, they are poorly biodegradable and this issue complicates their translation to clinical application [143, 144].

Acetazolamide functionalized gold NP (**Fig. 2.10 K**) were used to

deliver DOX to human colon cancer cells [145]. NP effectively overcame hypoxia-caused cell resistance as it possessed favorable pH-triggered drug release properties and showed enhanced DOX penetration in cell spheroids.

Stiti et al. used gold as a base of NP to study CA inhibition properties of couple targeting moieties [146]. NP with sulfonamidic group (**Fig. 2.10 J**) were able to effectively inhibit CA IX function, whereas inhibition of non-cancer-related isoforms CA I and II inhibition was assessed to be moderate-high. Further studies aimed to facilitate the NP modification reactions to find optimal targeted compound amount on the surface of NP, and enhance their aqueous stability [147]. This targeting moiety was later on applied for killing CA IX positive human breast and colorectal cells with gold nanorods after optical sensitization (**Fig. 2.10 L**) [148]. Nanorods with targeting molecule accumulated better in CA IX positive cells as compared to CA IX negative ones. Gold nanorods, attached with CA IX specific antibody GT-12 (**Fig. 2.10 M**), were more effective than those without an antibody in killing hypoxic colorectal tumor cells and tumors in mice xenografts during photothermal ablation [149].

Metal oxide NP are being broadly investigated in biomedical studies. There are huge differences in the physical properties and the NP application depending on the metal used for their fabrication. For example, some metal oxides (e.g., Fe_3O_4) are used as drug carriers or a tool for magnetic imaging, while others (e.g., CuO, ZnO) induce cell apoptosis, because of their physical damage to the cells, and reactive oxygen species synthesis [150, 151]. Doping with other metals in metal oxide structures enhances the appearance of structural defects (sharp pricks) of the NP and membrane damaging effects towards the organisms [152]. For example, Zn doped CuO NP (**Fig. 2.10 N**) have multiple pricks on the surface and mechanically kill cancer cells as well as microorganisms even those, which are resistant to drugs [153, 154].

Polymer poly-L-lysine coated and CA IX antibody M75 attached Fe_3O_4 NP (**Fig. 2.10 O**) were investigated as cancer cells detecting and targeting system [155]. *In vitro* cell cytotoxicity studies showed that these NP selectively killed CA IX highly expressing cells. Antibody modified NP were able to bind to CA IX, and were internalized inside

the cells. Magnetic NP attached with benzene sulfonamide (**Fig. 2.10 P**) were investigated as an agent for colon lesion visualization [156]. NP were nontoxic to HT-29 cells, and showed superior tumor contrasting ability in mice xenografts.

Inorganic materials are less applied in clinically approved and tested nano formulated anticancer drugs (**Fig. 2.8**). However, due to the easier production, longer shelf-life, and multifunctionality, inorganic NP are often used as a model material for investigating the targeting moiety capacities. Systems G and N from **Fig. 2.10** are described in this thesis.

3. MATERIALS AND METHODS

3.1 Materials and cell culturing

Reagents were obtained from Sigma-Aldrich (USA) if not specified otherwise.

Human breast adenocarcinoma cell lines MDA-MB-231 and MCF-7, and also human foreskin fibroblasts BJ-5ta were cultured in Dulbecco's Modified Eagle Medium (DMEM) (Gibco, USA), supplemented with 10% fetal bovine serum (FBS) (Gibco, USA), 1% penicillin-streptomycin (10 000 U/ml) (Gibco, USA) at 37 °C in a humidified atmosphere with 5% CO₂ and 21% O₂ until passage number of 20. Hypoxia was artificially induced by incubating cells in medium supplemented with CoCl₂ (240 μM) for 48 h (these conditions are further termed as hypoxia mimicking conditions and in figures is referred to as hypoxia).

3.2 Optical microscopy studies

CAIX expression was monitored by immunofluorescence study. Compound VD11-4-2 accumulation within the cells was monitored by confocal microscopy.

3.2.1 Immunofluorescence staining

MDA-MB-231, MCF-7, and BJ-5ta cells were grown on 13 mm No.1 thickness glass coverslips (VWR, USA) in 24 well plate (8×10^4 cells/well) under normoxia and hypoxia mimicking conditions for 48 h, and then fixed with ice cold methanol for 20 min. Then, methanol was aspirated, and cells were incubated with an incubation

buffer (phosphate saline buffer (PBS) (Gibco, USA) containing 2% bovine serum albumin (BSA) and 2% FBS. Afterward, cells were incubated with 1:200 CAIX-specific monoclonal antibody (mAb) H7 [157] for 1 h, thoroughly washed and then incubated with 1:500 goat anti-mouse AlexaFluor 488-conjugated IgG antibody (Life Technologies, USA) for 1 h. Cell nucleus were stained with DAPI (1 $\mu\text{g}/\text{ml}$) in PBS for 10 min. Coverslips with cells were placed on microscope slides covered with proLong diamond antifade mountant (Invitrogen, US). EVOS FL Auto Imaging System (Thermo Fisher Scientific, USA) was used for immunofluorescence imaging by using a magnification of 20 \times . Program ImageJ (National Institute of Health, USA) was used to evaluate fluorescence intensity of labelled antibodies in cells (at least 50 cells from three different images per group).

3.2.2 CA IX inhibitor accumulation in cells by confocal microscopy

CA IX inhibitor VD11-4-2 was supplied by the Department of Biothermodynamics and Drug Design, Institute of Biotechnology, Life Sciences Center, Vilnius University.

MDA-MB-231 cells were grown on 13 mm No. 1 thickness glass coverslips (VWR, USA) in 24 well plate (8×10^4 cells/well) under normoxia and hypoxia mimicking conditions for 48 h. Then, the medium was aspirated, and compound VD11-4-2 solution (1 μM) in PBS for 1 min was placed on cells. PBS without compound was used for control wells. Afterward, cells were thoroughly washed with PBS three times and fixed in ice-cold methanol for 15 min. Subsequently, coverslips were washed with PBS and placed on microscope slides covered with proLong diamond antifade mountant. Images were obtained by Fluoview FV1000 (Olympus, Japan) confocal laser scanning microscope, after excitation with diode laser (405 nm) using a magnification of 60 \times . Fluorescence intensity from cells and their different zones were measured by the program ImageJ (at least 60 cells in each group).

Cells were prepared identically for imaging with ALPHA300 S confocal microscope (WITec, Germany) with diode laser of 405 nm wavelength (ALPHALAS, Germany). Fluorescence spectra were recorded for each

investigated image pixel, and emission intensity maps at specific values of (510 ± 50) nm were plotted and compared between the experimental groups. Measurements were performed by Dr. Augustas Vaitkevičius (Institute of Photonics and Nanotechnology, Vilnius University).

3.3 Cell migration assay

Individual single-cell motility was monitored using two experimental models in the presence, absence or gradient of EGF. During 6 h experiment, images of cells were taken every hour by using bright-field microscopy. Then, cells movements were followed, translated into trajectories by using the program ImageJ plugin MTrackJ (developed by E. Meijering, Erasmus University Medical Center Rotterdam), and velocities were calculated.

3.3.1 Migration in a μ -dish

A 35 mm imaging dish (**Fig. 3.1 A**) with a glass bottom and an imprinted cell location grid (Ibidi, Germany) was used for the migration study. Glass surface was covered with 50 μ l of Rat tail Collagen type I (Thermo Fisher Scientific, USA) and diluted to 1 mg/ml with the cell culture medium alkalized with 0.075% NaHCO_3 solution (Merk, USA). Collagen was left to polymerize for 1 h at 37°C , and then 1.6×10^4 cells/plate were seeded and left overnight to attach. Then, medium, containing 0, 5 or 20 μM of VD11-4-2 and 0 or 50 ng/ml recombinant human EGF (Invitrogen, US), was replaced. Images of cells (at least 120 of cancer cells and at least 30 fibroblasts per experimental group) in three different locations from at least two μ -dishes were taken by using EVOS FL Auto Imaging System (Thermo Fisher Scientific, USA) by using a magnification of $10\times$.

3.3.2 Migration in microfluidic device

Dr. Linas Mažutis from Sector of Microtechnologies, Institute of Biotechnology, Life Sciences Center, Vilnius University supplied silicon wafer templates of gradient microfluidic device. The microfluidic device was prepared by pouring poly(dimethyl)siloxane (PDMS base) and

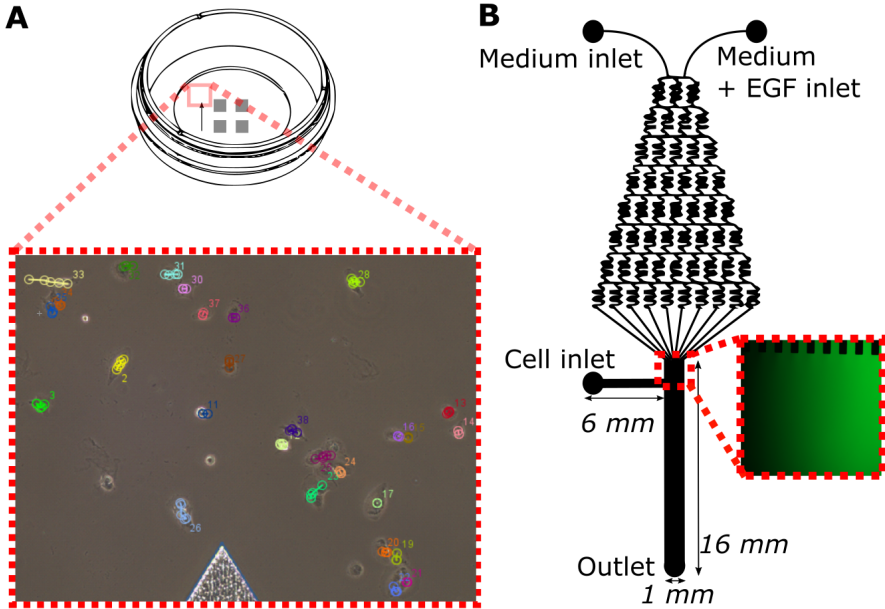


Figure 3.1: Schematic view of μ -dish (A) with the inset of tracked cells and microfluidic device (B) with fluorescence image (inset) of the main channel where gradient flow of the fluorescein could be seen.

cross-linker (Dow Corning) mixture (10:1) into the Petri dish with a silicon wafer, degassing it, and incubated at 65°C for 12 h. Device scheme is shown in **Fig. 3.1 B** 1.2 mm gauge needle was used to punch inlets and outlets in PDMS. Afterward, PDMS was treated with oxygen plasma and bound to the clean glass slide. The main channel of microfluidic device was covered with collagen type I solution (1 mg/ml) through a cell outlet and left for 1 h at 37°C . After that, a syringe with the cell medium containing $20\ \mu\text{M}$ of VD11-4-2 was connected. Medium in one syringe contained $100\ \text{ng/ml}$ EGF. Syringes (1 ml) with the medium were hung above the microfluidic device, and the medium flowed through the channels due to the gravitational force. Gradient flow inside the device was monitored by flowing fluorescein (**Fig. 3.1 B**).

The main channel was carefully filled with MDA-MB-231 cells ($\approx 1 \times 10^6$ cell/ml) mixed with fibronectin (10 mg/ml) until the number of cells in monitored field reached a number of at least 20. Cells were left to attach at 37°C for 1 h, and then the main channel was imaged with Eclipse Ti-U microscope (Nikon, USA) by using a magnification of $4\times$. Medium without inhibitor was used to control experiments. Results

obtained from three experiments are presented.

3.4 Preparation of functionalized NS

Undecylenic acid-modified, thermally hydrocarbonized PSi (Un-THCPSi) NP were supplied by Laboratory of Industrial Physics (Department of Physics and Astronomy, University of Turku), where it was fabricated and characterized. Prickly Zn-CuO NP were fabricated, encapsulated in spermine-modified acetylated dextran, and characterized in the Division of Pharmaceutical Chemistry and Technology, Faculty of Pharmacy, University of Helsinki [158].

3.4.1 Chemical modification of PSi based NS

UnTHCPSi (**Fig. 4.9 (1)**, 1 μg) was dispersed in of anhydrous *N,N*-dimethylformamide (DMF, 1 ml) then 1-ethyl-3-(3-dimethylaminopropyl)-carbodiimide (EDC, 8 μl) and *N*-hydroxysuccinimide (NHS, 6 mg) were added. The solution was left to stir for 2 h at room temperature (r.t.). *t*-butoxycarbonyl-amine-PEG-amine (*tboc*-NH-PEG-NH₂, 5 mg) was dissolved in 1 ml anhydrous DMF and added to NP solution. The solution was left to stir for 24 h at r.t. Then, *boc*-NH-PEG-UnTHCPSi was washed three times with DMF and redispersed in dichloromethane (3 ml) with trifluoroacetic acid (1.8 ml), and left to stir for 3 h at r.t. to remove *boc* from amine group in PEG and obtain product **Fig. 4.9 (2)**. Afterward, particles were washed with dichloromethane (1 ml) for once and dispersed in toluene (1 ml). VD11-4-2 (**Fig. 4.9 (3)**, 1 mg) and carbonyldiimidazole (CDI) (0.4 mg) solution in toluene (2 ml) were stirred and heated at 60 °C for 3 h in round-bottom flask with argon protection. Previously prepared NP (**Fig. 4.9 (2)**) were added to CDI attached VD11-4-2 (**Fig. 4.9 (4)**) solution dropwise and left to stir overnight at 60 °C. Final product – PSi NP attached with compound VD11-4-2 (VD-PSi, **Fig. 4.9 (5)**) was collected by centrifuge (16 000 g for 5 min) at r.t., washed 2 times with ethanol, and stored at 4 °C.

3.4.2 Chemical modification of Zn-CuO based NS

VD11-4-2 (1 mg) (**Fig. 4.9 (3)**) was mixed with CDI (0.4 mg) in toluene (5 ml) for 3 h at 60 °C in argon atmosphere protection. Then, NH₂-PEG-COOH (5 mg) was added and after another 3 h reaction product **Fig. 4.9 (7)** was dried in vacuum. Afterward, VD11-4-2-PEG-COOH was dispersed in HEPES pH=5.5 buffer (2 ml) with NHS (6 mg) and EDC (8 µl), and left to stir for 2 h r.t. Then, the pH of the solution was adjusted to 7.8 with NaOH and Prickly nanoparticles encapsulated in spermine-modified acetylated dextran (Prickly@SpAcDX, **Fig. 4.9 (6)**) NP (5 mg) was added and left to stir for 1 h at r.t. Afterward, obtained particles **Fig. 4.9 (8)** were collected by centrifugation 16×g 5 min at r.t.), washed with water, and stored in alkalized to pH=8.0 water at 4 °C.

3.4.3 Characterization of NS

Size and zeta potential of NP dispersed in water were measured by Zetasizer Nano ZS (Malvern Instruments, UK) at r.t.

NP chemical composition, before and after chemical modification with VD11-4-2, was assessed by using VERTEX 70 series FTIR spectrometer (Bruker Optics, Germany) equipped with a horizontal ATR sampling accessory (MIRacle, Pike Technology, Inc.), recording spectra between 4000 and 400 cm⁻¹ wavelengths with a 2 cm⁻¹ resolution.

During the evaluation of quantitative conjugation efficacy, VD-PSi (2 mg) was hydrolyzed with 2 ml of 0.1 M NaOH (pH=12). VD11-4-2 was extracted with ethyl acetate (3 × 4 ml), which was further evaporated and residues were dissolved in ethanol. Fluorescence intensity was measured by Varioskan Flash Multimode Reader (Thermo Fisher Scientific, USA). VD11-4-2 concentration was assessed by using standard curves obtained by measuring fluorescence intensities (λ_{ex} =360 nm, λ_{em} =500 nm).

3.5 Inhibition and binding studies of CA IX

Protein CA IX used in the experiments was supplied by the Laboratory of Biothermodynamics and Drug Design, Institute of Biotechnology,

Life Sciences Center, Vilnius University. Experiments were performed by Dr. Lina Baranauskienė from the same laboratory.

3.5.1 NS binding of CA IX study

Protein-ligand binding was carried out by using Fluorescent thermal shift assay (FTSA). For experiments with VD-PSi, samples contained 100 μM solvatochromic dye 8-anilino-1-naphthalene sulfonate, 50 mM PBS, 10 % ethanol, 8 μM or 4 μM of CA IX mixed with 0 μM to 40 μM VD11-4-2 or 0 mg/ml to 0.3 mg/ml VD-PSi, respectively. For prickly NP, samples contained 50 μM dye, 50 mM PBS, and 4 μM protein CA IX mixed with 0 μM to 40 μM VD11-4-2 or 0 mg/ml to 1.5 mg/ml NP. Samples were heated from 25 $^{\circ}\text{C}$ to 99 $^{\circ}\text{C}$ (1 $^{\circ}\text{C}/\text{min}$) in a Corbett Rotor-Gene 6000 (Qiagen Rotor-Gene Q) instrument and fluorescence of dye was observed at λ_{ex} of (365 \pm 20) nm and λ_{em} (460 \pm 15) nm. Protein melting temperature at different ligand concentration was determined and plotted against protein concentration. The melting temperature of each sample was determined using a sigmoidal model [159].

3.5.2 NS inhibition of CA IX study

Catalytic inhibition of protein CA IX was performed by stopped-flow kinetic CO_2 hydration assay. Samples contained 20 μM CA IX, 0 μM to 2 μM VD11-4-2 or 0 $\mu\text{g}/\text{ml}$ to 75 $\mu\text{g}/\text{ml}$ of particles, 20 mM HEPES with 100 mM NaCl, 10 % FBS, 2.5 % ethanol and 60 μM phenol red during the tests with VD-PSi nanoparticles. For testing Prickly particles, samples contained 10 μM CA IX, 0 μM to 1 μM VD-11-4-2, 0 $\mu\text{g}/\text{ml}$ to 37.5 $\mu\text{g}/\text{ml}$ of particles, 25 μM HEPES, 50 μM NaCl, and 30 μM phenol red. Samples were diluted with CO_2 saturated MiliQ-water (1:1), and then phenol red absorbance changes at 557 nm were measured by Applied Photophysics SX.18MV-R stopped-flow spectrometer. Samples without protein and samples without inhibitors were used as controls. Experimental values were fitted by Hill equation [160].

3.6 NS influence on medium acidification

MCF-7 cells were seeded in 24 well plates (1×10^4 cells/well) and incubated in normoxia and hypoxia mimicking conditions for 48 h 37 °C. Then, medium, which contained NP at a concentration of 0.1 mg/ml or VD11-4-2 (6.4 µg/ml), was added to the wells. After another 48 h incubation at 37 °C medium from the cell culturing wells was aspirated, and its pH values were measured after collected samples reached r.t. by using SevenCompact pH/Ion meter S220 (Mettler Toledo, Spain).

3.7 Drugs loading into PSi and release

Particles in the following experiments were collected using centrifugation at $16 \times g$ for 5 min at r.t.

High-performance liquid chromatography (HPLC) was used to assess PTX (TCI, Tokyo, Japan) loading into NP and its release rate. For drug loading studies, 50 µg of VD-PSi were suspended in 1 ml of acetonitrile (ACN) containing 10 mg of PTX and left overnight to stir at r.t. Then NP were collected, washed 3 times, redispersed in ACN, sonicated (1 min), and the supernatant was analyzed for PTX release. During *in vitro* release studies, after loading PTX overnight, particles were collected, washed, redispersed in 2 ml PBS pH=7.0 containing 0.1 % Tween 80, and shaken 200 rpm at 37 °C for the experimental time. At subsequent time points (0,5, 1, 2, 4, 24 h), supernatants were collected for HPLC analysis, and particles were dispersed in a fresh medium. For the quantification of PTX in the supernatant HPLC system (Shimadzu, Japan) equipped LC-10 AT VP pump, SIL-10 AD VP sample injector, FCV-10 AL UV/vis detector (wavelength of 227 nm), and analytic column C-18 (GL Sciences Inc.) was used. The buffer A (5 % ACN, 0.7 % trifluoroacetic acid) and buffer B (95 % ACN, 0.1 % trifluoroacetic acid) were pumped at a flow rate of 1 ml/min. The amount of PTX in the samples was assessed by using standard curves.

Fluorescence properties of DOX were utilized during its loading and release into NP studies. 1 mg of NP (PSi and VD-PSi) were dispersed in 2 ml of PBS (pH=7.4) with 3 mg of DOX (TCI, Japan). Suspensions were left to stir overnight at r.t. and then collected, washed three times

with PBS pH=7.4.

NP were redispersed in PBS pH=5, sonicated, centrifuged (repeated 5 times), and supernatants were collected for fluorescence analysis during drug loading studies. During *in vitro* drug release studies 50 μg of DOX loaded NP were dispersed in 2 ml of PBS buffer (pH 5.0 or 7.4) and left shaking (200 rpm) at 37 °C for the experimental time. At subsequent time points (1, 2, 3, 4, 6, 24 h), 100 μl of the sample were taken and centrifuged. The supernatants were collected and analyzed while NP were dispersed in fresh 100 μl medium and returned to the testing solution. The fluorescence intensities of DOX at λ_{ex} =490 nm and λ_{em} from 490 nm to 700 nm in supernatants were measured by a UV-1600PC spectrophotometer (VWR, USA). The amount of DOX in the samples was assessed using a standard curve.

Drug loading efficiency was calculated by the following formula:

$$\text{Loading Efficiency}(\%) = \frac{\text{mass of drug loaded into NP}}{\text{mass of drug loaded NP}} \times 100\% \quad (3.1)$$

While cumulative drug release (%) was calculated by this formula:

$$\text{Cumulative drug release}(\%) = \frac{\text{mass of drug released from NP}}{\text{mass of drug loaded into NP}} \times 100\% \quad (3.2)$$

During UV-Vis spectroscopy study 40 $\mu\text{g}/\text{ml}$ DOX and VD11-4-2 (10 mg/ml stock solution in DMSO) solutions together with 200 $\mu\text{g}/\text{ml}$ of VD-PSi were prepared in an 8.7 mM PBS buffer. Spectra were recorded by full-length scanning by UV-1600PC spectrophotometer (VWR, USA).

3.8 Cell viability studies

MCF-7 cells were seeded in 96 well plate (3×10^3 cells/well for PSi and 5×10^3 cells/well for Zn-doped CuO NP) and left to attach overnight. The medium was replaced with the other one containing different concentrations (10, 25, 50, 100 $\mu\text{g}/\text{ml}$ for PSi and 0.1, 0.5, 1, 5, 10, 50, 100, 500 $\mu\text{g}/\text{ml}$ for Zn-doped CuO NP). Free compounds DOX, PTX, and VD11-4-2 were used at concentrations corresponding their amounts in NP (21, 5.5 and 1.2 $\mu\text{g}/\text{ml}$). 10 $\mu\text{g}/\text{ml}$ of VD11-4-2 were

used additionally with NP in a group of free VD11-4-2 with NP. Cells were grown in a medium without compounds or NP and in medium with 1% of Triton X-10 for negative and positive controls, respectively. After 48 h (experiments with DOX loaded NP) or 24 h (experiments with PTX loaded NP and Zn-doped CuO NP) incubation of live cell numbers was determined by ATP-based luminescence cell viability kit (CellTiter-Glo, Promega, USA). The luminescence was measured with a Varioskan Flashfluorometer (Thermo Fisher Scientific, USA). Each concentration was tested in triplicate.

Experiments with PSi NP were done together with Dr. Zehua Liu. Experiments with Zn-doped CuO NP were done by Dr. Hongbo Zhang (Faculty of Pharmacy, University of Helsinki, Finland).

3.9 Evaluation of FRET effect

Initially, VD11-4-2 and DOX fluorescence spectra (excitation and emission) were recorded. Then, constant concentration (12 $\mu\text{g}/\text{ml}$) of VD11-4-2 solutions were prepared in 6.7 mM PBS buffer, and increasing molar ratio of DOX (0, 0.5, 1, 2, 4, 8 and 16) were added and vortexed. pH influence on FRET effect was tested by using buffers (75 mM) to make compound solutions with different pH values: acetate (pH = 4.97), MES (pH = 5.31), and HEPES (pH = 7.42). Spectra were recorded at 25 $^{\circ}\text{C}$ and 37 $^{\circ}\text{C}$. Ionic strength influence on FRET effect was tested by adding different NaCl concentration (0.02 M and 0.1 M) in the VD11-4-2 and DOX solution. The fluorescence spectra of solutions were also recorded where the increasing molar concentrations of VD11-4-2 were added to fixed concentrations (21 μM) of DOX solutions. DOX uploaded VD-PSi NP (DOX@VD-PSi) and VD-PSi concentration of 5 mg/ml were used to obtain fluorescence spectra of NP. Fluorescence emission spectra in all experiments were recorded at the range of 400 nm to 700 nm after excitation of $\lambda_{ex} = 360$ nm by Synergy H4 Hybrid Multi-Mode Microplate Reader (BioTek, USA).

3.10 NS uptake by cell and drug release

For confocal microscopy experiment, MCF-7 cells (1×10^4 cells/well) were seeded in Lab-Tek Chamber Slides (Thermo Fisher Scientific, USA) and incubated for 48 h in normoxia and hypoxia mimicking conditions. Then cells were rinsed with Hank's Balanced Salt Solution (HBSS), and a medium containing DOX@VD-PSi (100 $\mu\text{g}/\text{ml}$) was added to wells. 3 h and 24 h after the incubation, medium was removed, cells washed with HBSS and then cell membranes were stained (37 °C for 3 min) with CellMaskTM DeepRed (Life Technologies, USA). After 3 min of incubation, cells were washed and fixed with 2.5 % glutaraldehyde at r.t. for 20 min, then washed and stored in HBSS. Images were taken with an SP2 inverted confocal microscope (Leica Microsystems, Germany).

During flow cytometric study MCF-7 cells were seeded in a 6-well plate (2.5×10^5 cells/well) and incubated for 48 h in normoxia and hypoxia. Then cells were washed with HBSS, and a medium containing DOX@VD-PSi (100 $\mu\text{g}/\text{ml}$) was added to wells. After 3 h of incubation, cells were collected or further cultured in a medium without particles for another 3 h and then collected. Collected cells were fixed with 2.5 % glutaraldehyde for 30 min. DOX fluorescence of total 1×10^4 cell counts was measured by LSRII flow cytometer (BD Biosciences, USA) using an excitation wavelength of $\lambda_{ex}=488$ nm. VD11-4-2 fluorescence was measured by LSR Fortessa flow cytometer (BD Biosciences, USA) with a laser excitation wavelength of $\lambda_{ex}=405$ nm.

Experiments were performed together with Zehua Liu (Faculty of Pharmacy, University of Helsinki, Finland).

3.11 Statistical analysis

Measurements were carried out in at least three independent experiments. Values are reported as mean and standard deviation (\pm). Student's t-test was used to statistically evaluate the obtained values with the level of significance set at probabilities of * $p < 0.05$, ** $p < 0.01$, and *** $p < 0.005$.

4. RESULTS AND DISCUSSION

4.1 Visualization of CA IX in cells by immunofluorescence

Immunofluorescence study was carried out in order to observe CA IX expression in breast cancer MDA-MB-231 and MCF-7 cells under exposure of hypoxia mimetic agent CoCl_2 in concentration of 240 μM . Fluorescence of FITC labeled secondary antibody was observed in MDA-MB-231 and MCF-7 cells incubated under hypoxia mimicking conditions (**Fig. 4.1 A**). Quantitative fluorescence intensity analysis showed that signals from cells in hypoxia mimicking conditions were about 5-fold higher than normoxia ones in both breast cancer lines. This result coincides with other researchers' observations that CA IX expression in these breast cancer cells could be induced by their exposure to CoCl_2 [34,161]. It should be noted, that CoCl_2 in concentration of 100 μM was not able to effectively induce CA IX expression.

Human foreskin fibroblasts (non-cancerous cells) showed a ground-level fluorescence in both normoxia and hypoxia mimicking conditions (**Fig. 4.1 B**). This result corresponds to literature results, showing no expression of CA IX in tissues harboring human skin fibroblasts [162].

4.2 Properties of CA IX inhibitor accumulation in cancer cells

Fluorescence of the compound VD11-4-2 was utilized to monitor its accumulation properties within the cells. The excitation and emission wavelength maximum of VD11-4-2 are around 360 nm and 500 nm, re-

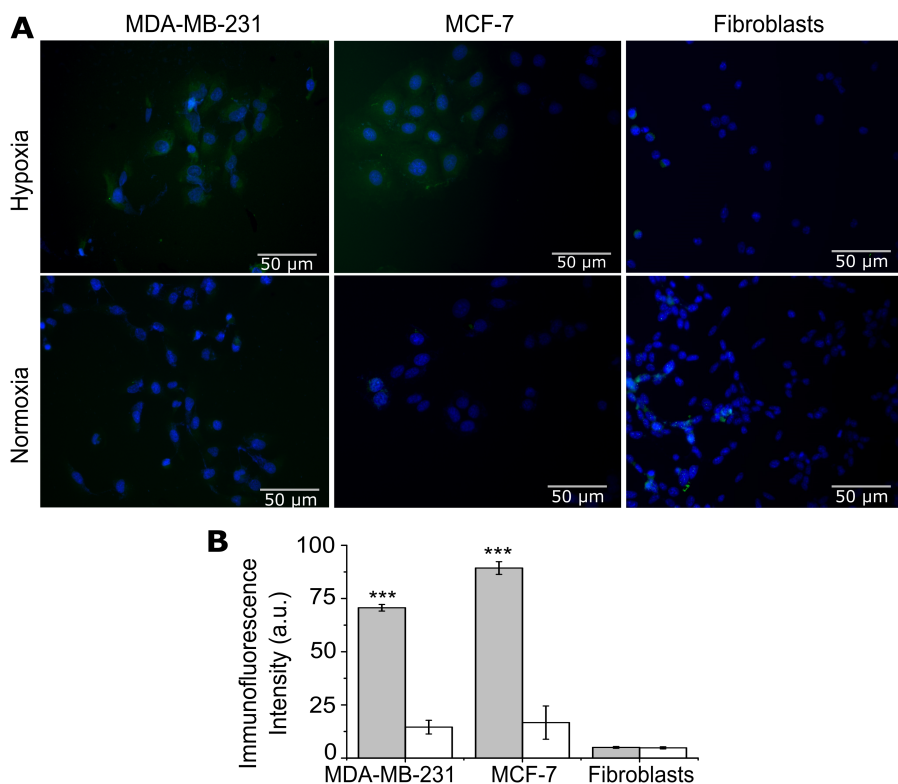


Figure 4.1: Immunofluorescence images (A) of MDA-MB-231 and MCF-7 cells, green and blue colors show CA IX and nucleus stainings, respectively. Quantitative fluorescence intensities (B) of CA IX immunofluorescence in MDA-MB-231, MCF-7 and fibroblasts.

spectively (**Fig. 4.2 A**). Therefore, a laser of 405 nm was used to excite specimens and to monitor compound accumulation within the cell (**Fig. 4.2 C**).

Cell autofluorescence after excitation of such wavelength could vary regarding the amount of several molecules (NAD(P)H, FAD, etc.) [163]. Therefore, compound's fluorescence was evaluated by subtracting the average fluorescence intensity of control cells incubated with PBS with 1 μM of the compound or without it. Fluorescence intensity of VD11-4-2 in hypoxia mimicking conditions incubated MDA-MB-231 cells was significantly higher compared to cells incubated in normoxia (**Fig. 4.2 B**).

Fluorescence intensities from different cell parts (nucleus, around the nucleus, and cell membrane corresponding distal cell part) were calcu-

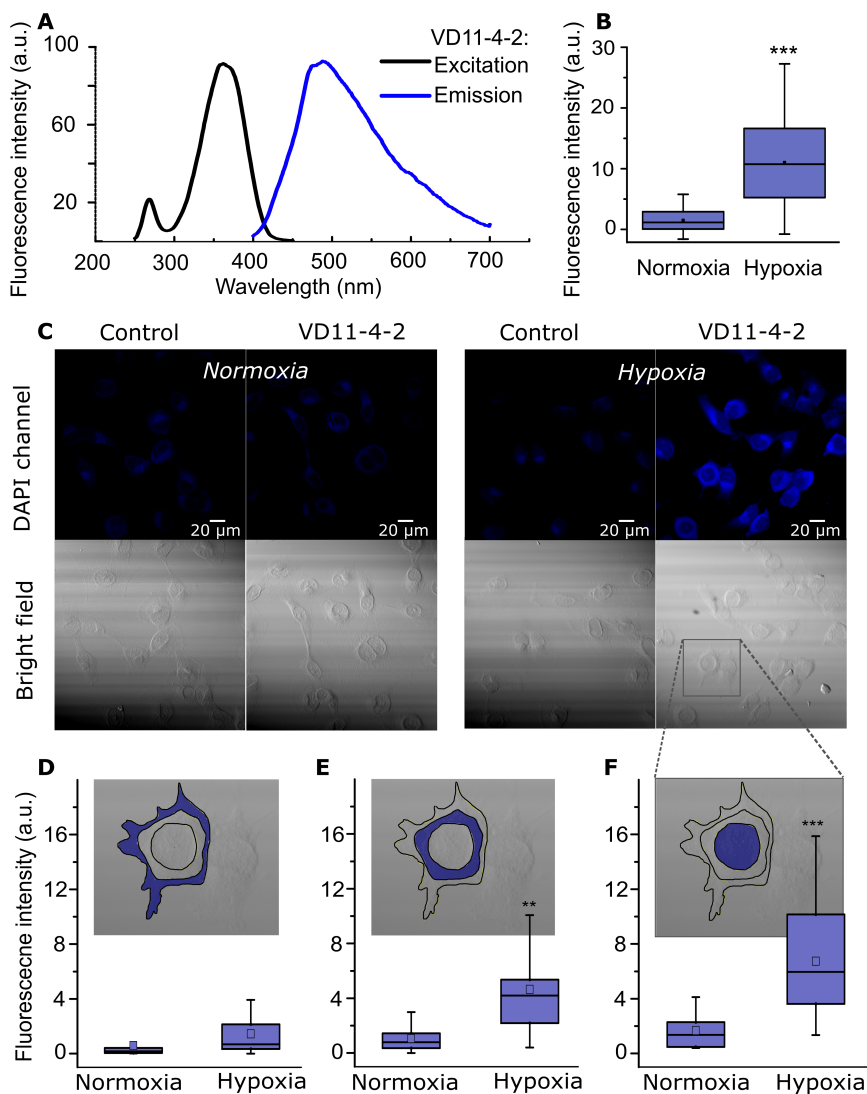


Figure 4.2: VD11-4-2 fluorescence excitation and emission spectra(A); calculated cell fluorescence intensities (B), and confocal images (C) of VD11-4-2 (1 μM) treated, and untreated MDA-MB-231 cells in normoxia and hypoxia mimicking conditions; calculated fluorescence intensities of different parts of the cells: distal part of the cell (corresponding to the fluorescence of cytoplasmic membrane D), zone around nucleus (corresponding to the cytoplasm E), nucleus (F) (**p<0.01; ***p<0.001).

lated. The most interesting part of the cell in this experiment was cell edges, where CAIX is localized. The group of cells incubated with compound VD11-4-2 in hypoxia mimicking conditions showed a larger fluorescence intensity from the distal cell parts as compared to other groups

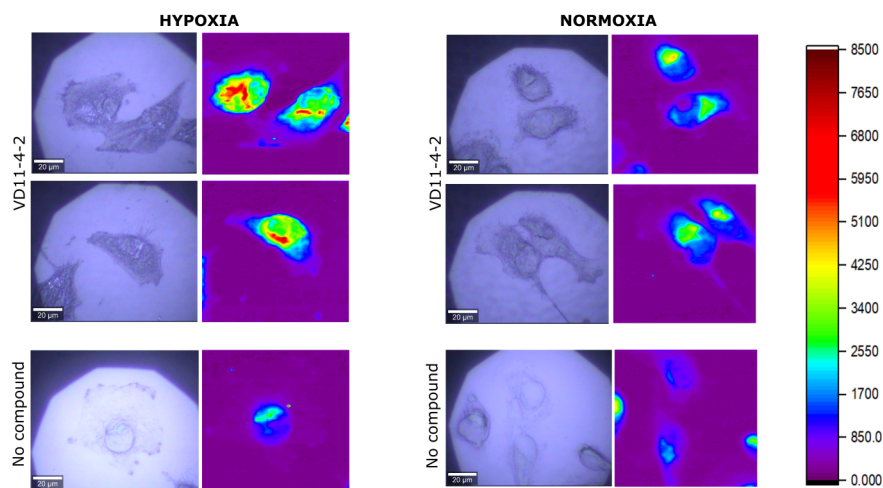


Figure 4.3: MDA-MB-231 cell fluorescence in the range of (510 ± 50) nm.

(normoxic cells incubated with compound and control cells) (**Fig. 4.2 D**). However, fluorescence intensities from the nucleus and zones around the nucleus were also observed to be more fluorescent in cells incubated under hypoxia mimicking compared to normoxia condition (**Fig. 4.2 E and F**). VD11-4-2, being a small molecule, should be able to cross the cytoplasmic cell membrane [164]. Such compound accumulation within inner parts of the cell could be observed due to possible compound binding towards cytosolic isoform of CA IX [38] or to other proteins inside the cell. Such strong fluorescence signal from the inner cell parts after incubation with fluorescent CA IX inhibitors could be also seen in other researchers works [165, 166].

Partially identical compound accumulation manner differences between cells in normoxia and hypoxia mimicking conditions were observed after fluorescence spectra ($\lambda_{em} = (510 \pm 50)$ nm) analysis in separate points obtained with another imaging system. Fluorescence signal intensity was higher in hypoxia than normoxia (max value 8500 and 4500 a.u., respectively). The maximum value for control cells fluorescence reached about 2000 a.u. The most intense signal was observed in the nucleus zone (**Fig. 4.3**). Cell membrane zones (the localization of CA IX) could be seen more accurately in cells incubated with VD11-4-2 in hypoxia mimicking conditions rather than normoxia.

4.3 Impact of CA IX inhibition to cell migration

Influence of CA IX inhibition by compound VD11-4-2 on cell motility was evaluated in two independent studies carried out using μ -dish and gradient flow microfluidic device. Single-cell paths were tracked during the experimental time and cell velocities together with movement toward chemoattractant were calculated. To closer simulate the physiological environment migration, surfaces were coated with collagen and cell suspension mixed with fibronectin (in the study with microdevice) before the seeding. It has been previously shown that the amount of these ECM components is boosted in breast cancer areas [167,168]. None of the earlier studies aiming to test the influence of CA IX inhibition on cell migration have used ECM coated surfaces.

4.3.1 Influence of CA IX inhibitor on cancer cell velocities

Collagen coated glass-bottomed μ -dish with the imprinted grid as a reference was used to evaluate compound VD11-4-2 influence on CA IX over-expressing cell migration. The compound was tested at concentrations of 5 and 20 μ M, which does not cause severe toxicity to MDA-MB-231 cells. Half maximal effective concentration (EC_{50}) for these cells was determined to be not lower than 50 μ M in previous studies [95]. In some of the experiments 50 ng/ml of EGF was added to the cell medium in the beginning of experiment, in order to induce epithelial-mesenchymal transition in MDA-MB-231 and MCF-7 cell lines [169].

MDA-MB-231 cell velocities were observed to be lower under hypoxia compared to normoxia conditions. No significant changes in cell speeds were observed in normoxic cells incubated with or without the 20 μ M of the compound. Under hypoxia mimicking conditions, 20 μ M of the compound reduced cell velocity from 10.0 to 7.7 μ m/h ($p < 0.001$) in the presence of EGF and from 3.9 μ m/h to 3.1 μ m/h ($p < 0.01$) in the absence of EGF (**Fig. 4.4 A and B**). The concentration of 5 μ M VD11-4-2 also reduced EGF non-treated MDA-MB-231 cell, incubated in hypoxia mimicking conditions, migration rate; however, not significantly.

Swayampakula et al. results showed that CA IX inhibitor U-104 (25 μ M) also reduced MDA-MB-231 cell migration by 10% under hy-

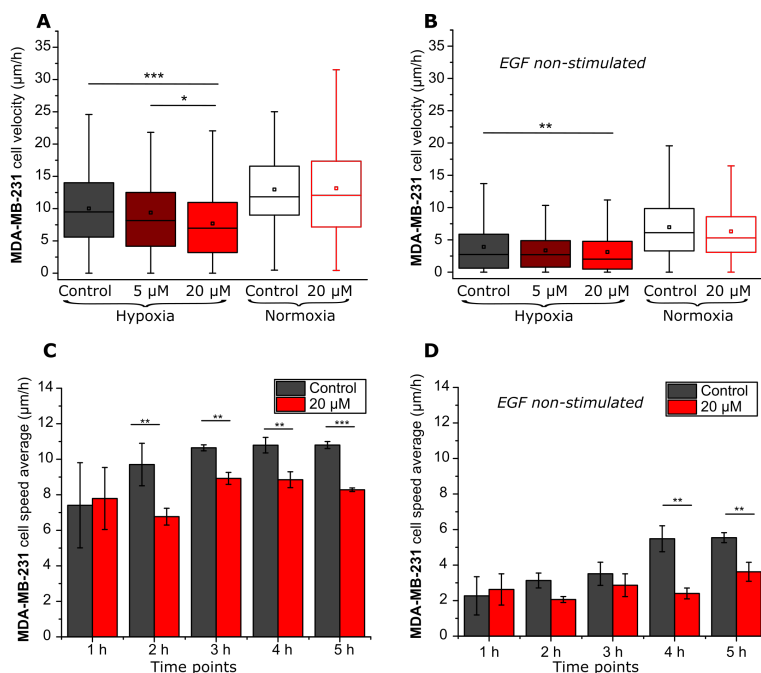


Figure 4.4: VD11-4-2 influence on MDA-MB-231 cell velocities (A,B) and under hypoxia mimicking condition incubated cell speed changes during the time (B,D) when cells are treated (A, C) or non-treated (B, D) with EGF (* $p < 0.05$; ** $p < 0.01$; *** $p < 0.001$).

poxia condition [56]. In comparison, VD11-4-2 showed cell migration rate reduction by more than 20 % at even lower concentration of 20 μM . Ward et al. demonstrated that a group of sulfamate inhibitors influence MDA-MB-231 cell migration in both normoxia and hypoxia conditions [107]. However, they used scratch assay while evaluating gap closure after 48 h, which is longer than cell population doubling time.

In our experiment, cell velocity rates in the hypoxia mimicking condition were calculated at every hour of the experiment. It was observed, that EGF treated MDA-MB-231 cell velocity reached the steady state of $(10.6 \pm 0.2) \mu\text{m/h}$ after 3 h of experiment. Whereas EGF-non stimulated cells reached the steady-state velocity of $(5.5 \pm 0.7) \mu\text{m/h}$ after 4 h. Maximum cell velocities were reduced by 20 μM of VD11-4-2 and reached $(8.9 \pm 0.3) \mu\text{m/h}$ and $(3.6 \pm 0.5) \mu\text{m/h}$ for EGF stimulated and non-stimulated cells (respectively **Fig. 4.4 C** and **D**).

Similar influence of the compound on migration was observed in MCF-7 breast cancer cell line. MCF-7 cell line as well as MDA-MB-231

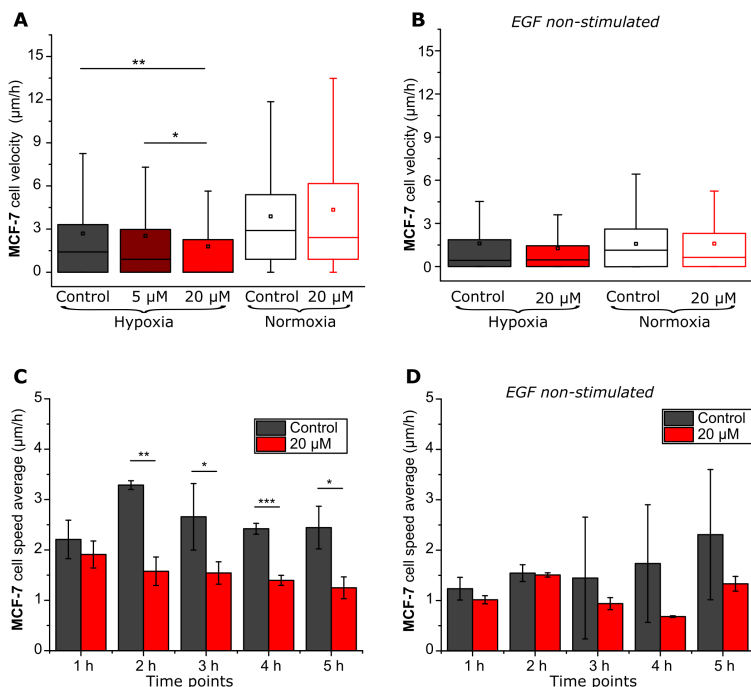


Figure 4.5: VD11-4-2 influence on MCF-7 cell velocities (A,B) and under hypoxia mimicking condition incubated cell speed changes during the time (B,D) when cells are treated (A, C) or non-treated (B, D) with EGF (* $p < 0.05$; ** $p < 0.01$; *** $p < 0.001$).

was derived from a metastatic tumor site [170]; however, it showed lower migration rates than MDA-MB-231 cells. EGF non-stimulated MCF-7 cell velocities were low (from 1.3 $\mu\text{m}/\text{h}$ to 2.0 $\mu\text{m}/\text{h}$, **Fig. 4.6 B**), and no significant differences between the groups were observed. U-104 previously showed no influence on MCF-7 cell migration during scratch assay as well [105]. MCF-7 cell velocities increased after their stimulation with EGF (**Fig. 4.6 A**). The presence of compound VD11-4-2 20 μM reduced ($p < 0.01$) cell velocities from 2.7 $\mu\text{m}/\text{h}$ to 2.0 $\mu\text{m}/\text{h}$. Maximum speed of (3.3 ± 0.1) $\mu\text{m}/\text{h}$ for cells under hypoxia mimicking conditions treated with EGF was reached after the second hour of incubation. Meanwhile the maximum speed of VD11-4-2 treated cells did not exceed 2.0 $\mu\text{m}/\text{h}$ during the experiment (**Fig. 4.6 C**). Compound also slowed the speed increment of EGF-non stimulated cells, however with no statistical significance (**Fig. 4.6 D**).

Influence of CA IX inhibitor on migration velocities of CA IX non-expressing fibroblasts under hypoxia mimicking conditions was inves-

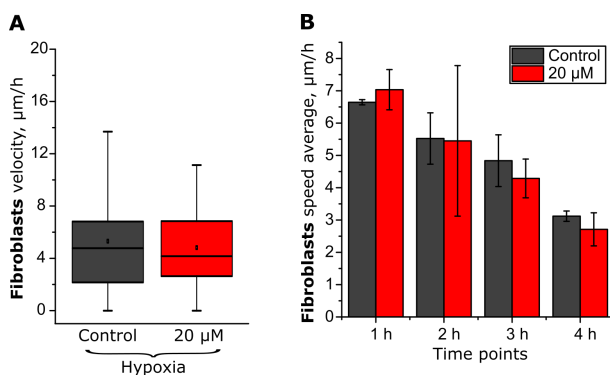


Figure 4.6: VD11-4-2 influence on EGF treated fibroblast cell velocities and speed changes during the time when cells are incubated under hypoxia mimicking condition.

tigated in order to ensure VD11-4-2 acts only on CAIX expressing cells. No statistically significant changes in cell velocities after addition of 20 μM VD11-4-2 were observed (**Fig. 4.6 B**). CAIX inhibitor did not cause significant changes in cell speed during the observed hours (**Fig. 4.6 D**).

All in all, compound VD11-4-2 at 20 μM was able to diminish CAIX positive cell speed by more than 20%. However, it is not the greatest effect observed in the migrastatic agent exploration. For example, several compounds, which inhibits cell contractility, reduced MDA-MB-231 cell migration in concentrations below 3 μM in wound healing assays [171, 172]. Some studies suggest that agents inhibiting protrusion formations are the most perspective in developing of migrastatic agents, as this effect is difficult to bypass [24]. However, agents disturbing cell contractility would affect the motility of not only tumor cells, but healthy ones as well [173]. They can affect the immune response, neuronal processes, tissue rebuilding, etc., and in such a way cause damage in a long time perspective. Therefore, VD11-4-2 with its ability to influence only CAIX positive cancer cell velocity makes it a prominent feature.

4.3.2 Influence of CAIX inhibition on cell chemotaxis

Influence of CAIX inhibition on MDA-MB-231 cell chemotaxis towards EGF was further investigated. A microfluidic device with gradient flow of EGF 0 ng/ml to 100 ng/ml was used for this study. Previous

studies have shown that microfluidic systems with EGF gradients are highly suitable to investigate the influence of anticancer drug on cancer cell migration [174].

Cell migration direction was assessed by tracking the location of individual cells in the x and y directions, and setting the start position at 0;0 coordinate (**Fig. 4.7 A**). The majority of control cells (>55 %, $p < 0.01$) in both normoxia and hypoxia mimicking conditions migrated toward higher concentrations of the EGF (**Fig. 4.7 B, C**). This coincides with Wang et al. results, showing that more than half of MDA-MB-231 cells migrate towards higher EGF concentrations in a microchip with gradient flow of EGF at the concentration range of 0 ng/ml to 100 ng/ml [175].

CA IX inhibitor VD11-4-2 in a concentration of 20 μ M altered cell attraction toward EGF in hypoxia mimicking condition: no significant difference between amount of cells migrating toward and from EGF were observed. As the number of cells moving in both directions becomes almost equal, it leads to the outcome that cells were non-chemotactic in the presence of inhibitor. Such VD11-4-2 influence on chemotaxis was not observed in normoxia condition, as more than 64 % of cells ($p < 0.001$) migrated toward higher EGF concentration.

A previous study showed that MDA-MB-231 cells migration through the membrane with pores toward EGF is enhanced if cells are stably expressing CA IX [56]. The study also demonstrates that inhibitor U-104 at the concentration of 50 μ M could reduce the motility of these cells. MDA-MB-231 cell treatment with EGF has been shown to increase CA IX reorganization into lipid rafts, where EGF receptors reside, under hypoxia condition [176]. However, the precise mechanism of how CA IX inhibition disturbs cell movement toward EGF is unclear.

Cell velocities were lower in hypoxia mimicking condition (**Fig. 4.8 A**), and this coincides with the results obtained from experiment in μ -dish. However, no statistically significant differences between control and compound incubated groups were observed in normoxia and hypoxia mimicking conditions.

Under hypoxia mimicking conditions incubated cells were grouped according to their migration rate intervals (bins) and cell numbers normalized to the maximum bin size. VD11-4-2 (20 μ M) caused about three-fold increase of cells migrating in speeds lower than 5 μ m/h (**Fig. 4.8 B**).

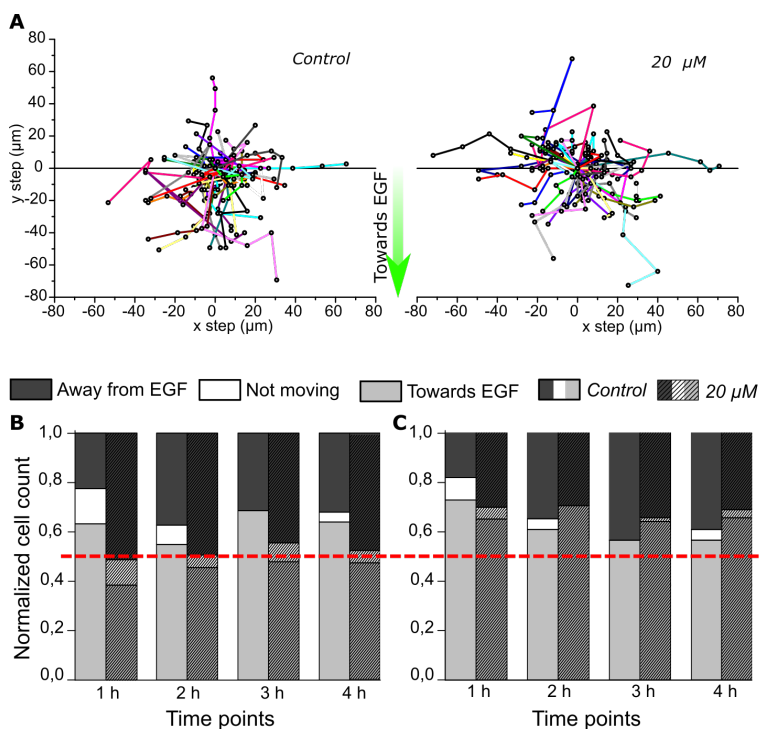


Figure 4.7: The migration paths of MDA-MB-231 cells (marked in different colors for individual cells) in control group (left) and group treated with 20 μM of VD11-4-2 (right). Paths toward a negative y values show migration to higher EGF concentrations. Normalized count of cells migrating toward or away from higher EGF concentrations under hypoxia mimicking (B) and normoxia (C) conditions. Numbers of cells per group are as following: 61 (control) and 78 (VD11-4-2 treated) in hypoxia mimicking conditions; 64 (control) and 42 (VD11-4-2 treated) in normoxia.

The compound also reduced the number of cells migrating in the speed range of 10 to 20 $\mu\text{m}/\text{h}$.

Influence of the compound on cell migration speed was observed to be dependent on starting EGF concentration (**Fig. 4.8 C**). Previous studies in chemotactic MDA-MB-231 migration showed that cell speed is not EGF-dose dependent [177]. VD11-4-2 reduced the migration rate for cells in hypoxia mimicking conditions by almost 2 $\mu\text{m}/\text{h}$ ($p < 0.05$), when the starting EGF concentration was from 0 to 50 ng/ml. No effect was observed when starting EGF concentration was between 50 ng/ml to 100 ng/ml.

Influence of VD11-4-2 on cell motility could also be seen in migra-

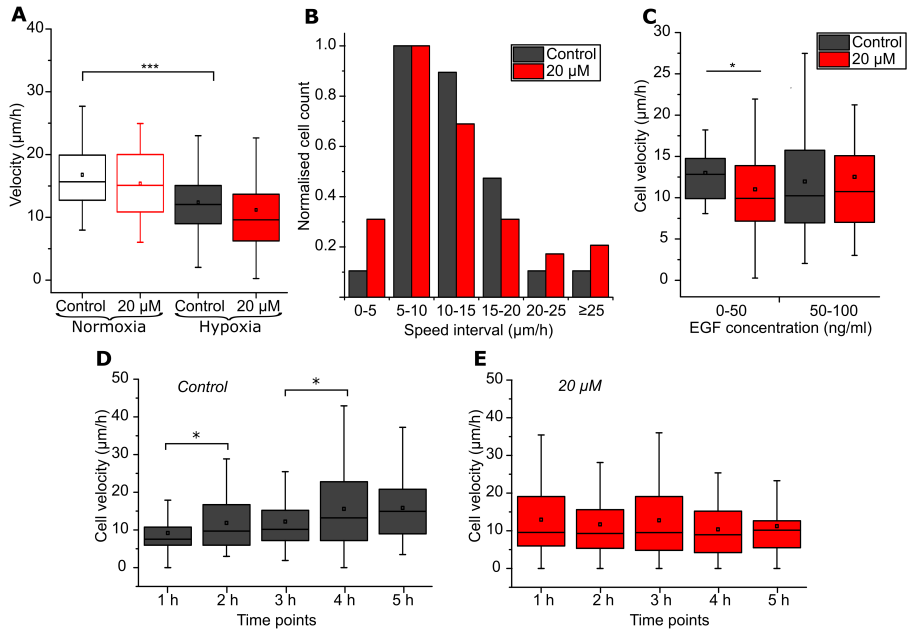


Figure 4.8: MDA-MB-231 cell velocities (A) under normoxia or hypoxia and in the presence or absence of 20 μM VD11-4-2; cells under hypoxia mimicking condition amount in different speed ranges (B); velocity differences dependence on starting EGF concentrations ($n=30, 49, 31, 27$) (C), and velocity changes during the time (D) (* $p<0.05$; *** $p<0.001$).

tion speed changes over the time. The migration rate of cells under hypoxia mimicking conditions in the control group increased monotonically and reached a steady state during the fourth hour of the experiment (15.6 $\mu\text{m}/\text{h}$). Meanwhile cell speed in group treated with 20 μM of VD11-4-2 reached maximum speed of 12.8 $\mu\text{m}/\text{h}$ during the third hour of experiment (**Fig. 4.8 D**).

Overall, two independent experiments (in μ -dish and microfluidic device) showed that VD11-4-2 inhibits both EGF stimulated and non-stimulated CA IX cell velocity, and disturbs their chemotaxis toward a higher concentration of EGF. Such VD11-4-2 effect occurs only in the presence of its target, and suggests it could be further tested as an antimetastatic drug and as a guide for specific drug delivery toward tumor cells under hypoxia conditions. The study of this VD11-4-2 application is described in the next part of the thesis.

4.4 Characteristics of prepared NS

Due to its high affinity and selectivity toward CAIX properties inhibitor VD11-4-2 was tested as a targeting moiety for breast cancer in several different NS based on PSi NP and Zn-CuO NP encapsulated in SpAcDX (Prickly@SpAcDX). Chemical modification reactions were performed by using VD11-4-2 “tail” part (**Fig. 4.9 (3)**), containing the hydroxy group while preserving the sulfonamide group, which is essential for compound binding to CAIX active center.

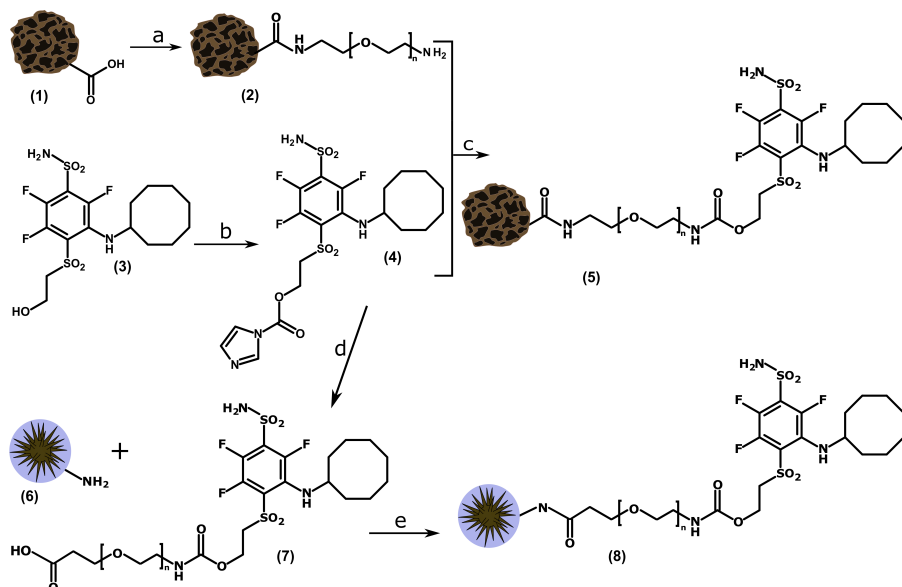


Figure 4.9: Steps of NP chemical modification: EDC, NHS, *t*boc-NH-PEG-NH₂ in DMF at r.t. and afterward DCM, TFA, r.t. (a); CDI, in toluene at 60 °C (b); 2 and 4 mixed in toluene at 60 °C (c); NH₂-PEG-COOH in toluene at 60 °C (d); EDC, NHS in HEPES at r.t. (e). Reactions a, b, c were performed to prepare VD-PSi, while b, d, e reactions were done during Prickly@SpAcDX-PEG-VD11-4-2 preparation.

PEG with a molecular weight of 5000 was chosen as a linker between the compound and the NP due to the long and flexible chain, which could ensure VD11-4-2 access protein CAIX active center. It has been previously observed that attachment of CAIX targeting moiety to NP via PEG linker reduces the nonspecific NS uptake by CAIX negative cell and enhances endocytosis by CAIX positive ones further enhancing cytotoxicity of NP [145]. Moreover, PEG in NS is used as a

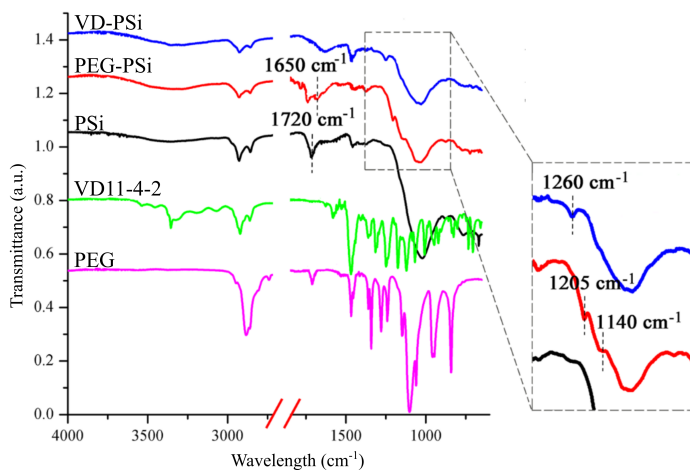


Figure 4.10: FTIR spectra of VD11-4-2, PEG, PSi, PEG-PSi, and VD-PSi representing successful NP modification.

stabilizer, preserving them from charge-based contact with proteins and small molecules [178].

During VD-PSi (**Fig. 4.9 (5)**) preparation, carboxyl groups from UnTHCPSi (**Fig. 4.9 (1)**) were coupled with amine groups of NH_2 -PEG-NH-Boc during EDC/NHS coupling reaction (**Fig. 4.9 a**). Boc protection avoided both PEG ending crosslinking with NP. After PEG conjugation, boc was removed and amine groups from PEG-modified PSi (**Fig. 4.9 (2)**) were used to attach VD11-4-2 via CDI mediated coupling (**Fig. 4.9 b and c**). The size, zeta potential, and FTIR spectra were measured for bare PSi, PEG-modified PSi, and VD-PSi. The size of the NP increased after each step of modification: from (184.0 ± 0.8) nm of bare PSi to (190.0 ± 0.7) nm of VD-PSi. Zeta potentials remarkably changed after the chemical reactions steps: (-24.0 ± 0.7) mV for PSi, (22.0 ± 0.4) mV for PEG modified PSi and (-22.0 ± 0.5) mV for VD-PSi. FTIR spectra after NP modification with PEG showed new bands at 1205 cm^{-1} (C-N-C moiety), at 1140 (N-C=O moiety) and a shift of C=O moiety band from 1720 to 1650 cm^{-1} (**Fig. 4.10**). Further modification with VD11-4-2 resulted in appearance of a band at 1260 cm^{-1} , which could be attributed to aryl fluorine. Quantitative analysis showed that VD11-4-2 conjugation efficiency to the NP was 1.2% ($100 \mu\text{g/ml}$ of VD-PSi contains $1.2 \mu\text{g/ml}$ VD11-4-2).

During the preparation of Prickly@SpAcDX (**Fig. 4.9 (8)**), the hydroxyl group of the inhibitor was initially activated (**Fig. 4.9 (4)**) with CDI for further coupling with the amine group of NH₂-PEG-COOH (**Fig. 4.9 d**). Afterward, amine groups of Prickly NP (**Fig. 4.9 (6)**) were utilized to bind with hydroxy group of PEG bound with VD11-4-2 (**Fig. 4.9 (7)**) via EDC/NHS reaction (**Fig. 4.9 e**). Size of the compound modified NP increased to (274.0 ± 1.2) nm (unmodified Prickly@SpAcDX size was (226.0 ± 1.7) nm), together with decreased zeta-potential: (41.0 ± 0.4) mV for Prickly@SpAcDX and (7.4 ± 1.0) mV Prickly@SpAcDX-PEG-VD11-4-2. FTIR analysis showed a number of a bands obtained from VD11-4-2 repeated in Prickly@SpAcDX-PEG-VD11-4-2, indicating the successful synthesis.

The sizes of both functionalized NP were relatively large (190 and 274 nm). Such size of NP could lead to its preferential accumulation in tumor compared to healthy tissues, as the smaller size (e.g., 15 nm and smaller) particles can accumulate in various healthy organs and could even cross the blood-brain barrier [179]. At the cellular level, the entering to non-targeted cells is less probable with the increasing NP size [180, 181]. However, the greater sizes of the NP could burden its binding to the cell due to the steric hindrance [182]. Therefore, VD-PSi NP targeting ability was tested in experiments with CA IX protein and on CA IX overexpressing and not-expressing cells.

4.5 CA IX targeting capability of the prepared NS

Binding and inhibition of CA IX protein were studied in order to ensure the affinity of VD11-4-2 toward CA IX after the chemical modification of NP. FTSA was used to study NP binding to CA IX properties. It showed that after the attachment to both of NP, compound retains its affinity toward CA IX, as both of the NS increased protein melting temperature by about 15 °C (**Fig. 4.11 A and B**). These values were similar to those of free VD11-4-2 binding to CA IX. Prickly@SpAcDX-PEG was used as a negative CA IX non-binding group and showed only a very slight T_m shift, which was only up to 1 °C.

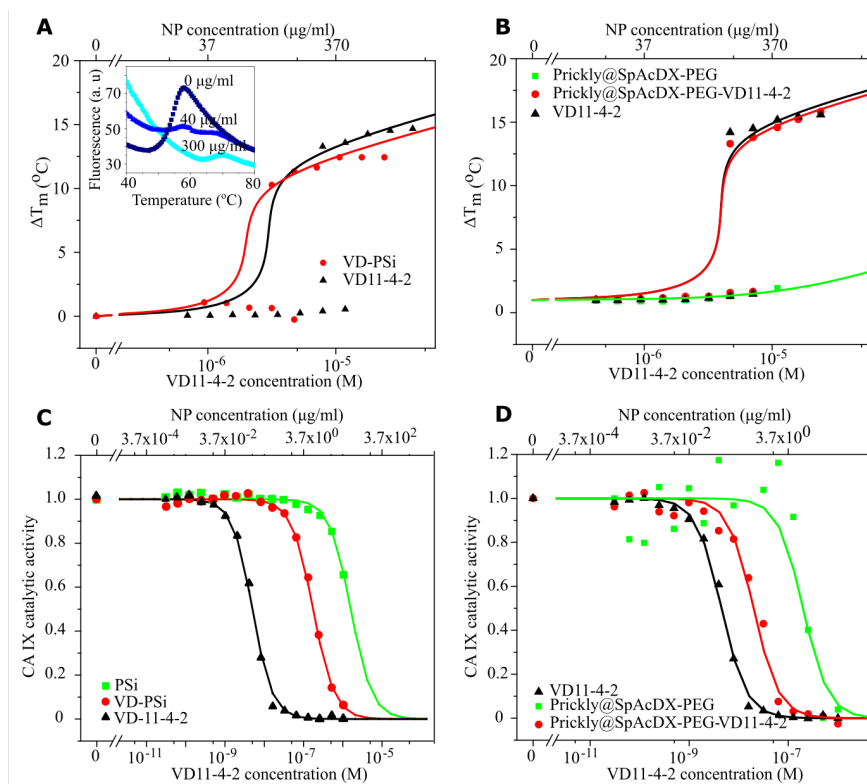


Figure 4.11: Protein melting temperature changes during FTSA assay representing VD-PSi (A) and Prickly@SpAcDX-PEG-VD11-4-2 (B) binding to CAIX. Insert in the (A) represents the raw FTSA data points (fluorescence intensities during the gradient temperature increase) when 0 $\mu\text{g/ml}$ to 300 $\mu\text{g/ml}$ of VD-PSi is added. VD-PSi (C) and Prickly@SpAcDX-PEG-VD11-4-2 (D) influence on CAIX protein inhibition determined by stopped-flow kinetic CO_2 hydration.

Afterward, inhibition of CAIX catalytic activity by NP was measured using stopped-flow CO_2 hydration method. Both VD11-4-2 modified NP were able to inhibit CAIX. The inhibition was observed to be weaker as compared to free compound VD11-4-2 (**Fig. 4.11 C and D**). It is important to mention, that binding and inhibition data obtained during these experiments does not represent the binding and inhibition constants of VD11-4-2 or NP.

Most of the developed CAIX targeting NS (except for works of [146, 147]) were directly tested in cell or animal studies while skipping the protein binding or inhibition tests. In the case of antibodies, it is reasonable to start NS studies from *in vitro* or *in vivo* investigation,

as even degraded parts of G250 were observed to retain the ability to bind to CA IX in cell [183]. Meanwhile small molecule inhibitors have to reach an active site for protein binding, this action could be altered due to the attachment of inhibitor on NP surface [184]. For example, sulfonamide group of VD11-4-2 binds the active site of CA IX. However, the substituent cyclooctylamine group in benzene ring is necessary for its binding to CA IX, as its absence leads to a 1000-fold reduction in affinity [10].

After CA IX binding and inhibition assays showed that NS retained affinity toward CA IX protein, tests in cancer cells were carried out in order to see how NP will behave in CA IX expressing cells.

4.6 Influence of the NS on medium pH changes

The main function of protein CA IX under hypoxia conditions is to help maintain neutral intracellular pH while producing bicarbonate from the excess of carbon dioxide [43]. Another this reaction product is protons, which accumulates in the extracellular space and acidifies it. Therefore, the pH changes measured by the pH-meter in the medium were used to evaluate the activity of CA IX protein *in vitro*. pH value of the medium was lower in hypoxia mimicking as compared to normoxia conditions: $7.5 \pm 1.5\%$ and $7.8 \pm 2.5\%$, respectively. Compound VD11-4-2 alone, VD-PSi, and PSi all reduced the medium acidification in hypoxia mimicking conditions (**Fig. 4.12 A**). Influence of PSi on pH value changes could be explained through a non-specific CA IX protein adsorption and function disruption. Inhibitor modified NP showed the highest influence on pH value, which was $7.8 \pm 0.9\%$ compared to control value of $7.5 \pm 1.5\%$.

Afterward, the pH values of the medium collected from normoxic cell wells were measured. NP or free VD11-4-2 caused no significant changes in pH values under normoxia condition (**Fig. 4.12 B**). Free VD11-4-2 inhibitor has been shown to reduce hypoxia-induced acidosis in four different cancer cell lines, including MDA-MB-231 [95]. Previous studies showed that CA IX silencing in 4T1 cells and inhibition by 100 μM of U-104 in B16F10 cells decreases extracellular medium acidification in hypoxia conditions [5, 185].

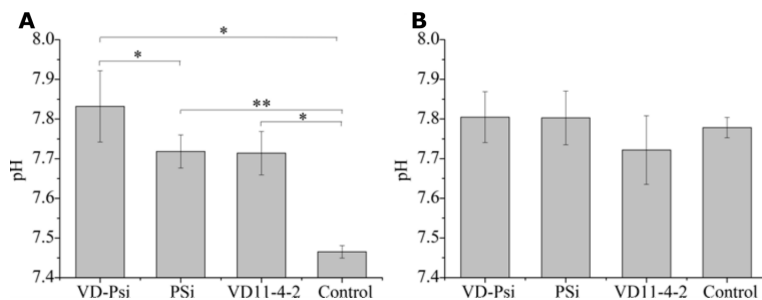


Figure 4.12: pH values of cell culture medium after its incubation with MCF-7 cells for 48 h in A hypoxia mimicking and B normoxia conditions.

4.7 Properties of NS drug loading and release profiles

PSi modified VD11-4-2 was then investigated as a carrier for PTX and DOX. These two drugs are commonly used for node-positive receptor-negative breast cancer treatment during chemotherapy [186]. Nanoformulations of albumin bound PTX and liposomal DOX have been already approved for use in clinics [17]. Despite that, various other NS loaded with PTX and DOX are intensively studied to minimize the premature drug leakage during circulation in the blood and maximize its release of the drug at the tumor site [187, 188]. Therefore, VD-PSi was tested for drug loading degree and release profiles.

4.7.1 Properties of paclitaxel loading and release

Modification with inhibitor did not influence the PTX loading degree: both bare PSi and VD-PSi were able to upload about 5.5% of the drug. PSi modification with CAIX inhibitor also barely affected PTX release profile (**Fig. 4.13 A**). PTX is very poorly water-soluble; therefore 0.1% Tween 80 was added to the medium as a serum mimicking agent. It was previously shown that Tween is a more stable agent than FBS and, therefore, is more recommended during poorly water-soluble drug release tests [189].

The majority of the drug was released at pH=7.0 within the first hour of the experiment. PTX release study from VD-PSi was further repeated at FBS containing medium at pH=7.4, which again showed a rapid drop of the payload in the first two hours of experiments (data not

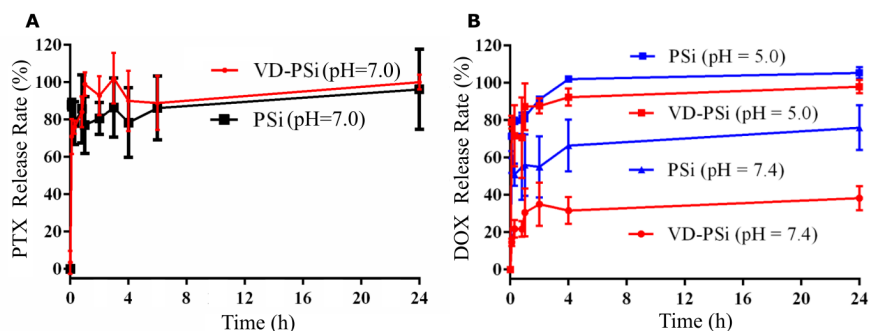


Figure 4.13: Release of PTX (A) from VD-PSi (red) and PSi (black) NP at pH=7.0 (containing 0.1 % Tween 80); release of DOX (B) from VD-PSi (red) and PSi (blue) NP at pH=5.0 and pH=7.4

shown). Such a fast payload leak at physiological conditions is not a desirable feature of a nanocarrier, as it can lead to a CA IX non-specific cell toxicity. A promising nanoformulation should at least show a sequential time-release [190]. It was previously observed, that PTX release from the mesoporous NP could be reduced with a downsized NP pores. However, in such NP with a size up to 10 nm drug release rate was not higher than 40 % even after 120 h of the experiment [191]. Therefore, stimulus-responsive NS, such as prodrug nanoassemblies, could be identified as more prominent PTX delivery systems [192].

4.7.2 Properties of doxorubicin loading and release

Modification with VD-11-4-2 was shown to cause two-fold increase in the DOX loading capacity: VD-PSi uploaded (21.4 ± 0.1) % of DOX whereas PSi reached (10.1 ± 0.1) %. In comparison CA IX specific antibody modified mesoporous silica NP, showed the loading efficiency of 14 % [139].

PSi attachment with inhibitor changed DOX release properties, which were observed to be pH value-dependent. DOX release rate (**Fig. 4.13 B**) within 1 h at pH value 7.4 is only (30.6 ± 12.6) %, while at pH value 5.0 it reaches (87.2 ± 14.2) %. The observed pH-dependent release profile could be caused by the formation of hydrogen bonds between VD11-4-2 and DOX, which is disturbed in an acidic medium containing excess protons.

To further confirm this effect, the UV-Vis absorption spectra of

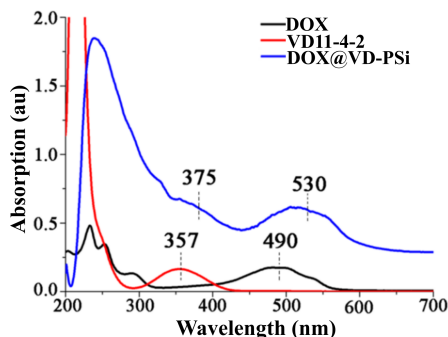


Figure 4.14: UV-vis absorption spectra of DOX, VD11-4-2, and DOX@VD-PSi measured in aqueous solution.

DOX, VD11-4-2 and DOX@VD-PSi were recorded (**Fig. 4.14**). Absorption spectra show that free DOX and VD11-4-2 compounds have peaks, which could also be observed in the solution of DOX@VD-PSi. Compared to free compounds, DOX@VD-PSi shows a red-shift in both DOX (490 and 530 nm) and VD11-4-2 (357 and 375 nm) wavelengths. This indicates the hydrogen bonding, as it is known that absorption band's shift is one of the characteristic feature of the hydrogen bond formation [193,194].

The maximum antitumor activity of currently used DOX nanoformulations could not be reached due to the poor release of the drug at the tumor sites, as the specific clear drug release mechanisms are still unknown [188,195]. Therefore, novel NS with heat, magnetic field, and pH triggered DOX release is broadly investigated [196,197]. Acidic pH-sensitive NS (such as VD-PSi) is considered to be valuable for controlling drug release in tumors, because of several reasons [198].

A nanocarrier, actively targeting cancer cells, is internalized through endocytosis and is trapped by the acidic organelles (pH=4.5-5.5), which is beneficial for acid pH release of the payload [199]. Moreover, the pH-triggered release of DOX is also beneficial for cancer-targeted systems, as pH values in hypoxia malignant tumor sites are acidic (pH=5.6-7.7) [200,201]. Therefore, VD-PSi is expected to be carrying the drugs in an environment with neutral pH (e.g., blood) with minimal leak and to accelerate the release after entering acidic pH (e.g., acidic cell organelles). Therefore, VD-PSi was the pioneer in stimulus-controlled DOX delivery via the CAIX targeting nanosystem. Following stud-

ies were done for mesoporous silica and gold NP constructed to release the DOX in the presence of pH stimulus, respectively [139,145]. The increasing number of studies aiming to find stimulus-triggered drug release from NS further proves their high demand.

4.8 NS caused cytotoxicity

ATP-luminescent based assay *in vitro* cell viability tests were done further to study designed NP ability to target CAIX. Breast cancer cells MCF-7 were chosen for this study, as they were shown to express CAIX under hypoxia mimicking conditions (**Fig. 4.1**). Free VD11-4-2, at the highest concentration tested (1.2 $\mu\text{g}/\text{ml}$, which correspond to VD11-4-2 amount in 100 $\mu\text{g}/\text{ml}$ of VD-PSi), was not able to kill more than 12% of cells (data not shown). A similar result was obtained with VD-PSi, where the highest concentration of 100 $\mu\text{g}/\text{ml}$ did not disturb the viability of 85% of the cells (**Fig. 4.15 A**). In comparison, inhibitor non-modified PSi showed a little higher cytotoxicity ($\approx 80\%$ of viable cells) (**Fig. 4.15 D, E**). This might be because VD-PSi modification with PEG is making particles more biocompatible [202]. VD-PSi was shown to alter viability of the cells, incubated under hypoxia mimicking conditions, which could be linked with its binding to CAIX receptors and the disturbance of its function.

4.8.1 Paclitaxel loaded NS

Influence PTX on both normoxia and hypoxia mimicking conditions incubated cell viability was similar: (75.7 ± 2.0)% and (76.0 ± 2.3)% of viable cells at the highest concentration tested (**Fig. 4.15 B, C**). Under normoxic conditions, PTX uploaded VD-PSi NP (PTX@VD-PSi) was less effective ($(85.5 \pm 3.2)\%$ of viable cells) than PTX alone in killing cells ($p < 0.05$). VD-PSi showed higher activity of (63.0 ± 0.4)% comparing to PTX alone ($p < 0.01$) under hypoxia mimicking conditions, which presumably is influenced due to alleviated NP uptake via CAIX.

Unmodified PSi uploaded with PTX showed better activity than PTX alone or PTX@VD-PSi in both normoxic ($(67.2 \pm 8.4)\%$ of viable cells) and hypoxia mimicking ($(55.0 \pm 1.4)\%$ of viable cells) conditions.

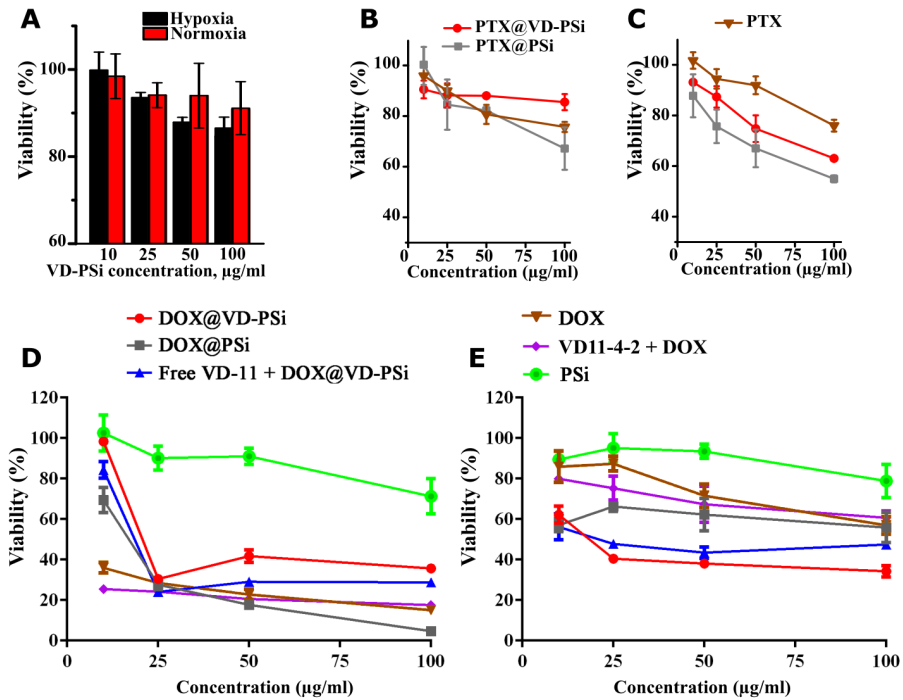


Figure 4.15: VD-PSi influence on MCF-7 cell viability (A); Results obtained from under normoxia (B, D) and hypoxia mimicking conditions (C, E) incubated cell with different formulations of PTX (B, C) and DOX (D, E).

Such effect could be attributed to higher toxicity of PEG unmodified NP and to uncontrolled PTX drop from both of NP in the presence of FBS as observed in release studies. In comparison, CAIX targeted systems exhibiting lower leakage of PTX at pH=7.4 have a superior anticancer effect towards hypoxic MDA-MB-231 cells as compared to non-targeted ones [132]. Therefore, cell toxicity studies were switched to DOX loaded VD-PSi, which showed more promising release profiles.

Overall, PTX formulated in NP showed higher anticancer activity than PTX alone, and advantages of similar PTX nanoformulations were observed during numerous studies [203, 204].

4.8.2 Doxorubicin loaded NS

DOX loaded VD-PSi NP were then tested for their anticancer activity. Under normoxic conditions, when CAIX was not expressed, DOX@VD-PSi particles were less active than other formulations with

DOX. Even bare DOX loaded PSi (DOX@PSi) were more active than DOX@VD-PSi (**Fig. 4.15 D**). This effect could also be related to higher DOX release rates from unmodified NP at neutral pH values. Furthermore, bare PSi, in comparison with VD-PSi, were not modified with PEG, which diminishes NP interaction with cells.

Different anticancer activities were observed in viability tests of hypoxic cells (**Fig. 4.15 E**). In such conditions, free DOX showed to be less active in killing the cells in hypoxia mimicking conditions (56.9 ± 4.3 %) as compared to normoxia condition (15.1 ± 1.3 %) at the highest concentrations tested. Such decreased DOX effectivity could be linked with hypoxia caused resistance to DOX, which was observed in previous studies with various cancer cell lines, including MCF-7 [205,206]. Meanwhile DOX@VD-PSi were observed to have the highest anticancer activity among all groups at 100 $\mu\text{g/ml}$, as only (34.2 ± 2.7 %) of cells were viable. Other DOX formulations (DOX, DOX@PSi, DOX combination with VD11-4-2) were less effective (not less than 55 % of viable cells).

One of the tested groups were cells with preincubated free VD11-4-2, which were used to monitor if the cancer cell killing effect was due to CA IX targeting. Preincubation with free VD11-4-2 diminished the anticancer activity of DOX@VD-PSi as viable cell number increased ($p < 0.005$) to (47.4 ± 2.1 %). This result proved that VD11-4-2 on the surface of NP can target CA IX in breast cancer cells and overcome hypoxia-caused cell resistance. Later studies with gold NP targeting CA IX along with acetazolamide-like compound confirm that this is an option to overcome hypoxia-caused drug resistance in human colorectal cells as well [145].

Different DOX nanoformulations for receptor-mediated delivery into the cell are broadly investigated [207, 208]. Among them, HER2 receptors targeted pegylated liposomes carrying DOX were already tested in clinical trials and showed limited toxicity to healthy cells compared to unmodified particles [209]. Uptake of NP uploaded with DOX is important, because DOX is a weak basic drug, and is protonated in an acidic tumor environment, and this state hinders cellular uptake of free DOX [210]. Therefore, such targeting moieties, which alleviates NP uptake, would be highly beneficial, and further experiments were done with Zn doped CuO NP in order to further prove VD11-4-2 targeting

capacity.

4.8.3 Zn-CuO based NS

Zn doped CuO (Prickly) NP have needle shaped edges, which cause cell death by disrupting the cell membranes, and in concentration of 500 $\mu\text{g}/\text{ml}$ NP leave no viable MCF-7 cells after 24 h in hypoxia mimicking conditions (**Fig. 4.16 A** black line). Prickly NP coated with a polymer and attached with PEG (Prickly@SpAcDX-PEG) have low toxicity to cells, leaving more than 82% of them viable at a maximum concentration of 500 $\mu\text{g}/\text{ml}$. Prickly particles killed cells only when polymer coating was corrupted in cell organelles with acidic conditions such as lysosomes.

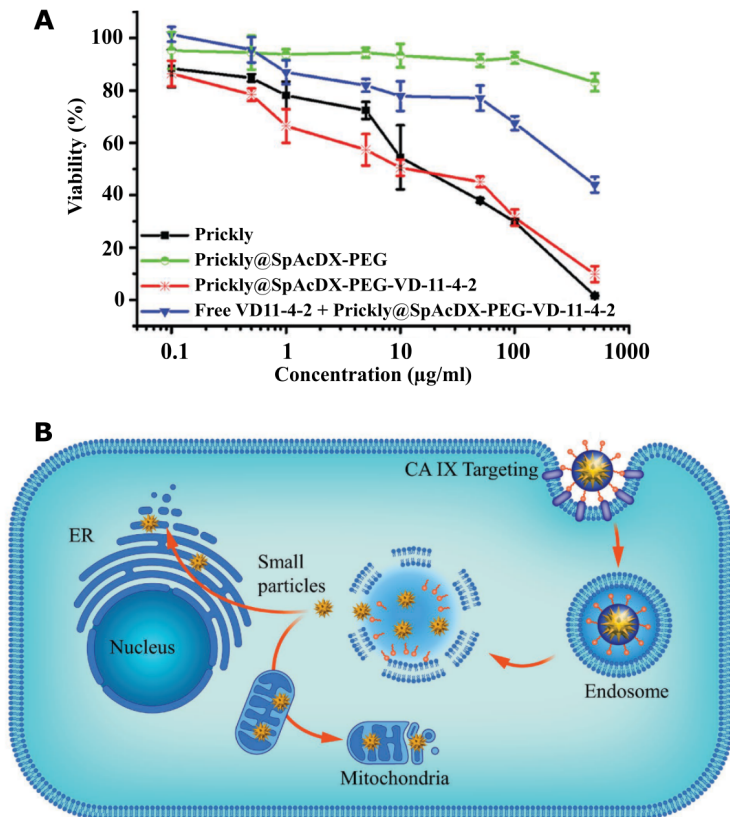


Figure 4.16: Influence of Prickly NP on MCF-7 cell viability under hypoxia mimicking conditions (A) and schematic explanation (B) of Prickly@SpAcDX-PEG-VD11-4-2 mechanism of action reprinted with permission from [158].

Coated and compound modified NS (Prickly@SpAcDX-PEG-VD11-4-2) was similarly effective as bare Prickly (**Fig. 4.16 A**), which indicates that presence of CA IX inhibitor alleviates NP uptake. Previous studies have shown that CA IX targeting systems bind to its active site, and enter the cell through protein internalization [94]. CA IX receptor saturation with free inhibitor VD11-4-2 preincubation, led to a reduced anticancer activity as cell viability increased ($p < 0.005$) from $(10.1 \pm 2.6) \%$ to $(42.3 \pm 2.2) \%$. Prickly@SpAcDX-PEG-VD11-4-2 was observed to act in DOX resistant MCF-7 cells in the same manner while they did not exhibit such toxicity to CA IX negative NIH-3T3 human fibroblasts cells [158].

Overall, the *in vitro* cytotoxicity studies lead to the idea that Prickly@SpAcDX-PEG-VD11-4-2 mechanism of anticancer activity could be explained by the scheme in **Fig. 4.16 B**. Briefly, coated and VD11-4-2 modified particles bind CA IX, and are internalized inside the cell via endocytosis and fused with lysosomes [211]. The acidic NP environment in the cell organelles degrades the polymer, and then Prickly NP kills the cell through mechanical disruption of cell membranes. NS usually need activation by external stimulus (magnetic field, heating etc) [212–215]. The fact that Prickly@SpAcDX-PEG-VD11-4-2 acts on targeting cells and kills them without any external stimulus, makes its possible application less complicated.

4.9 FRET effect

Both of the compounds VD11-4-2 and DOX, respectively utilized as CA IX targeting part and cytotoxic agents in the VD-PSi NS, are fluorescent. Excitation wavelength of VD11-4-2 is 360 nm with emission peak of 500 nm, while DOX excitation wavelength is 490 nm with emission peak at around 600 nm. These compounds were tested as a potential pair for FRET effect with VD11-4-2 as fluorophore donor and DOX as acceptor. If the FRET effect occurs between these two molecules, VD11-4-2 excitation of 360 nm would lead to observation of DOX fluorescence instead of the fluorescence signal of VD11-4-2 emission peak.

Initially, the FRET effect was tested by measuring fluorescence spectra of a compound VD11-4-2 (12 $\mu\text{g/ml}$ or 27 μM) solutions with the

increasing concentration of DOX. Samples were excited with VD11-4-2 excitation wavelength of 360 nm. Increasing molar ratio of DOX results in decrease of VD11-4-2 fluorescence emission at ≈ 500 nm and enhanced DOX emission at ≈ 600 nm could be also observed (**Fig. 4.17 A**). Then, fluorescence spectra of solutions were recorded, where a fixed DOX amount (0.021 mM) was mixed with the increasing molar ratios of VD11-4-2. Excitation with the wavelength of 360 nm led to a DOX fluorescence increase together with an increasing molar ratio of VD11-4-2 in the solution (**Fig. 4.17 B**). This led to a conclusion that the FRET effect occurs between VD11-4-2 and DOX.

The influence of environment conditions (temperature, pH, and ionic strength) on FRET was determined. Fluorophore properties could be altered by the environmental conditions, which could disturb the FRET effect [216]. Such FRET hindrances are used in the development of FRET-based biosensors [217]. However, if the NP drug release is monitored, the surrounding factors should not interfere with fluorescence tracking in the best scenario.

To observe how ionic strength influences FRET, fluorescence spectra of VD11-4-2 and DOX solutions containing 0.02 or 0.1 M NaCl were measured. 0.1 M NaCl was observed to slightly decrease (less than 10 %) the fluorescence intensity of DOX when VD11-4-2:DOX ratio is 1:8 (**Fig. 4.17 C**). Subsequently, fluorescence intensities were measured in different pH buffers: acetate (pH=4.97), MES (pH=5.31), and HEPES (pH=7.42) at room (25 °C) and in physiological (37 °C) temperatures. Fluorescence of DOX was observed to be about 10 % more intense in acidic acetate and MES buffers compared to more neutral HEPES buffer (**Fig. 4.17 D**). Solution temperature did not have notable influence on the fluorescence intensities. The FRET effect occurred in all conditions, and the experiments were further done with the DOX@VD-PSi NS.

FRET effect between DOX and VD-PSi was then investigated. VD11-4-2:DOX molar ratio is 1:12 when DOX is uploaded to VD-PSi. FRET between these two compounds occurs in such a ratio as seen from (**Fig. 4.17 E**). When VD-PSi is excited with 360 nm wavelength the fluorescence signal of VD11-4-2 could be observed (**Fig. 4.17 F**) with slight fluorescence emission shift from 500 nm to 475 nm. This shift could be due to the binding of VD11-4-2 and PSi [218].

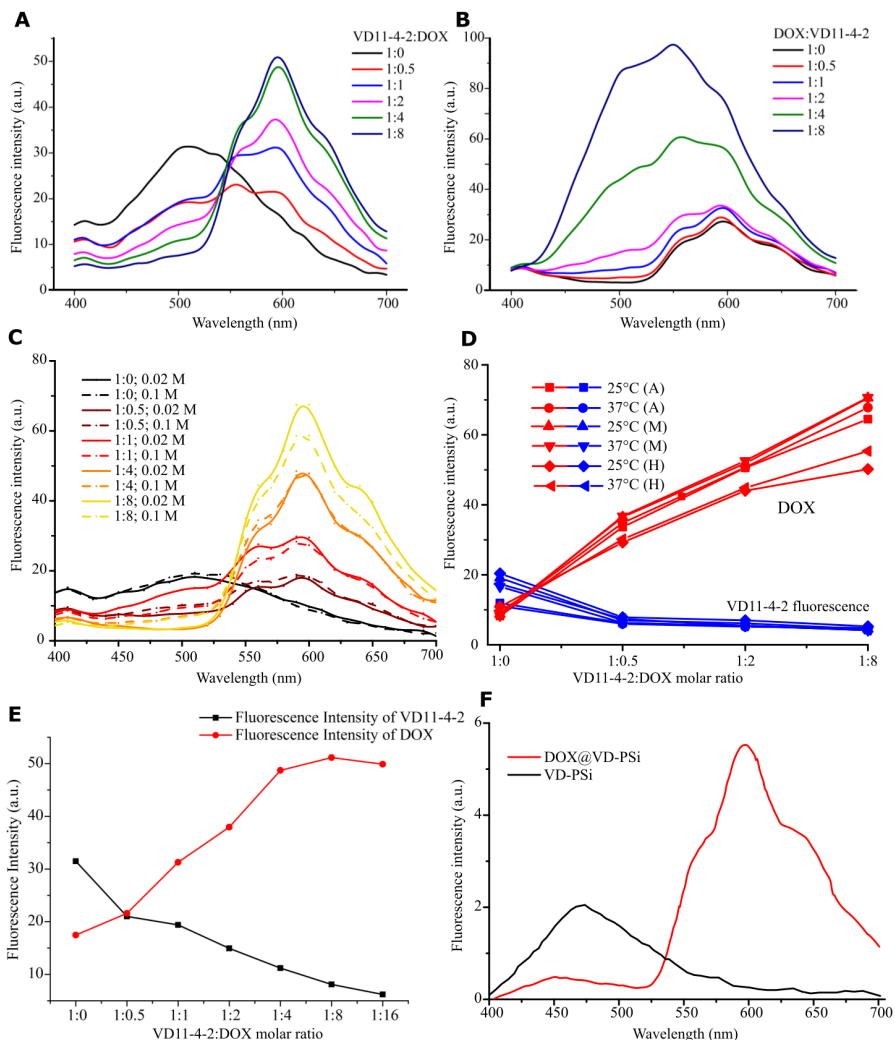


Figure 4.17: Fluorescence emission spectra of VD11-4-2 solution with increased molar ratios of DOX (A) or DOX with increased molar ratios of VD11-4-2 (B), $\lambda_{ex}=360$ nm. Fluorescence spectra (C) after addition of 0.02 M (solid lines) or 0.1 M (dashed lines) of NaCl to the VD11-4-2 solutions with increased molar concentration of DOX. pH and temperature influence on fluorescence intensities of DOX (red line) and VD11-4-2 (blue line) (D). A, M, H correspond the type of buffer used: acetate, MES and HEPES, respectively. DOX (red) and VD11-4-2 (black) fluorescence intensities (E) after solution $\lambda_{ex}=360$ nm. Fluorescence emission spectra (F) of VD-PSi and DOX@VD-PSi.

Afterward, DOX uploaded NP fluorescence spectrum, after excitation with the same wavelength, was recorded. In this case fluorescence

of VD11-4-2 is diminished to minimum intensities, and DOX emission (600 nm) is observed as expected in the case of FRET effect. Such changes in emission peaks confirm that DOX presence or absence in the VD-PSi could be distinguished after its excitation with 360 nm wavelength. Therefore, it was further applied for monitoring NP uptake and DOX release within the cell by confocal microscopy and flow cytometry.

4.10 Cell uptake of VD-PSi and intracellular doxorubicin release

Fluorescence properties of DOX@VD-PSi were then tested for their ability to show DOX release from NP within the cell during the experiments of confocal microscopy and flow cytometry (**Fig. 4.18**). The limiting distance for FRET is about 10 nm [219]. Therefore, while DOX is not released from NP, FRET effect should appear, resulting in no observed fluorescence of VD11-4-2 after its excitation. After DOX is released and distanced from NP by more than 10 nm the fluorescence of VD11-4-2 could be observed, because it is no longer a donor for FRET.

MCF-7 cells incubated with DOX@VD-PSi for 3 and 24 h were imaged by confocal microscopy. No signal of VD11-4-2 was observed after 3 h of cell incubation with NP (**Fig. 4.18 A**). Whereas, DOX fluorescence could be seen from inside the cell, which indicates that NP entered the cells. The fluorescence signal of VD11-4-2 appears after 24 h of NP incubation with cells, indicating DOX is released from the NS.

Fluorescence intensities of VD11-4-2 and DOX in cells were measured by flow cytometry after cell incubation with DOX@VD-PSi for 3 and 6 h. Signal of VD11-4-2 significantly increased after 6 h as compared to 3 h cell incubation (**Fig. 4.18 B**). Meanwhile, the DOX fluorescence signal showed only a slight increase (no statistical significance) between the 3 h and 6 h incubation times. This coincides with confocal microscopy results: VD11-4-2 fluorescence increases as DOX is released and distanced from VD-PSi, and FRET effect no longer occurs.

Overall, confocal microscopy and flow cytometry studies showed that DOX@VD-PSi fluorescence properties could be applied in tracking NP uptake by the cell. Such ability is achieved without additional NP mod-

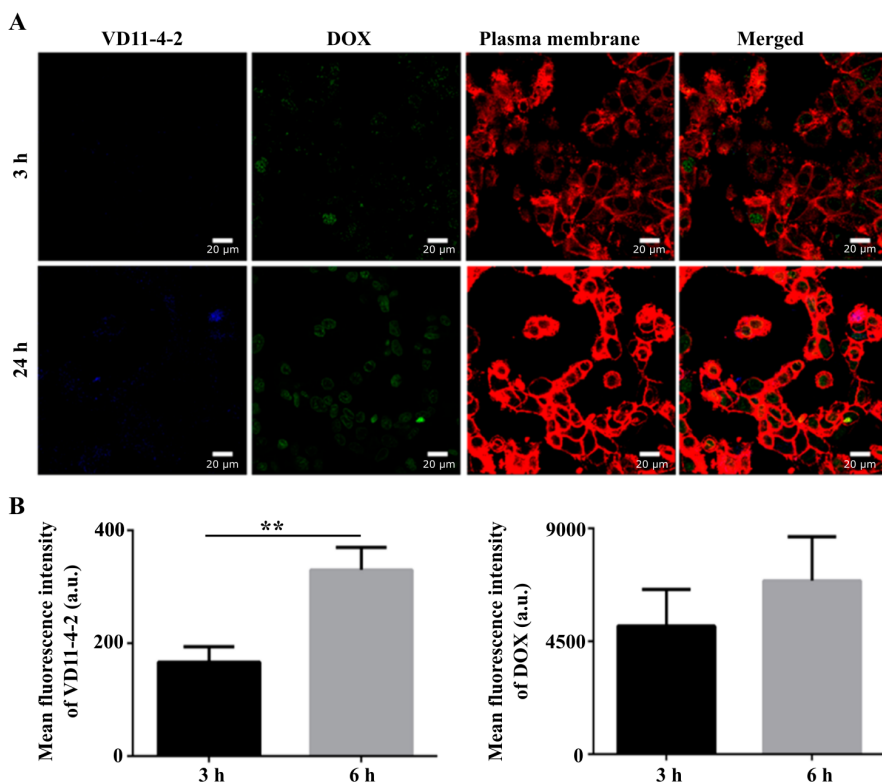


Figure 4.18: Images of MCF-7 cells incubated with DOX@VD-PSi for 3 and 24 h obtained by confocal microscopy (A). Cell membranes are stained with CellMaskTM DeepRed. Scale bar is 20 μm . Flow cytometry experiment results (B), showing VD11-4-2 (left) and DOX (right) fluorescence in cell after 3 and 6 h incubation with DOX@VD-PSi (** $p < 0.01$).

ification with fluorescent molecules, which is often needed to monitor NP distribution within the cell in other systems [138]. Application of VD11-4-2 for *in vivo* tracking would be complicated due to the strong intrinsic tissue scattering of short wavelength radiation and blue autofluorescence of the tissues [220]. Nevertheless, the possibility of tracking the payload release within the cell is highly favorable in the NS development field [221, 222]. FRET effect between anticancer drug DOX and targeting moiety VD11-4-2 enabled NS and payload tracking without additional modification steps, which makes this system applicable for various *in vitro* studies.

5. CONCLUSIONS

- CA IX selective VD11-4-2 compound preferentially accumulates in breast cancer cells under hypoxia mimicking conditions rather than normoxia *in vitro*.
- CA IX inhibitor VD11-4-2 reduces CA IX expressing breast cancer cell MDA-MB-231 and MCF-7 migration velocities at a concentration of 20 μM by at least 20% as observed after single-cell movement tracking. The same concentration of inhibitor VD11-4-2 reduces MDA-MB-231 cell movement toward chemoattractant and disturbs hourly cell velocity increment under hypoxia mimicking conditions.
- VD11-4-2, attached through polyethylene glycol to porous silicon and zinc-copper oxide nanoparticles, retains its affinity towards CA IX protein. Modification with inhibitor increases the anti-cancer activity of the nanosystems toward CA IX expressing breast cancer cells.
- Attachment of VD11-4-2 to porous silicon nanoparticles leads to a two-fold increase of doxorubicin loading capacity and results in an acidic pH-responsive drug release profile, while in the case of paclitaxel attachment of VD11-4-2 causes no significant changes to the uploading and release profiles. Uptake of the nanosystem and doxorubicin release within the cell can be monitored by the fluorescence resonance energy transfer effect, occurring between VD11-4-2 and doxorubicin, which is not hindered by pH, temperature or ionic strength.

REFERENCES

- [1] J. W. Lee, J. Ko, C. Ju, and H. K. Eltzschig, “Hypoxia signaling in human diseases and therapeutic targets,” *Experimental and Molecular Medicine*, vol. 51, no. 6, pp. 1–13, 2019.
- [2] G. L. Semenza, “Expression of hypoxia-inducible factor 1: Mechanisms and consequences,” *Biochemical Pharmacology*, vol. 59, no. 1, pp. 47–53, 2000.
- [3] S. J. Van Kuijk, A. Yaromina, R. Houben, R. Niemans, P. Lambin, and L. J. Dubois, “Prognostic significance of carbonic anhydrase IX expression in cancer patients: A meta-analysis,” *Frontiers in Oncology*, vol. 6, no. MAR, pp. 1–16, 2016.
- [4] S. Pastorekova, P. J. Ratcliffe, and J. Pastorek, “Molecular mechanisms of carbonic anhydrase IX-mediated pH regulation under hypoxia,” *BJU International, Supplement*, vol. 101, no. SUPPL.4, pp. 8–15, 2008.
- [5] Y. Lou, P. C. McDonald, A. Oloumi, S. Chia, C. Ostlund, A. Ahmadi, A. Kyle, U. Auf Dem Keller, S. Leung, D. Huntsman, B. Clarke, B. W. Sutherland, D. Waterhouse, M. Bally, C. Roskelley, C. M. Overall, A. Minchinton, F. Pacchiano, F. Carta, A. Scozzafava, N. Touisni, J. Y. Winum, C. T. Supuran, and S. Dedhar, “Targeting tumor hypoxia: Suppression of breast tumor growth and metastasis by novel carbonic anhydrase IX inhibitors,” *Cancer Research*, vol. 71, no. 9, pp. 3364–3376, 2011.
- [6] A. Nocentini and C. T. Supuran, “Carbonic anhydrase inhibitors as antitumor/antimetastatic agents: a patent review (2008–2018),” *Expert Opinion on Therapeutic Patents*, vol. 28, no. 10, pp. 729–740, 2018.
- [7] A. Janonienė and V. Petrikaite, “In Search of Advanced Tumor Diagnostics and Treatment: Achievements and Perspectives of Carbonic Anhydrase IX Targeted Delivery,” *Molecular Pharmaceutics*, vol. 17, no. 6, pp. 1800–1815, 2020.

- [8] C. T. Supuran, “Carbonic anhydrases: from biomedical applications of the inhibitors and activators to biotechnological use for CO₂ capture,” *Journal of Enzyme Inhibition and Medicinal Chemistry*, vol. 28, no. October, pp. 229–230, 2015.
- [9] C. Lomelino and R. Mckenna, “Carbonic anhydrase inhibitors: a review on the progress of patent literature (2011–2016),” *Expert Opinion on Therapeutic Patents*, vol. 26, no. 8, pp. 947–956, 2016.
- [10] V. Dudutienė, J. Matulienė, A. Smirnov, D. D. Timm, A. Zubrienė, L. Baranauskienė, V. Morkūnaitė, J. Smirnovienė, V. Michailovienė, V. Juozapaitienė, A. Mickeviciūtė, J. Kazokaitė, S. Bakšytė, A. Kasiliauskaitė, J. Jachno, J. Revuckienė, M. Kišonaitė, V. Pilipuitytė, E. Ivanauskaitė, G. Milinavičiūtė, V. Smirnovas, V. Petrikaitė, V. Kairys, V. Petrauskas, P. Norvaišas, D. Lingė, P. Gibieža, E. Čapkaukaite, A. Žakšauskas, E. Kazlauskas, E. Manakova, S. Gražulis, J. E. Ladbury, and D. Matulis, “Discovery and Characterization of Novel Selective Inhibitors of Carbonic Anhydrase IX,” *Journal of Medicinal Chemistry*, vol. 57, pp. 9435–9446, 2014.
- [11] J. Kazokaitė, S. Ames, H. M. Becker, J. W. Deitmer, and D. Matulis, “Selective inhibition of human carbonic anhydrase IX in *Xenopus* oocytes and MDA-MB-231 breast cancer cells,” *Journal of Enzyme Inhibition and Medicinal Chemistry*, vol. 31, pp. 38–44, 2016.
- [12] J. Kazokaitė, A. Aspatwar, V. Kairys, S. Parkkila, and D. Matulis, “Fluorinated benzenesulfonamide anticancer inhibitors of carbonic anhydrase IX exhibit lower toxic effects on zebrafish embryonic development than ethoxzolamide,” *Drug and Chemical Toxicology*, vol. 40, no. 3, pp. 309–319, 2017.
- [13] I. A. for Research on Cancer, *Latest global cancer data: Cancer burden rises to 19.3 million new cases and 10.0 million cancer deaths in 2020*, 2020 (accessed January 12, 2021).
- [14] R. Cagan and P. Meyer, “Rethinking cancer: Current challenges and opportunities in cancer research,” *DMM Disease Models and Mechanisms*, vol. 10, no. 4, pp. 349–352, 2017.
- [15] M. Dobbstein and U. Moll, “Targeting tumour-supportive cellular machineries in anticancer drug development,” *Nature Reviews Drug Discovery*, vol. 13, no. 3, pp. 179–196, 2014.
- [16] T. O. Olusanya, R. R. H. Ahmad, D. M. Ibegbu, J. R. Smith, and A. A. Elkordy, “Liposomal drug delivery systems and anticancer drugs,” *Molecules*, vol. 23, no. 4, pp. 1–17, 2018.

- [17] A. C. Anselmo and S. Mitragotri, “Nanoparticles in the clinic: An update,” *Bioengineering & Translational Medicine*, vol. 4, no. 3, pp. 1–16, 2019.
- [18] C. Holohan, S. Van Schaeybroeck, D. B. Longley, and P. G. Johnston, “Cancer drug resistance: An evolving paradigm,” *Nature Reviews Cancer*, vol. 13, no. 10, pp. 714–726, 2013.
- [19] D. L. Jardim, D. De Melo Gagliato, M. Nikanjam, D. A. Barkauskas, and R. Kurzrock, “Efficacy and safety of anticancer drug combinations: a meta-analysis of randomized trials with a focus on immunotherapeutics and gene-targeted compounds,” *OncoImmunology*, vol. 9, no. 1, pp. 1–12, 2020.
- [20] Y. T. Lee, Y. J. Tan, and C. E. Oon, “Molecular targeted therapy: Treating cancer with specificity,” *European Journal of Pharmacology*, vol. 834, no. January, pp. 188–196, 2018.
- [21] Y. R. Kim, J. K. Yoo, C. W. Jeong, and J. W. Choi, “Selective killing of circulating tumor cells prevents metastasis and extends survival,” *Journal of Hematology and Oncology*, vol. 11, no. 1, pp. 1–4, 2018.
- [22] E. Y. Lukianova-Hleb, Y. S. Kim, I. Belatsarkouski, A. M. Gillenwater, B. E. O’Neill, and D. O. Lapotko, “Intraoperative diagnostics and elimination of residual microtumours with plasmonic nanobubbles,” *Nature Nanotechnology*, vol. 11, no. 6, pp. 525–532, 2016.
- [23] H. Dillekås, M. S. Rogers, and O. Straume, “Are 90% of deaths from cancer caused by metastases?,” *Cancer Medicine*, vol. 8, no. 12, pp. 5574–5576, 2019.
- [24] A. Gandalovičová, D. Rosel, M. Fernandes, P. Veselý, P. Heneberg, V. Čermák, L. Petruželka, S. Kumar, V. Sanz-Moreno, and J. Brábek, “Migrastatics—Anti-metastatic and Anti-invasion Drugs: Promises and Challenges,” *Trends in Cancer*, vol. 3, no. 6, pp. 391–406, 2017.
- [25] L. Gomez-Cuadrado, N. Tracey, R. Ma, B. Qian, and V. G. Brunton, “Mouse models of metastasis: Progress and prospects,” *DMM Disease Models and Mechanisms*, vol. 10, no. 9, pp. 1061–1074, 2017.
- [26] F. Lefranc, J. Brotchi, and R. Kiss, “Possible future issues in the treatment of glioblastomas: Special emphasis on cell migration and the resistance of migrating glioblastoma cells to apoptosis,” *Journal of Clinical Oncology*, vol. 23, no. 10, pp. 2411–2422, 2005.

-
- [27] C. Roma-Rodrigues, R. Mendes, P. V. Baptista, and A. R. Fernandes, "Targeting tumor microenvironment for cancer therapy," *International Journal of Molecular Sciences*, vol. 20, no. 4, 2019.
- [28] V. Petrova, M. Annicchiarico-Petruzzelli, G. Melino, and I. Amelio, "The hypoxic tumour microenvironment," *Oncogenesis*, vol. 7, no. 1, 2018.
- [29] W. R. Wilson and M. P. Hay, "Targeting hypoxia in cancer therapy," *Nature Reviews Cancer*, vol. 11, no. 6, pp. 393–410, 2011.
- [30] P. H. Maxwell, C. W. Pugh, and P. J. Ratcliffe, "Inducible operation of the erythropoietin 3' enhancer in multiple cell lines: Evidence for a widespread oxygen-sensing mechanism," *Proceedings of the National Academy of Sciences of the United States of America*, vol. 90, no. 6, pp. 2423–2427, 1993.
- [31] C. K. Davis, S. A. Jain, O. N. Bae, A. Majid, and G. K. Rajanikant, "Hypoxia mimetic agents for ischemic stroke," *Frontiers in Cell and Developmental Biology*, vol. 6, no. January, pp. 1–12, 2019.
- [32] A. Amiri, P. U. Le, A. Moquin, G. Machkalyan, K. Petrecca, J. W. Gillard, N. Yoganathan, and D. Maysinger, "Inhibition of carbonic anhydrase IX in glioblastoma multiforme," *European Journal of Pharmacology*, vol. 109, pp. 81–92, 2016.
- [33] C. L. Chen, J. S. Chu, W. C. Su, S. C. Huang, and W. Y. Lee, "Hypoxia and metabolic phenotypes during breast carcinogenesis: Expression of HIF-1 α , GLUT1, and CAIX," *Virchows Archiv*, vol. 457, no. 1, pp. 53–61, 2010.
- [34] C. Y. Chu, Y. T. Jin, W. Zhang, J. Yu, H. P. Yang, H. Y. Wang, Z. J. Zhang, X. P. Liu, and Q. Zou, "CA IX is upregulated in CoCl₂-induced hypoxia and associated with cell invasive potential and a poor prognosis of breast cancer," *International Journal of Oncology*, vol. 48, no. 1, pp. 271–280, 2016.
- [35] E. El-Abd, C. Matta, M. Sheta, Y. El-Kerm, M. Afifi, T. Benhassine, S. Meftahi, S. Sakr, and B. Elsherbini, "Relation between Hypoxic Markers P65, P50, CAIX, and Tumor Stages in Invasive Ductal Carcinoma Subtypes," *Adv. Cancer: Res. Treat.*, vol. 2015, pp. 1–19, 2015.
- [36] L. Liu and M. C. Simon, "Regulation of transcription and translation by hypoxia," *Cancer Biology and Therapy*, vol. 3, no. 6, pp. 492–497, 2004.
- [37] A. Nocentini and C. T. Supuran, "Advances in the structural annotation of human carbonic anhydrases and impact on future drug discovery," *Expert Opinion on Drug Discovery*, vol. 14, no. 11, pp. 1175–1197, 2019.

- [38] M. Barathova, M. Takacova, T. Holotnakova, A. Gibadulinova, A. Ohradanova, M. Zatovicova, A. Hulikova, J. Kopacek, S. Parkkila, C. T. Supuran, S. Pastorekova, and J. Pastorek, "Alternative splicing variant of the hypoxia marker carbonic anhydrase IX expressed independently of hypoxia and tumour phenotype," *British Journal of Cancer*, vol. 98, no. 1, pp. 129–136, 2008.
- [39] S. Aslam and V. Gupta, "Carbonic Anhydrase Inhibitors.," in *StatPearls [Internet]*, Treasure Island (FL): StatPearls Publishing, Jan. 2021.
- [40] C. T. Supuran and J.-Y. Winum, "Carbonic anhydrase IX inhibitors in cancer therapy: an update," *Future Medicinal Chemistry*, vol. 7, pp. 1407–1414, 2015.
- [41] S. Pastorekova, J. Kopacek, and J. Pastorek, "Carbonic Anhydrase Inhibitors and the Management of Cancer," *Current Topics in Medicinal Chemistry*, vol. 7, no. 9, pp. 865–878, 2007.
- [42] A. Waheed, W. S. Sly, and E. A. Doisy, "Carbonic Anhydrase XII Functions in Health and Disease," *Gene*, vol. 623, pp. 33–40, 2017.
- [43] O. Sedlakova, E. Svastova, M. Takacova, J. Kopacek, J. Pastorek, and S. Pastorekova, "Carbonic anhydrase IX, a hypoxia-induced catalytic component of the pH regulating machinery in tumors," *Frontiers in Membrane Physiology and Membrane Biophysics*, vol. 4, pp. 1–14, 2014.
- [44] Z. Chen, L. Ai, M. Y. Mboge, C. Tu, R. McKenna, K. D. Brown, C. D. Heldermon, and S. C. Frost, "Differential expression and function of CAIX and CAXII in breast cancer: A comparison between tumorgraft models and cells," *PLoS ONE*, vol. 13, no. 7, pp. 1–25, 2018.
- [45] B. P. Mahon, M. A. Pinard, and R. McKenna, "Targeting carbonic anhydrase IX activity and expression.," *Molecules*, vol. 20, no. 2, pp. 2323–48, 2015.
- [46] P. E. Morgan, S. Pastoreková, A. K. Stuart-Tilley, S. L. Alper, and J. R. Casey, "Interactions of transmembrane carbonic anhydrase, CAIX, with bicarbonate transporters," *American Journal of Physiology - Cell Physiology*, vol. 293, no. 2, pp. 738–748, 2007.
- [47] S. Ames, S. Pastorekova, and H. M. Becker, "The proteoglycan-like domain of carbonic anhydrase IX mediates non-catalytic facilitation of lactate transport in cancer cells," *Oncotarget*, vol. 9, no. 46, pp. 27940–27957, 2018.

- [48] S. Jamali, M. Klier, S. Ames, L. Felipe Barros, R. McKenna, J. W. Deitmer, and H. M. Becker, “Hypoxia-induced carbonic anhydrase IX facilitates lactate flux in human breast cancer cells by non-catalytic function,” *Scientific Reports*, vol. 5, no. January, p. 13605, 2015.
- [49] N. Rohani, L. Hao, M. S. Alexis, B. A. Joughin, K. Krismer, M. N. Moufarrej, A. R. Soltis, D. A. Lauffenburger, M. B. Yaffe, C. B. Burge, S. N. Bhatia, and F. B. Gertler, “Acidification of tumor at stromal boundaries drives transcriptome alterations associated with aggressive phenotypes,” *Cancer Research*, vol. 79, no. 8, pp. 1952–1966, 2019.
- [50] L. Csaderova, M. Debreova, P. Radvak, M. Stano, M. Vrestiakova, J. Kopacek, S. Pastorekova, and E. Svastova, “The effect of carbonic anhydrase IX on focal contacts during cell spreading and migration,” *Frontiers in Membrane Physiology and Membrane Biophysics*, vol. 4, pp. 1–12, 2013.
- [51] E. Švastová, N. Žilka, M. Zat’ovičová, A. Gibadulinová, F. Čiampor, J. Pastorek, and S. Pastoreková, “Carbonic anhydrase IX reduces E-cadherin-mediated adhesion of MDCK cells via interaction with β -catenin,” *Experimental Cell Research*, vol. 290, no. 2, pp. 332–345, 2003.
- [52] P. Ditte, F. Dequiedt, E. Svastova, A. Hulikova, A. Ohradanova-Repic, M. Zatovicova, L. Csaderova, J. Kopacek, C. T. Supuran, S. Pastorekova, and J. Pastorek, “Phosphorylation of carbonic anhydrase IX controls its ability to mediate extracellular acidification in hypoxic tumors,” *Cancer Research*, vol. 71, no. 24, pp. 7558–7567, 2011.
- [53] T. Dorai, I. S. Sawczuk, J. Pastorek, P. H. Wiernik, and J. P. Dutcher, “The role of carbonic anhydrase IX overexpression in kidney cancer,” *European Journal of Cancer*, vol. 41, no. 18, pp. 2935–2947, 2005.
- [54] A. McIntyre, S. Patiar, S. Wigfield, J. L. Li, I. Ledaki, H. Turley, R. Leek, C. Snell, K. Gatter, W. S. Sly, R. D. Vaughan-Jones, P. Swietach, and A. L. Harris, “Carbonic anhydrase IX promotes tumor growth and necrosis in vivo and inhibition enhances anti-VEGF therapy,” *Clinical Cancer Research*, vol. 18, no. 11, pp. 3100–3111, 2012.
- [55] J. Chiche, K. Ilc, J. Laferrière, E. Trottier, F. Dayan, N. M. Mazure, M. C. Brahimi-Horn, and J. Pouyssegur, “Hypoxia-inducible carbonic anhydrase IX and XII promote tumor cell growth by counteracting acidosis through the regulation of the intracellular pH,” *Cancer Research*, vol. 69, no. 1, pp. 358–368, 2009.
- [56] M. Swayampakula, P. C. McDonald, M. Vallejo, E. Coyaud, S. C. Chafe, A. Westerback, G. Venkateswaran, J. Shankar, G. Gao, E. M. Laurent,

- Y. Lou, K. L. Bennewith, C. T. Supuran, I. R. Nabi, B. Raught, and S. Dedhar, “The interactome of metabolic enzyme carbonic anhydrase IX reveals novel roles in tumor cell migration and invadopodia/MMP14-mediated invasion,” *Oncogene*, vol. 36, no. 45, pp. 6244–6261, 2017.
- [57] M. Choschzick, E. Oosterwijk, V. Müller, L. Woelber, R. Simon, H. Moch, and P. Tennstedt, “Overexpression of carbonic anhydrase IX (CAIX) is an independent unfavorable prognostic marker in endometrioid ovarian cancer,” *Virchows Archiv*, vol. 459, no. 2, pp. 193–200, 2011.
- [58] D. J. Brennan, K. Jirstrom, Å. Kronblad, R. C. Millikan, G. Landberg, M. J. Duffy, L. Rydén, W. M. Gallagher, and S. L. O’Brien, “CA IX is an independent prognostic marker in premenopausal breast cancer patients with one to three positive lymph nodes and a putative marker of radiation resistance,” *Clinical Cancer Research*, vol. 12, no. 21, pp. 6421–6431, 2006.
- [59] M. Lie, N. M. Mazure, V. Hofman, R. E. Ammadi, C. Ortholan, C. Bonnetaud, K. Havet, N. Venissac, B. Mograbi, J. Mouroux, J. Pouysségur, and P. Hofman, “High levels of carbonic anhydrase IX in tumour tissue and plasma are biomarkers of poor prognostic in patients with non-small cell lung cancer,” *British Journal of Cancer*, vol. 102, no. 11, pp. 1627–1635, 2010.
- [60] ClinicalTrials.gov, “Ca-ix, p16, proliferative markers, and hpv in diagnosing cervical lesions in patients with abnormal cervical cells.” <https://clinicaltrials.gov/ct2/show/NCT00892866?term=CA+IX&draw=2&rank=1>, urldate = 2021-01-27.
- [61] ClinicalTrials.gov, “Serum ca9 level as biological marker of the treatment response in metastatic renal cell cancer (ca9crm).” <https://clinicaltrials.gov/ct2/show/NCT00942058?term=CA+IX&recrs=efghm&draw=2&rank=4>, urldate = 2021-01-27.
- [62] V. Müller, S. Riethdorf, B. Rack, W. Janni, P. A. Fasching, E. Solomayer, B. Aktas, S. Kasimir-Bauer, J. Zeitz, K. Pantel, and T. Fehm, “Prospective evaluation of serum tissue inhibitor of metalloproteinase 1 and carbonic anhydrase IX in correlation to circulating tumor cells in patients with metastatic breast cancer,” *Breast Cancer Research*, vol. 13, no. 4, 2011.
- [63] ClinicalTrials.gov, “89zr-tlx250 for pet/ct imaging of ccrcc- zircon study (89zr-tlx250).” <https://clinicaltrials.gov/ct2/show/NCT03849118?term=CA+IX&recrs=a&draw=2&rank=7>, urldate = 2021-01-27.

- [64] ClinicalTrials.gov, “Zirconium-89-girentuximab pet/ct imaging in renal cell carcinoma.” <https://clinicaltrials.gov/ct2/show/NCT02883153?term=CA+IX&recrs=efghm&draw=3&rank=14>, urldate = 2021-01-27.
- [65] ClinicalTrials.gov, “Evaluate the utility of 124i-cg250 for the early detection of response to therapy in patients with metastatic renal cell carcinoma.” <https://clinicaltrials.gov/ct2/show/NCT01582204?term=CA+IX&recrs=d&draw=2&rank=2>, urldate = 2021-01-27.
- [66] M. M. Kijanka, A. S. A. V. Brussel, E. V. D. Wall, W. P. T. M. Mali, P. J. V. Diest, P. M. P. V. Bergen en Henegouwen, and S. Oliveira, “Optical imaging of pre-invasive breast cancer with a combination of VHHs targeting CAIX and HER2 increases contrast and facilitates tumour characterization,” *EJNMMI Research*, vol. 6, pp. 1–13, 2016.
- [67] A. S. A. V. Brussel, A. Adams, S. Oliveira, B. Dorresteyn, M. E. Khat-tabi, J. F. Vermeulen, E. V. D. Wall, W. P. T. M. Mali, P. W. B. Derksen, P. J. V. Diest, and P. M. P. V. Bergen en Henegouwen, “Hypoxia-Targeting Fluorescent Nanobodies for Optical Molecular Imaging of Pre-Invasive Breast Cancer,” *Molecular Imaging and Biology*, vol. 18, pp. 535–544, 2016.
- [68] N. K. Tafreshi, M. M. Bui, K. Bishop, M. C. Lloyd, S. A. Enkemann, A. S. Lopez, D. Abrahams, B. W. Carter, J. Vagner, S. R. Grobmyer, R. J. Gillies, and D. L. Morse, “Noninvasive Detection of Breast Cancer Lymph Node Metastasis Using Carbonic Anhydrases IX and XII Targeted Imaging Probes,” *Clinical Cancer Research*, vol. 18, pp. 207–219, 2012.
- [69] C. H. Lamers, S. Sleijfer, S. Van Steenberghe, P. Van Elzaker, B. Van Krimpen, C. Groot, A. Vulto, M. Den Bakker, E. Oosterwijk, R. Debets, and J. W. Gratama, “Treatment of metastatic renal cell carcinoma with CAIX CAR-engineered T cells: Clinical evaluation and management of on-target toxicity,” *Molecular Therapy*, vol. 21, no. 4, pp. 904–912, 2013.
- [70] ClinicalTrials.gov, “Inhibition of carbonic anhydrase in combination with platinum and etoposide-based radiochemotherapy in patients with localized small cell lung cancer (icar).” <https://clinicaltrials.gov/ct2/show/NCT03467360?term=CA+IX&recrs=a&draw=2&rank=9>, urldate = 2021-01-29.
- [71] ClinicalTrials.gov, “A study of slc-0111 and gemcitabine for metastatic pancreatic ductal cancer in subjects positive for caix (slc-0111-

- 17-01)." <https://clinicaltrials.gov/ct2/show/NCT03450018?term=CA+IX&recrs=a&draw=2&rank=2>, urldate = 2021-01-29.
- [72] E.-M. E. Hedlund, Paul C. McDonald, Oksana Nemirovsky, Shannon Awrey, Lasse D.E. Jensen, and Shoukat Dedhar, "Harnessing Induced Essentiality: Targeting Carbonic Anhydrase IX and Angiogenesis Reduces Lung Metastasis of Triple Negative Breast Cancer Xenografts," *Cancers*, vol. 11, no. 7, p. 1002, 2019.
- [73] M. Fragai, G. Comito, L. Di Cesare Mannelli, R. Galdani, V. Calderone, A. Louka, B. Richichi, O. Francesconi, A. Angeli, A. Nocentini, P. Grateri, P. Chiarugi, C. Ghelardini, F. Tadini-Buoninsegni, C. T. Supuran, and C. Nativi, "Lipoyl-Homotaurine Derivative (ADM-12) Reverts Oxaliplatin-Induced Neuropathy and Reduces Cancer Cells Malignancy by Inhibiting Carbonic Anhydrase IX (CAIX)," *Journal of Medicinal Chemistry*, vol. 60, no. 21, pp. 9003–9011, 2017.
- [74] K. Chamie, N. M. Donin, P. Klöpfer, P. Bevan, B. Fall, O. Wilhelm, S. Störkel, J. Said, M. Gambla, R. E. Hawkins, G. Jankilevich, A. Kapoor, E. Kopyltsov, M. Staehler, K. Taari, A. J. Wainstein, A. J. Pantuck, and A. S. Belldegrun, "Adjuvant weekly girentuximab following nephrectomy for high-risk renal cell carcinoma: The ARISER randomized clinical trial," *JAMA Oncology*, vol. 3, no. 7, pp. 913–920, 2017.
- [75] W. R. Chegwiddden and I. M. Spencer, "Sulphonamide Inhibitors of Carbonic Anhydrase Inhibit the Growth of Human Lymphoma Cells in Culture," *Inflammopharmacology*, vol. 3, pp. 231–239, 1995.
- [76] B. A. Teicher, S. D. Liu, H. S. A, W. R. Herman T SChegwiddden, and I. M. Spencer, "A carbonic anhydrase inhibitor as a potential modulator of cancer therapies," *Inflammopharmacology*, vol. 13, pp. 1549–56, 1993.
- [77] C. T. Supuran, F. Briganti, S. Tilli, W. R. Chegwiddden, and A. Scozzafava, "Carbonic anhydrase inhibitors: Sulfonamides as antitumor agents?," *Bioorganic and Medicinal Chemistry*, vol. 9, no. 3, pp. 703–714, 2001.
- [78] J. Kazokaitė, A. Aspatwar, S. Parkkila, and D. Matulis, "An update on anticancer drug development and delivery targeting carbonic anhydrase IX," *PeerJ*, vol. 5, p. e4068, 2017.
- [79] D. P. Logsdon, M. Grimard, M. Luo, S. Shahda, Y. Jiang, Y. Tong, Z. Yu, N. Zyromski, E. Schipani, F. Carta, C. T. Supuran, M. Korc, M. Ivan, M. R. Kelley, and M. L. Fishel, "Regulation of HIF1 α under hypoxia by APE1/Ref-1 impacts CA9 expression: Dual targeting in patient-derived

- 3D pancreatic cancer models,” *Molecular Cancer Therapeutics*, vol. 15, no. 11, pp. 2722–2732, 2016.
- [80] D. P. Logsdon, F. Shah, F. Carta, C. T. Supuran, M. Kamocka, M. H. Jacobsen, G. E. Sandusky, M. R. Kelley, and M. L. Fishel, “Blocking HIF signaling via novel inhibitors of CA9 and APE1/Ref-1 dramatically affects pancreatic cancer cell survival,” *Scientific Reports*, vol. 8, no. 1, pp. 1–14, 2018.
- [81] P. C. McDonald, S. C. Chafe, W. S. Brown, S. Saberi, M. Swayampakula, G. Venkateswaran, O. Nemirovsky, J. A. Gillespie, J. M. Karasinska, S. E. Kalloger, C. T. Supuran, D. F. Schaeffer, A. Bashashati, S. P. Shah, J. T. Topham, D. T. Yapp, J. Li, D. J. Renouf, B. Z. Stanger, and S. Dedhar, “Regulation of pH by Carbonic Anhydrase 9 Mediates Survival of Pancreatic Cancer Cells With Activated KRAS in Response to Hypoxia,” *Gastroenterology*, vol. 157, no. 3, pp. 823–837, 2019.
- [82] D. Ramchandani, D. Unruh, C. S. Lewis, V. Y. Bogdanov, and G. F. Weber, “Activation of Carbonic Anhydrase IX by Alternatively Spliced Tissue Factor Under Late-Stage Tumor Conditions,” *Laboratory Investigation*, vol. 96, no. 12, pp. 1234–1245, 2016.
- [83] E. Andreucci, J. Ruzzolini, S. Peppicelli, F. Bianchini, A. Laurenzana, F. Carta, C. T. Supuran, and L. Calorini, “The carbonic anhydrase IX inhibitor SLC-0111 sensitises cancer cells to conventional chemotherapy,” *Journal of Enzyme Inhibition and Medicinal Chemistry*, vol. 34, no. 1, pp. 117–123, 2019.
- [84] F. E. Lock, P. C. McDonald, Y. Lou, I. Serrano, S. C. Chafe, C. Ostlund, S. Aparicio, J. Y. Winum, C. T. Supuran, and S. Dedhar, “Targeting carbonic anhydrase IX depletes breast cancer stem cells within the hypoxic niche,” *Oncogene*, vol. 32, no. 44, pp. 5210–5219, 2013.
- [85] A. Nocentini, E. Trallori, S. Singh, C. L. Lomelino, G. Bartolucci, L. Di Cesare Mannelli, C. Ghelardini, R. McKenna, P. Gratteri, and C. T. Supuran, “4-Hydroxy-3-nitro-5-ureido-benzenesulfonamides Selectively Target the Tumor-Associated Carbonic Anhydrase Isoforms IX and XII Showing Hypoxia-Enhanced Antiproliferative Profiles,” *Journal of Medicinal Chemistry*, vol. 61, no. 23, pp. 10860–10874, 2018.
- [86] S. Faes, A. Planche, E. Uldry, T. Santoro, C. Pythoud, J.-c. Stehle, J. Horlbeck, I. Letovanec, N. Riggi, N. Demartines, and O. Dormond, “Targeting carbonic anhydrase IX improves the anti-cancer efficacy of mTOR inhibitors,” *Oncotarget*, vol. 7, no. 24, 2016.

- [87] L. Dubois, S. Peeters, N. G. Lieuwes, N. Geusens, A. Thiry, S. Wigfield, F. Carta, A. McIntyre, A. Scozzafava, J. M. Dogné, C. T. Supuran, A. L. Harris, B. Masereel, and P. Lambin, "Specific inhibition of carbonic anhydrase IX activity enhances the in vivo therapeutic effect of tumor irradiation," *Radiotherapy and Oncology*, vol. 99, no. 3, pp. 424–431, 2011.
- [88] L. Dubois, S. G. J. A. Peeters, S. J. A. V. Kuijk, A. Yaromina, N. G. Lieuwes, R. Saraya, R. Biemans, M. Rami, N. K. Parvathaneni, D. Vullo, M. Vooijs, C. T. Supuran, J.-Y. Winum, and P. Lambin, "Targeting carbonic anhydrase IX by nitroimidazole based sulfamides enhances the therapeutic effect of tumor irradiation : A new concept of dual targeting drugs," *Radiotherapy and Oncology*, vol. 108, no. 3, pp. 523–528, 2013.
- [89] J. Y. Winum, F. Carta, C. Ward, P. Mullen, D. Harrison, S. P. Langdon, A. Cecchi, A. Scozzafava, I. Kunkler, and C. T. Supuran, "Ureido-substituted sulfamates show potent carbonic anhydrase IX inhibitory and antiproliferative activities against breast cancer cell lines," *Bioorganic and Medicinal Chemistry Letters*, vol. 22, no. 14, pp. 4681–4685, 2012.
- [90] C. Federici, L. Lugini, M. L. Marino, F. Carta, E. Iessi, T. Azzarito, C. T. Supuran, and S. Fais, "Lansoprazole and carbonic anhydrase IX inhibitors synergize against human melanoma cells," *Journal of Enzyme Inhibition and Medicinal Chemistry*, vol. 31, pp. 119–125, 2016.
- [91] N. Touisni, A. Maresca, P. C. McDonald, Y. Lou, A. Scozzafava, S. Dedhar, J. Y. Winum, and C. T. Supuran, "Glycosyl coumarin carbonic anhydrase IX and XII inhibitors strongly attenuate the growth of primary breast tumors," *Journal of Medicinal Chemistry*, vol. 54, no. 24, pp. 8271–8277, 2011.
- [92] C. H. Muselaers, M. Rijpkema, D. L. Bos, J. F. Langenhuijsen, W. J. Oyen, P. F. Mulders, E. Oosterwijk, and O. C. Boerman, "Radionuclide and Fluorescence Imaging of Clear Cell Renal Cell Carcinoma Using Dual Labeled Anti-Carbonic Anhydrase IX Antibody G250," *Journal of Urology*, vol. 194, pp. 532–538, 2015.
- [93] J. C. Oosterwijk-Wakka, O. C. Boerman, P. F. A. Mulders, and E. Oosterwijk, "Application of Monoclonal Antibody G250 Recognizing Carbonic Anhydrase IX in Renal Cell Carcinoma," *International Journal of Molecular Sciences*, vol. 14, pp. 11402–11423, 2013.
- [94] M. Zatovicova, L. Jelenska, A. Hulikova, L. Csaderova, Z. Ditte, P. Ditte, T. Goliasova, J. Pastorek, and S. Pastorekova, "Carbonic Anhydrase IX as an Anticancer Therapy Target: Preclinical Evaluation of Internalizing

- Monoclonal Antibody Directed to Catalytic Domain,” *Current Pharmaceutical Design*, vol. 16, no. 29, pp. 3255–3263, 2010.
- [95] J. Kazokaitė, R. Niemans, V. Dudutienė, H. M. Becker, J. Leitans, A. Zubrienė, L. Baranauskienė, G. Gondi, R. Zeidler, J. Matulienė, K. Tars, A. Yaromina, P. Lambin, L. J. Dubois, and D. Matulis, “Novel fluorinated carbonic anhydrase IX inhibitors reduce hypoxia-induced acidification and clonogenic survival of cancer cells,” *Oncotarget*, vol. 9, no. 42, pp. 26800–26816, 2018.
- [96] C. Decaestecker, O. Debeir, P. Van Ham, and R. Kiss, “Can anti-migratory drugs be screened in vitro? A review of 2D and 3D assays for the quantitative analysis of cell migration,” *Medicinal Research Reviews*, vol. 27, no. 2, pp. 149–176, 2007.
- [97] M. B. Chen, J. A. Whisler, J. S. Jeon, and R. D. Kamma, “Mechanisms of tumor cell extravasation in an in vitro microvascular network platform Michelle,” *Integr Biol (Camb)*, vol. 5, no. 10, pp. 1262–1271, 2013.
- [98] H.-J. Shin, S. B. Rho, D. C. Jung, I.-O. Han, E.-S. Oh, and J.-Y. Kim, “Carbonic anhydrase IX (CA9) modulates tumor-associated cell migration and invasion.,” *Journal of cell science*, vol. 124, pp. 1077–1087, 2011.
- [99] E. Svastova and S. Pastorekova, “Carbonic anhydrase IX: A hypoxia-controlled "catalyst" of cell migration,” *Cell Adhesion and Migration*, vol. 7, no. 2, pp. 226–231, 2013.
- [100] E. Svastova, W. Witariski, L. Csaderova, I. Kosik, L. Skvarkova, A. Hulikova, M. Zatovicova, M. Barathova, J. Kopacek, J. Pastorek, and S. Pastorekova, “Carbonic anhydrase IX interacts with bicarbonate transporters in lamellipodia and increases cell migration via its catalytic domain,” *Journal of Biological Chemistry*, vol. 287, no. 5, pp. 3392–3402, 2012.
- [101] S. Pastorekova and R. J. Gillies, “The role of carbonic anhydrase IX in cancer development: links to hypoxia, acidosis, and beyond,” *Cancer and Metastasis Reviews*, vol. 38, no. 1-2, pp. 65–77, 2019.
- [102] S. C. Chafe, Y. Lou, J. Sceneay, M. Vallejo, M. J. Hamilton, P. C. McDonald, K. L. Bennewith, A. Möller, and S. Dedhar, “Carbonic anhydrase IX promotes myeloid-derived suppressor cell mobilization and establishment of a metastatic niche by stimulating G-CSF production,” *Cancer Research*, vol. 75, no. 6, pp. 996–1008, 2015.
- [103] F. Pacchiano, F. Carta, P. C. McDonald, Y. Lou, D. Vullo, A. Scozzafava, S. Dedhar, and C. T. Supuran, “Ureido-substituted benzenesulfonamides

- potently inhibit carbonic anhydrase IX and show antimetastatic activity in a model of breast cancer metastasis,” *Journal of Medicinal Chemistry*, vol. 54, no. 6, pp. 1896–1902, 2011.
- [104] M. E. Katt, A. L. Placone, A. D. Wong, Z. S. Xu, and P. C. Searson, “In vitro tumor models: Advantages, disadvantages, variables, and selecting the right platform,” *Frontiers in Bioengineering and Biotechnology*, vol. 4, no. FEB, 2016.
- [105] A. Güttler, K. Theuerkorn, A. Riemann, H. Wichmann, J. Kessler, O. Thews, M. Bache, and D. Vordermark, “Cellular and radiobiological effects of carbonic anhydrase IX in human breast cancer cells,” *Oncology Reports*, vol. 41, no. 4, pp. 2585–2594, 2019.
- [106] R. G. Gieling, M. Babur, L. Mamnani, N. Burrows, B. A. Telfer, F. Carta, J. Y. Winum, A. Scozzafava, C. T. Supuran, and K. J. Williams, “Antimetastatic effect of sulfamate carbonic anhydrase IX inhibitors in breast carcinoma xenografts,” *Journal of Medicinal Chemistry*, vol. 55, no. 11, pp. 5591–5600, 2012.
- [107] C. Ward, J. Meehan, P. Mullen, C. Supuran, J. Michael Dixon, J. S. Thomas, J. Y. Winum, P. Lambin, L. Dubois, N. K. Pavathaneni, E. J. Jarman, L. Renshaw, I. H. Um, C. Kay, D. J. Harrison, I. H. Kunkler, and S. P. Langdon, “Evaluation of carbonic anhydrase IX as a therapeutic target for inhibition of breast cancer invasion and metastasis using a series of in vitro breast cancer models,” *Oncotarget*, vol. 6, no. 28, pp. 24856–24870, 2015.
- [108] F. Kai, A. P. Drain, and V. M. Weaver, “The extracellular matrix modulates the metastatic journey,” *Developmental Cell*, vol. 49, no. 3, pp. 332–346, 2019.
- [109] W. Jin, E. T. Shah, C. J. Penington, S. W. McCue, P. K. Maini, and M. J. Simpson, “Logistic Proliferation of Cells in Scratch Assays is Delayed,” *Bulletin of Mathematical Biology*, vol. 79, no. 5, pp. 1028–1050, 2017.
- [110] K. I. Hulkower and R. L. Herber, “Cell migration and invasion assays as tools for drug discovery,” *Pharmaceutics*, vol. 3, pp. 107–24, Jan. 2011.
- [111] V. Shah, O. Taratula, O. B. Garbuzenko, O. R. Taratula, L. Rodriguez-Rodriguez, and T. Minko, “Targeted nanomedicine for suppression of CD44 and simultaneous cell death induction in ovarian cancer: An optimal delivery of siRNA and anticancer drug,” *Clinical Cancer Research*, vol. 19, no. 22, pp. 6193–6204, 2013.

- [112] C. Shi, X. Guo, Q. Qu, Z. Tang, Y. Wang, and S. Zhou, "Actively targeted delivery of anticancer drug to tumor cells by redox-responsive star-shaped micelles," *Biomaterials*, vol. 35, no. 30, pp. 8711–8722, 2014.
- [113] A. R. Mohammed, N. Weston, A. G. Coombes, M. Fitzgerald, and Y. Perrie, "Liposome formulation of poorly water soluble drugs: Optimisation of drug loading and ESEM analysis of stability," *International Journal of Pharmaceutics*, vol. 285, no. 1-2, pp. 23–34, 2004.
- [114] R. Huang, S. Harmsen, J. M. Samii, H. Karabeber, K. L. Pitter, E. C. Holland, and M. F. Kircher, "High precision imaging of microscopic spread of glioblastoma with a targeted ultrasensitive SERRS molecular imaging probe," *Theranostics*, vol. 6, no. 8, pp. 1075–1084, 2016.
- [115] H. Zhou, W. Qian, F. M. Uckun, L. Wang, Y. A. Wang, D. Kooby, Q. Yu, M. Lipowska, C. A. Staley, H. Mao, and L. Yang, "IGF1 Receptor Targeted Theranostic Nanoparticles for Targeted and Image-Guided Therapy of Pancreatic Cancer," *ACS Nano*, vol. 9, no. 8, pp. 7976–7991, 2015.
- [116] S. Hossen, M. K. Hossain, M. K. Basher, M. N. H. Mia, M. T. Rahman, and M. J. Uddin, "Smart nanocarrier-based drug delivery systems for cancer therapy and toxicity studies : A review," *Journal of Advanced Research*, vol. 15, pp. 1–18, 2018.
- [117] J. W. Nichols and Y. H. Bae, "EPR: Evidence and fallacy," *Journal of Controlled Release*, vol. 190, pp. 451–464, 2014.
- [118] J. Shi, P. W. Kantoff, R. Wooster, and O. C. Farokhzad, "Cancer nanomedicine: progress, challenges and opportunities," *Nature Reviews Cancer*, vol. 17, no. 1, pp. 20–37, 2017.
- [119] N. Muhamad, T. Plengsuriyakarn, and K. Na-Bangchang, "Application of active targeting nanoparticle delivery system for chemotherapeutic drugs and traditional/herbal medicines in cancer therapy: A systematic review," *International Journal of Nanomedicine*, vol. 13, pp. 3921–3935, 2018.
- [120] S. Cazzamalli, A. D. Corso, and D. Neri, "Targeted Delivery of Cytotoxic Drugs: Challenges, Opportunities and New Developments," *CHIMIA International Journal for Chemistry*, vol. 71, no. 10, pp. 712–715, 2017.
- [121] Q. He, J. Chen, J. Yan, S. Cai, H. Xiong, Y. Liu, D. Peng, M. Mo, and Z. Liu, "Tumor microenvironment responsive drug delivery systems," *Asian Journal of Pharmaceutical Sciences*, vol. 15, no. 4, pp. 416–448, 2020.

- [122] Q. Jin, Y. Deng, X. Chen, and J. Ji, "Rational Design of Cancer Nanomedicine for Simultaneous Stealth Surface and Enhanced Cellular Uptake," *ACS Nano*, vol. 13, no. 2, pp. 954–977, 2019.
- [123] A. E. Nel, L. Mädler, D. Velegol, T. Xia, E. M. V. Hoek, P. Somasundaran, F. Klaessig, V. Castranova, and M. Thompson, "Understanding biophysicochemical interactions at the nano–bio interface," *Nature Materials*, vol. 8, no. 7, pp. 543–557, 2009.
- [124] B. Pelaz, P. Del Pino, P. Maffre, R. Hartmann, M. Gallego, S. Rivera-Fernández, J. M. De La Fuente, G. U. Nienhaus, and W. J. Parak, "Surface Functionalization of Nanoparticles with Polyethylene Glycol: Effects on Protein Adsorption and Cellular Uptake," *ACS Nano*, vol. 9, no. 7, pp. 6996–7008, 2015.
- [125] Y. Wang, M. S. Shim, N. S. Levinson, H.-W. Sung, and Y. Xia, "Stimuli-Responsive Materials for Controlled Release of Theranostic Agents," *Advanced Functional Materials*, vol. 24, no. 27, pp. 4206–4220, 2014.
- [126] G. Bozzuto and A. Molinari, "Liposomes as nanomedical devices," *International Journal of Nanomedicine*, pp. 975–999, 2015.
- [127] M. Shinkai, B. Le, H. Honda, K. Yoshikawa, K. Shimizu, S. Saga, T. Wakabayashi, J. Yoshida, and T. Kobayashi, "Targeting Hyperthermia for Renal Cell Carcinoma Using Human MN Antigen-specific Magnetoliposomes," *Japanese Journal of Cancer Research*, vol. 92, no. 10, pp. 1138–1145, 2001.
- [128] B. C. K. Wong, H. Zhang, L. Qin, H. Chen, C. Fang, A. Lu, and Z. Yang, "Carbonic anhydrase IX-directed immunoliposomes for targeted drug delivery to human lung cancer cells in vitro," *Drug Design, Development and Therapy*, vol. 8, pp. 993–1001, 2014.
- [129] C. Lin, B. C. K. Wong, H. Chen, Z. Bian, G. Zhang, X. Zhang, M. Kashif Riaz, D. Tyagi, G. Lin, Y. Zhang, J. Wang, A. Lu, and Z. Yang, "Pulmonary delivery of triptolide-loaded liposomes decorated with anti-carbonic anhydrase IX antibody for lung cancer therapy," *Scientific Reports*, vol. 7, no. 1, pp. 1–12, 2017.
- [130] H. O. Alsaab, S. Sau, R. M. Alzhrani, V. T. Cheriyan, L. A. Polin, U. Vaishampayan, A. K. Rishi, and A. K. Iyer, "Tumor hypoxia directed multimodal nanotherapy for overcoming drug resistance in renal cell carcinoma and reprogramming macrophages," *Biomaterials*, vol. 183, pp. 280–294, 2018.

- [131] F. Liu, J. Mu, and B. Xing, “Recent Advances on the Development of Pharmacotherapeutic Agents on the Basis of Human Serum Albumin,” *Current Pharmaceutical Design*, vol. 21, no. 14, pp. 1866–1888, 2015.
- [132] K. Tatiparti, S. Sau, K. A. Gawde, and A. K. Iyer, “Copper-free ‘click’ chemistry-based synthesis and characterization of carbonic anhydrase-IX anchored albumin-paclitaxel nanoparticles for targeting tumor hypoxia,” *International Journal of Molecular Sciences*, vol. 19, no. 3, p. 838, 2018.
- [133] K. Tatiparti, M. A. Rauf, S. Sau, and A. K. Iyer, “A biomimetic drug delivery system targeting tumor hypoxia in triple-negative breast cancers,” *Applied Sciences (Switzerland)*, vol. 10, no. 3, 2020.
- [134] W. Zhu, Y. Liu, Z. Yang, L. Zhang, L. Xiao, P. Liu, J. Wang, C. Yi, Z. Xu, and J. Ren, “Albumin/sulfonamide stabilized iron porphyrin metal organic framework nanocomposites: Targeting tumor hypoxia by carbonic anhydrase IX inhibition and: T1- T2dual mode MRI guided photodynamic/photothermal therapy,” *Journal of Materials Chemistry B*, vol. 6, no. 2, pp. 265–276, 2018.
- [135] S. P. Hadipour Moghaddam, R. Mohammadpour, and H. Ghandehari, “In vitro and in vivo evaluation of degradation, toxicity, biodistribution, and clearance of silica nanoparticles as a function of size, porosity, density, and composition,” *Journal of Controlled Release*, vol. 311-312, no. May, pp. 1–15, 2019.
- [136] J.-H. Park, L. Gu, G. von Maltzahn, E. Ruoslahti, S. N. Bhatia, and M. J. Sailor, “Biodegradable luminescent porous silicon nanoparticles for in vivo applications,” *Nature materials*, vol. 8, no. 4, pp. 331–6, 2009.
- [137] V. Tokárová, A. Pittermannová, V. Král, P. Řezáčová, and F. Štěpánek, “Feasibility and constraints of particle targeting using the antigen-antibody interaction,” *Nanoscale*, vol. 5, no. 23, pp. 11490–11498, 2013.
- [138] D. Lizoňová, M. Majerská, V. Král, M. Pechar, R. Pola, M. Kovář, and F. Štěpánek, “Antibody-pHPMA functionalised fluorescent silica nanoparticles for colorectal carcinoma targeting,” *RSC Advances*, vol. 8, no. 39, pp. 21679–21689, 2018.
- [139] M. Chen, J. Hu, L. Wang, Y. Li, C. Zhu, C. Chen, M. Shi, Z. Ju, X. Cao, and Z. Zhang, “Targeted and redox-responsive drug delivery systems based on carbonic anhydrase IX-decorated mesoporous silica nanoparticles for cancer therapy,” *Scientific Reports*, vol. 10, no. 1, pp. 1–12, 2020.

- [140] Y. Ding, Z. Jiang, K. Saha, C. S. Kim, S. T. Kim, R. F. Landis, and V. M. Rotello, "Gold nanoparticles for nucleic acid delivery," *Molecular Therapy*, vol. 22, no. 6, pp. 1075–1083, 2014.
- [141] J. B. Vines, J. H. Yoon, N. E. Ryu, D. J. Lim, and H. Park, "Gold nanoparticles for photothermal cancer therapy," *Frontiers in Chemistry*, vol. 7, no. APR, pp. 1–16, 2019.
- [142] W. Li and X. Chen, "Gold nanoparticles for photoacoustic imaging," *Nanomedicine*, vol. 10, no. 2, pp. 299–320, 2015.
- [143] Y. P. Jia, B. Y. Ma, X. W. Wei, and Z. Y. Qian, "The in vitro and in vivo toxicity of gold nanoparticles," *Chinese Chemical Letters*, vol. 28, no. 4, pp. 691–702, 2017.
- [144] E. M. Higbee-Dempsey, A. Amirshaghghi, M. J. Case, M. Bouché, J. Kim, D. P. Cormode, and A. Tsourkas, "Biodegradable gold nanoclusters with improved excretion due to ph-triggered hydrophobic-to-hydrophilic transition," *Journal of the American Chemical Society*, vol. 142, no. 17, pp. 7783–7794, 2020.
- [145] A. M. Shabana, U. K. Mondal, M. R. Alam, T. Spoon, C. A. Ross, M. Madesh, C. T. Supuran, and M. A. Ilies, "PH-Sensitive Multiligand Gold Nanoplatfom Targeting Carbonic Anhydrase IX Enhances the Delivery of Doxorubicin to Hypoxic Tumor Spheroids and Overcomes the Hypoxia-Induced Chemoresistance," *ACS Applied Materials and Interfaces*, vol. 10, no. 21, pp. 17792–17808, 2018.
- [146] M. Stiti, A. Cecchi, M. Rami, M. Abdaoui, V. Barragan-Montero, A. Scozzafava, Y. Guari, J.-Y. Winum, and C. T. Supuran, "Carbonic Anhydrase Inhibitor Coated Gold Nanoparticles Selectively Inhibit the Tumor-Associated Isoform IX over the Cytosolic Isozymes I and II," *JACS*, vol. 130, pp. 16130–16131, 2008.
- [147] F. Bellissima, F. Carta, A. Innocenti, A. Scozzafava, P. Baglioni, C. T. Supuran, and D. Berti, "Structural modulation of the biological activity of gold nanoparticles functionalized with a carbonic anhydrase inhibitor," *European Physical Journal E*, vol. 36, no. 48, pp. 1–13, 2013.
- [148] F. Ratto, E. Witort, F. Tatini, S. Centi, L. Lazzeri, F. Carta, M. Lulli, D. Vullo, F. Fusi, C. T. Supuran, A. Scozzafava, S. Capaccioli, and R. Pini, "Plasmonic Particles that Hit Hypoxic Cells," *Advanced Functional Materials*, vol. 25, pp. 316–323, 2015.
- [149] Y. Chen, X. Bian, M. Aliru, A. A. Deorukhkar, O. Ekpenyong, S. Liang, J. John, J. Ma, X. Gao, J. Schwartz, P. Singh, Y. Ye, S. Krishnan,

- and H. Xie, "Hypoxia-targeted gold nanorods for cancer photothermal therapy," *Oncotarget*, vol. 9, no. 41, pp. 26556–26571, 2018.
- [150] X. H. Peng, X. Qian, H. Mao, A. Y. Wang, Z. G. Chen, S. Nie, and D. M. Shin, "Targeted magnetic iron oxide nanoparticles for tumor imaging and therapy," *International Journal of Nanomedicine*, vol. 3, no. 3, pp. 311–321, 2008.
- [151] Y. N. Chang, M. Zhang, L. Xia, J. Zhang, and G. Xing, "The toxic effects and mechanisms of CuO and ZnO nanoparticles," *Materials*, vol. 5, no. 12, pp. 2850–2871, 2012.
- [152] S. M. Dizaj, F. Lotfipour, M. Barzegar-Jalali, M. H. Zarrintan, and K. Adibkia, "Antimicrobial activity of the metals and metal oxide nanoparticles," *Materials Science and Engineering C*, vol. 44, pp. 278–284, 2014.
- [153] E. Malka, I. Perelshtein, A. Lipovsky, Y. Shalom, L. Naparstek, N. Perkas, T. Patick, R. Lubart, Y. Nitzan, E. Banin, and A. Gedanken, "Eradication of multi-drug resistant bacteria by a novel Zn-doped CuO nanocomposite," *Small*, vol. 9, no. 23, pp. 4069–4076, 2013.
- [154] N. Wu, C. Zhang, C. Wang, L. Song, W. Yao, A. Gedanken, X. Lin, and D. Shi, "Zinc-doped copper oxide nanocomposites reverse temozolomide resistance in glioblastoma by inhibiting AKT and ERK1/2," *Nanomedicine*, vol. 13, no. 11, pp. 1303–1318, 2018.
- [155] I. Khmara, M. Koneracka, M. Kubovcikova, V. Zavisova, I. Antal, K. Csach, P. Kopcansky, I. Vidlickova, L. Csaderova, S. Pastorekova, and M. Zatovicova, "Preparation of poly-L-lysine functionalized magnetic nanoparticles and their influence on viability of cancer cells," *Journal of Magnetism and Magnetic Materials*, vol. 427, pp. 114–121, 2017.
- [156] W. Chen, Y. Han, Yu'eQian, J. Tang, H. Hu, and Y. Shen, "Preparation and Imaging Study of Tumor-targeting MRI Contrast Agent Based on Fe₃O₄ Nanoparticles," *Chemistry Letters*, vol. 44, no. 12, pp. 1771–1773, 2015.
- [157] D. Stravinskiene, A. Imbrasaitė, V. Petrikaite, D. Matulis, J. Matulienė, and A. Zvirbliene, "New monoclonal antibodies for a selective detection of membrane-associated and soluble forms of carbonic anhydrase ix in human cell lines and biological samples," *Biomolecules*, vol. 9, no. 8, pp. 1–23, 2019.
- [158] H. Zhang, D. Liu, L. Wang, L. Zehua, R. Wu, A. Janoniene, M. Ma, G. Pan, L. Baranauskienė, L. Zhang, W. Cui, V. Petrikaite, D. Matulis, H. Zhao, J. Pan, and H. A. Santos, "Microfluidic Encapsulation of

- Prickly Zinc-doped Copper Oxide Nanoparticles with VD1142 Modified Spermine Acetalated Dextran for Efficient Cancer Therapy,” *Advanced Healthcare Materials*, vol. 6, no. 11, p. 1601406, 2017.
- [159] D. Matulis, J. K. Kranz, F. R. Salemme, and M. J. Todd, “Thermodynamic stability of carbonic anhydrase: Measurements of binding affinity and stoichiometry using thermofluor,” *Biochemistry*, vol. 44, no. 13, pp. 5258–5266, 2005.
- [160] M. Hilvo, L. Baranauskiene, A. M. Salzano, A. Scaloni, D. Matulis, A. Innocenti, A. Scozzafava, S. M. Monti, A. Di Fiore, G. De Simone, M. Lindfors, J. Jänis, J. Valjakka, S. Pastoreková, J. Pastorek, M. S. Kulomaa, H. R. Nordlund, C. T. Supuran, and S. Parkkila, “Biochemical characterization of CA IX, one of the most active carbonic anhydrase isozymes,” *Journal of Biological Chemistry*, vol. 283, no. 41, pp. 27799–27809, 2008.
- [161] V. Ciccone, A. Filippelli, A. Angeli, C. T. Supuran, and L. Morbidelli, “Pharmacological inhibition of CA-IX impairs tumor cell proliferation, migration and invasiveness,” *International Journal of Molecular Sciences*, vol. 21, no. 8, 2020.
- [162] S. Y. Liao, M. I. Lerman, and E. J. Stanbridge, “Expression of transmembrane carbonic anhydrases, CAIX and CAXII, in human development,” *BMC Developmental Biology*, vol. 9, no. 1, pp. 1–16, 2009.
- [163] O. I. Kolenc and K. P. Quinn, “Evaluating cell metabolism through autofluorescence imaging of NAD(P)H and FAD,” *Antioxidants and Redox Signaling*, vol. 30, no. 6, pp. 875–889, 2019.
- [164] A. Gautier and M. J. Hinner, “Site-Specific Protein Labeling: Methods and Protocols,” *Site-Specific Protein Labeling: Methods and Protocols*, pp. 1–267, 2015.
- [165] L. Dubois, K. Douma, C. T. Supuran, R. K. Chiu, M. A. M. J. van Zandvoort, S. Pastoreková, A. Scozzafava, B. G. Wouters, and P. Lambin, “Imaging the hypoxia surrogate marker CA IX requires expression and catalytic activity for binding fluorescent sulfonamide inhibitors,” *Radiotherapy and Oncology*, vol. 83, no. 3, pp. 367–373, 2007.
- [166] A. Cecchi, A. Hulikova, J. Pastorek, S. Pastoreková, A. Scozzafava, J. Y. Winum, J. L. Montero, and C. T. Supuran, “Carbonic anhydrase inhibitors. Design of fluorescent sulfonamides as probes of tumor-associated carbonic anhydrase IX that inhibit isozyme IX-mediated acidification of hypoxic tumors,” *Journal of Medicinal Chemistry*, vol. 48, pp. 4834–4841, 2005.

- [167] J. Insua-Rodríguez and T. Oskarsson, “The extracellular matrix in breast cancer,” *Advanced Drug Delivery Reviews*, vol. 97, pp. 41–55, 2016.
- [168] K. Wolfa, S. Alexanderb, V. Schachtc, L. M. Coussensd, U. H. von Andriane, J. van Rheenenf, E. Deryuginag, and P. Friedla, “Collagen-based cell migration models in vitro and in vivo,” *Seminars in Cell & Developmental Biology*, vol. 20, pp. 931–941, 2009.
- [169] J. Kim, J. Kong, H. Chang, H. Kim, and A. Kim, “EGF induces epithelial-mesenchymal transition through phospho-Smad2/3-Snail signaling pathway in breast cancer cells,” *Oncotarget*, vol. 7, no. 51, pp. 85021–85032, 2016.
- [170] S. Comsa, A. M. Cimpean, and M. Raica, “The story of MCF-7 breast cancer cell line: 40 Years of experience in research,” *Anticancer Research*, vol. 35, no. 6, pp. 3147–3154, 2015.
- [171] R. A. Patel, Y. Liu, B. Wang, R. Li, and S. M. Sebti, “Identification of novel ROCK inhibitors with anti-migratory and anti-invasive activities,” *Oncogene*, vol. 33, no. 5, pp. 550–555, 2014.
- [172] M. Unbekandt, D. R. Croft, D. Crighton, M. Mezna, D. McArthur, P. McConnell, A. W. Schüttelkopf, S. Belshaw, A. Pannifer, M. Sime, J. Bower, M. Drysdale, and M. F. Olson, “A novel small-molecule MRCK inhibitor blocks cancer cell invasion,” *Cell Communication and Signaling*, vol. 12, no. 1, pp. 1–15, 2014.
- [173] T. Svitkina, “The actin cytoskeleton and actin-based motility,” *Cold Spring Harbor Perspectives in Biology*, vol. 10, no. 1, pp. 1–21, 2018.
- [174] S. Lim, H. Nam, and J. S. Jeon, “Chemotaxis Model for Breast Cancer Cells Based on Signal/Noise Ratio,” *Biophysical Journal*, vol. 115, no. 10, pp. 2034–2043, 2018.
- [175] S. J. Wang, W. Saadi, F. Lin, C. Minh-Canh Nguyen, and N. Li Jeon, “Differential effects of EGF gradient profiles on MDA-MB-231 breast cancer cell chemotaxis,” *Experimental Cell Research*, vol. 300, no. 1, pp. 180–189, 2004.
- [176] Y. Li, H. Wang, C. Tu, K. T. Shiverick, D. N. Silverman, and S. C. Frost, “Role of hypoxia and EGF on expression, activity, localization and phosphorylation of carbonic anhydrase IX in MDA-MB-231 breast cancer cells,” *Biochimica et Biophysica Acta - Molecular Cell Research*, vol. 1813, no. 1, pp. 159–167, 2011.

- [177] V. Biswenger, N. Baumann, J. Jürschick, M. Häckl, C. Battle, J. Schwarz, E. Horn, and R. Zantl, “Characterization of EGF-guided MDA-MB-231 cell chemotaxis in vitro using a physiological and highly sensitive assay system,” *PLoS ONE*, vol. 13, no. 9, pp. 1–17, 2018.
- [178] J. V. Jokerst, T. Lobovkina, R. N. Zare, and S. S. Gambhir, “Nanoparticle PEGylation for imaging and therapy,” *Nanomedicine (Lond)*, vol. 6, no. 4, pp. 715–728, 2011.
- [179] R. Zein, W. Sharrouf, and K. Selting, “Physical Properties of Nanoparticles That Result in Improved Cancer Targeting,” *Journal of Oncology*, vol. 2020, 2020.
- [180] L. Q. Chen, L. Fang, J. Ling, C. Z. Ding, B. Kang, and C. Z. Huang, “Nanotoxicity of silver nanoparticles to red blood cells: Size dependent adsorption, uptake, and hemolytic activity,” *Chemical Research in Toxicology*, vol. 28, no. 3, pp. 501–509, 2015.
- [181] B. M. Rothen-Rutishauser, S. Schürch, B. Haenni, N. Kapp, and P. Gehr, “Interaction of fine particles and nanoparticles with red blood cells visualized with advanced microscopic techniques,” *Environmental Science and Technology*, vol. 40, no. 14, pp. 4353–4359, 2006.
- [182] V. Peretz, M. Motiei, C. N. Sukenik, and R. Popovtzer, “The Effect of Nanoparticle Size on Cellular Binding Probability,” *Journal of Atomic, Molecular, and Optical Physics*, vol. 2012, pp. 1–7, 2012.
- [183] M. Zatovicova, L. Jelenska, A. Hulikova, P. Ditte, Z. Ditte, L. Csaderova, E. Svastova, W. Schmalix, V. Boettger, P. Bevan, J. Pastorek, and S. Pastorekova, “Monoclonal antibody G250 targeting CA IX: Binding specificity, internalization and therapeutic effects in a non-renal cancer model,” *International Journal of Oncology*, vol. 45, no. 6, pp. 2455–2467, 2014.
- [184] N. Touisni, N. Kanfar, S. Ulrich, P. Dumy, C. T. Supuran, A. Mehdi, and J. Y. Winum, “Fluorescent Silica Nanoparticles with Multivalent Inhibitory Effects towards Carbonic Anhydrases,” *Chemistry - A European Journal*, vol. 21, no. 29, pp. 10306–10309, 2015.
- [185] S. C. Chafe, P. C. McDonald, S. Saberi, O. Nemirovsky, G. Venkateswaran, S. Burugu, D. Gao, A. Delaidelli, A. H. Kyle, J. H. Baker, J. A. Gillespie, A. Bashashati, A. I. Minchinton, Y. Zhou, S. P. Shah, and S. Dedhar, “Targeting hypoxia-induced carbonic anhydrase IX enhances immune-checkpoint blockade locally and systemically,” *Cancer Immunology Research*, vol. 7, no. 7, pp. 1064–1078, 2019.

- [186] K. L. Maughan, M. A. Lutterbie, and P. S. Ham, "Treatment of breast cancer," *American Family Physician*, vol. 81, no. 11, pp. 1339–1346, 2010.
- [187] M. J. Ernsting, M. Murakami, E. Undzys, A. Aman, B. Press, and S. D. Li, "A docetaxel-carboxymethylcellulose nanoparticle outperforms the approved taxane nanoformulation, Abraxane, in mouse tumor models with significant control of metastases," *Journal of Controlled Release*, vol. 162, no. 3, pp. 575–581, 2012.
- [188] Y. Zhao, D. Y. Alakhova, J. O. Kim, T. K. Bronich, and A. V. Kabanov, "A Simple Way to Enhance Doxil® Therapy: Drug Release from Liposomes at the Tumor Site by Amphiphilic Block Copolymer," *Journal of Controlled Release*, vol. 168, no. 1, pp. 61–69, 2013.
- [189] S. A. Abouelmagd, B. Sun, A. C. Chang, Y. J. Ku, and Y. Yeo, "Release Kinetics Study of Poorly Water-Soluble Drugs from Nanoparticles: Are We Doing It Right?," *Molecular Pharmaceutics*, vol. 12, no. 3, pp. 997–1003, 2015.
- [190] J. S. Baek and C. W. Cho, "A multifunctional lipid nanoparticle for co-delivery of paclitaxel and curcumin for targeted delivery and enhanced cytotoxicity in multidrug resistant breast cancer cells," *Oncotarget*, vol. 8, no. 18, pp. 30369–30382, 2017.
- [191] L. Jiaa, J. Shena, Z. Li, D. Zhang, Q. Zhang, G. Liu, D. Zheng, and X. Tian, "In vitro and in vivo evaluation of paclitaxel-loaded mesoporous silica nanoparticles with three pore sizes," *International Journal of Pharmaceutics*, vol. 445, pp. 12–19, 2013.
- [192] C. Luo, J. Sun, D. Liu, B. Sun, L. Miao, S. Musetti, J. Li, X. Han, Y. Du, L. Li, L. Huang, and Z. He, "Self-Assembled Redox Dual-Responsive Prodrug-Nanosystem Formed by Single Thioether-Bridged Paclitaxel-Fatty Acid Conjugate for Cancer Chemotherapy," *Nano Letters*, vol. 16, no. 9, pp. 5401–5408, 2016.
- [193] P. Hobza and Z. Havlas, "Blue-Shifting Hydrogen Bonds," *Chemical Reviews*, vol. 100, pp. 4253–4264, 2000.
- [194] S. Scheiner and T. Kar, "Red- versus blue-shifting hydrogen bonds: Are there fundamental distinctions?," *Journal of Physical Chemistry A*, vol. 106, no. 9, pp. 1784–1789, 2002.
- [195] L. Silverman and Y. Barenholz, "In vitro experiments showing enhanced release of doxorubicin from Doxil® in the presence of ammonia may explain drug release at tumor site," *Nanomedicine: Nanotechnology, Biology, and Medicine*, vol. 11, no. 7, pp. 1841–1850, 2015.

- [196] A. Agarwal, M. A. MacKey, M. A. El-Sayed, and R. V. Bellamkonda, "Remote triggered release of doxorubicin in tumors by synergistic application of thermosensitive liposomes and gold nanorods," *ACS Nano*, vol. 5, no. 6, pp. 4919–4926, 2011.
- [197] N. Griffete, J. Fresnais, A. Espinosa, C. Wilhelm, A. Bée, and C. Ménager, "Design of magnetic molecularly imprinted polymer nanoparticles for controlled release of doxorubicin under an alternative magnetic field in athermal conditions," *Nanoscale*, vol. 7, no. 45, pp. 18891–18896, 2015.
- [198] J. Liu, Y. Huang, A. Kumar, A. Tan, S. Jin, A. Mozhi, and X. J. Liang, "PH-Sensitive nano-systems for drug delivery in cancer therapy," *Biotechnology Advances*, vol. 32, no. 4, pp. 693–710, 2014.
- [199] L. Ma, Q. Ouyang, G. C. Werthmann, H. M. Thompson, and E. M. Morrow, "Live-cell microscopy and fluorescence-based measurement of luminal pH in intracellular organelles," *Frontiers in Cell and Developmental Biology*, vol. 5, no. AUG, pp. 1–18, 2017.
- [200] Y. Kato, S. Ozawa, C. Miyamoto, Y. Maehata, A. Suzuki, T. Maeda, and Y. Baba, "Acidic extracellular microenvironment and cancer," *Cancer Cell International*, vol. 13, no. 1, p. 1, 2013.
- [201] A. J. Thistlethwaite, D. Leeper, D. J. Moylan, and R. E. Nerlinger, "pH distribution in human tumors," *International Journal of Oncology*Biological*Physics*, vol. 11, no. 9, pp. 1647–1652, 1985.
- [202] A. S. Karakoti, S. Das, S. Thevuthasan, and S. Seal, "PEGylated inorganic nanoparticles," *Angewandte Chemie - International Edition*, vol. 50, no. 9, pp. 1980–1994, 2011.
- [203] Q. Gu, J. Z. Xing, M. Huang, X. Zhang, and J. Chen, "Nanoformulation of paclitaxel to enhance cancer therapy," *Journal of Biomaterials Applications*, vol. 28, no. 2, pp. 298–307, 2013.
- [204] P. Ma and R. J. Mumper, "Paclitaxel nano-delivery systems: A comprehensive review," *Journal of Nanomedicine and Nanotechnology*, vol. 4, no. 2, p. 6, 2013.
- [205] A. E. Greijer, M. C. De Jong, G. L. Scheffer, A. Shvarts, P. J. Van Diest, and E. Van Der Wall, "Hypoxia-induced acidification causes mitoxantrone resistance not mediated by drug transporters in human breast cancer cells," *Cellular Oncology*, vol. 27, no. 1, pp. 43–49, 2005.
- [206] R. Sullivan, G. C. Paré, L. J. Frederiksen, G. L. Semenza, and C. H. Graham, "Hypoxia-induced resistance to anticancer drugs is associated with

- decreased senescence and requires hypoxia-inducible factor-1 activity,” *Molecular Cancer Therapeutics*, vol. 7, no. 7, pp. 1961–1973, 2008.
- [207] L. Arabi, A. Badiee, F. Mosaffa, and M. R. Jaafari, “Targeting CD44 expressing cancer cells with anti-CD44 monoclonal antibody improves cellular uptake and antitumor efficacy of liposomal doxorubicin,” *Journal of Controlled Release*, vol. 220, pp. 275–286, 2015.
- [208] Z. C. Soe, J. B. Kwon, R. K. Thapa, W. Ou, H. T. Nguyen, M. Gautam, K. T. Oh, H. G. Choi, S. K. Ku, C. S. Yong, and J. O. Kim, “Transferrin-conjugated polymeric nanoparticle for receptor-mediated delivery of doxorubicin in doxorubicin-resistant breast cancer cells,” *Pharmaceutics*, vol. 11, no. 2, pp. 1–17, 2019.
- [209] P. Munster, I. E. Krop, P. LoRusso, C. Ma, B. A. Siegel, A. F. Shields, I. Molnár, T. J. Wickham, J. Reynolds, K. Campbell, B. S. Hendriks, B. S. Adiwijaya, E. Geretti, V. Moyo, and K. D. Miller, “Safety and pharmacokinetics of MM-302, a HER2-targeted antibody–liposomal doxorubicin conjugate, in patients with advanced HER2-positive breast cancer: a phase 1 dose-escalation study,” *British Journal of Cancer*, vol. 119, no. 9, pp. 1086–1093, 2018.
- [210] A. M. Shabana and M. A. Ilies, “Drug delivery to hypoxic tumors targeting carbonic anhydrase IX,” *ACS Symposium Series*, vol. 1309, pp. 223–252, 2019.
- [211] J. L. Jeger, “Endosomes, lysosomes, and the role of endosomal and lysosomal biogenesis in cancer development,” *Molecular Biology Reports*, vol. 47, no. 12, pp. 9801–9810, 2020.
- [212] A. Vegerhof, E. A. Barnoy, M. Motiei, D. Malka, Y. Danan, Z. Zalevsky, and R. Popovtzer, “Targeted magnetic nanoparticles for mechanical lysis of tumor cells by low-amplitude alternating magnetic field,” *Materials*, vol. 9, no. 11, 2016.
- [213] S. Wang, K.-J. Chen, T.-H. Wu, H. Wang, W.-Y. Lin, M. Ohashi, P.-Y. Chiou, and H.-R. Tseng, “Photothermal Effects of Supramolecularly Assembled Gold Nanoparticles for the Targeted Treatment of Cancer Cells,” *Angewandte Chemie*, vol. 122, no. 22, pp. 3865–3869, 2010.
- [214] M. Domenech, I. Marrero-Berrios, M. Torres-Lugo, and C. Rinaldi, “Lysosomal membrane permeabilization by targeted magnetic nanoparticles in alternating magnetic fields,” *ACS Nano*, vol. 7, no. 6, pp. 5091–5101, 2013.

- [215] L. Minai, D. Yeheskely-Hayon, and D. Yelin, “High levels of reactive oxygen species in gold nanoparticle-targeted cancer cells following femtosecond pulse irradiation,” *Scientific Reports*, vol. 3, pp. 1–7, 2013.
- [216] M. A. Meledeo, B. L. Ibey, D. P. O’Neal, M. V. Pishko, and G. L. Cote, “Investigation of pH and temperature effects on FRET systems for glucose sensing,” *Proceedings of SPIE - The International Society for Optical Engineering*, vol. 4624, no. May 2002, pp. 55–65, 2002.
- [217] L. Wu, C. Huang, B. P. Emery, A. C. Sedgwick, S. D. Bull, X. P. He, H. Tian, J. Yoon, J. L. Sessler, and T. D. James, “Förster resonance energy transfer (FRET)-based small-molecule sensors and imaging agents,” *Chemical Society Reviews*, vol. 49, no. 15, pp. 5110–5139, 2020.
- [218] J. Patwari, A. Chatterjee, S. Sardar, P. Lemmens, and S. K. Pal, “Ultrafast dynamics in co-sensitized photocatalysts under visible and NIR light irradiation,” *Physical Chemistry Chemical Physics*, vol. 20, no. 15, pp. 10418–10429, 2018.
- [219] P. C. Ray, Z. Fan, R. A. Crouch, S. S. Sinha, and A. Pramanik, “Nanoscale optical rulers beyond the FRET distance limit: Fundamentals and applications,” *Chemical Society Reviews*, vol. 43, no. 17, pp. 6370–6404, 2014.
- [220] J. Lifante, Y. Shen, E. Ximendes, E. Martín Rodríguez, and D. H. Ortigies, “The role of tissue fluorescence in in vivo optical bioimaging,” *Journal of Applied Physics*, vol. 128, no. 17, p. 171101, 2020.
- [221] F. Zheng, W. Xiong, S. Sun, P. Zhang, and J. J. Zhu, “Recent advances in drug release monitoring,” *Nanophotonics*, vol. 8, no. 3, pp. 391–413, 2019.
- [222] S. Y. Li, L. H. Liu, L. Rong, W. X. Qiu, H. Z. Jia, B. Li, F. Li, and X. Z. Zhang, “A dual-FRET-based versatile prodrug for real-time drug release monitoring and in situ therapeutic efficacy evaluation,” *Advanced Functional Materials*, vol. 25, no. 47, pp. 7317–7326, 2015.

CURRICULUM VITAE

Name, surname	Agnė Janonienė (previously Vegytė)
Date and place of birth	1990-07-13, Biržai, Lithuania
E-mail	agne.janoniene@gmail.com, agne.vegyte@bti.vu.lt

Education

2014-2020	Vilnius University, Institute of Biotechnology, PhD student in chemistry engineering.
2009-2014	Lithuanian University of Health Sciences, Faculty of Pharmacy. Qualification degree of master in pharmacy and professional qualification of pharmacist.
2009	Biržai Saulės gymnasium. School leaving certificate with honors.

Research work experience

From 2019	Junior researcher at Institute of Biotechnology, Vilnius University
2015-2019	Research biologist at Institute of Biotechnology, Vilnius University

Traineeship

2016 January-March	Visiting PhD student, University of Helsinki, Finland
--------------------	-------------------------------------------------------

Participation in research project

2015-2017	Investigation of human carbonic anhydrase IX as a cancer biomarker for application in cancer diagnostics, visualization and prognosis. SEN-04/2015 from the Research Council of Lithuania.
-----------	--------------------------------------------------------------------------------------------------------------------------------------------------------------------------------------------

Vilnius University Press
9 Saulėtekio Ave., Building III, LT-10222 Vilnius
Email: info@leidykla.vu.lt, www.leidykla.vu.lt
Print run copies 15